Department of Precision and Microsystems Engineering

The Effects of Dehydration, Microclimate and Growth on the Acoustic Emission Characteristics of Plants In-Vivo

Berend Bart de Klerk

TU Delft Delft
University of
Technology

Challenge the future

Delft University of Technology

THESIS
ME56035

The Effects of Dehydration, Microclimate and Growth on the Acoustic Emission Characteristics of Plants In-Vivo

Author:
B.B. de Klerk (4435168)

Examination Board:
Dr.ir. G.J. Verbiest (chair)
Prof.dr. P.G. Steeneken
Dr. S. Dutta
S. Malleshaiah, MSc (Deliflor)

A thesis presented for the M.Sc. Mechanical Engineering, track High Tech Engineering.
To be defended on August 4th 2022 in the Kronigzaal at the faculty TNW of the TU Delft.

July 27, 2022

TUDelft Delft University of Technology

Acknowledgement

Abstract

What can plants *tell* us? Plants are known to emit ultrasound pulses during transpiration. These pulses are formed in the xylem vessel elements: cylindrical-shaped chambers inside the plant that transport water. The pulses arise from bubble formation within the sap of xylem vessels under tension. In this thesis, I demonstrated how the time- and frequency domain characteristics of these ultrasound pulses change under various conditions of water loss, light intensity, temperature, humidity and during plant growth. By quantifying the acoustic response and mapping the qualitative characteristics under varying conditions, I found a novel way to map plant behavior. This could form the basis of a new wholesome sensor module, where the sensor can indicate the health and growth of plants and their response to changes in the microclimate. This consolidates the current transition from traditional human-driven crop management toward automatic data-driven crop management.

State-of-the-art research suggests that the physiological parameters of xylem vessel elements can be linked to the acoustic signal. However, we do not yet know how the acoustic signal changes with varying environmental parameters such as water content, temperature, humidity and light intensity, or intrinsic parameters such as stem length or plant variety. In this thesis, a method is proposed to determine the effects of these parameters on the acoustic signal. This method included creating an algorithm that automatically detected signals related to bubble formation in the xylem vessels.

Two experimental phases were carried out: the first set of experiments was performed on tomato plants in a greenhouse and the second set was performed on chrysanthemums in a climate chamber. Using a greenhouse as a practical environment, the relations between acoustic signals and varying environmental parameters were investigated. In the climate chamber, the environment (water content, temperature, light and humidity) remained constant. Here the effect of the growth of the plant stem on the acoustic signal was shown.

With the first experiment in the greenhouse, I found a positive correlation between the rate of acoustic emissions and values for temperature, light intensity and humidity. The peak value for the number of acoustic emissions was 75 minutes later than the peak value for light intensity. Compared to temperature, this delay was 20 minutes and with humidity no delay was found.

A clear relationship between the characteristics of the pulses and the water loss was found. The amplitude of the signals increased during dehydration, whereas the settling time of the signals decreased as a function of water loss. This first correlation can be explained by stating that dehydration might change the damping properties of the plant tissue. The change in settling time is possibly due to larger xylem vessels embolizing at relative low water loss compared to smaller xylem vessels. In the frequency domain, I found two main frequency clusters around 10 kHz and 30 kHz. This suggests two main types of modes in the frequency domain. These modes could be attributed to different vibration sources within the xylem vessel that drive the acoustic pressure waves.

From the climate chamber experiment, we saw a relation between the plant growth and the main frequency, where the frequency of the signals decreased sub-linearly as a function of plant growth.

For future research it is advised to use an exciter that allows for receiving data continuously and on-demand. This will be beneficial for the throughput of the sensor. This artificial response should be compared to the natural AEs from a scientific standpoint.

Contents

1 Introduction

Plants are known to emit ultrasound pulses during water loss. In this thesis, I refer to these sound pulses produced by plants as Acoustic Emissions (AEs). The first to detect these AEs was Milburn in 1973 [1]. AEs originate in the xylem vessel elements: cylindrically shaped chambers inside the plant that transport water. AEs are caused by small bubbles in liquid-filled xylem vessel elements due to tension. The tension is due to the evaporation of water through foliar stomata. Bubble formation mechanisms include cavitation and air-seeding. These bubbles will increase in size until the whole xylem vessel element is filled with gas, a process called embolism. This process was explained in 1983 by Zimmermann [2]. One year later, the first vulnerability curve was presented by Tyree et al. [3]. This curve plots the percentage of cumulative AEs at different water potential levels. Since then, many researchers performed similar experiments [4, 5, 6, 7, 8]. In this thesis, we are mainly interested in the information that the AEs entail. This information is of interest for several applications.

The most obvious application of measuring AEs is the vulnerability curve that can be constructed to map (deleterious) environmental variables [6]. The vulnerability curve shows at what value of water loss cavitation is initiated and thus how well a certain plant species can withstand drought stress. When the characteristics of the AEs change as a function of water content, these changes can be used to determine the water demand of plants. It may provide a useful tool to be used in greenhouses to automatically detect irrigation needs. The sensing of irrigation needs is in line with the demand for new sensors since there is a shift from traditional human-driven crop management toward data-driven crop management. During several conferences I attended, this shift was advocated [9, 10, 11]. This transition is driven by a lack of available experts and the need for increased efficiency. Observations and experience are expected to be replaced by sensors and data.

A second application focuses on insects. Khait et al. speculate that animals might use AEs for their benefit, e.g. moths might avoid laying eggs on plants that emit sound and therefore suffer from drought stress [12]. Whether or not this is beneficial for the plant itself is debated.

Recent research has suggested that the AE may contain more information about the plant's physiology than just a marker for drought stress. State-of-the-art research from Dutta et al. shows that when the AE pulse is analysed, several properties of the plant can be deduced, which are the radius, length and viscoelasticity of the xylem vessel elements [13]. Not only is this way of dissecting a plant much faster and cheaper, it is also a viable option for examining the plant in-vivo (meaning during life and leaving the plant intact). Recently, a market research team has investigated the application in the form of market pull. One point of interest was about *vase life* (VL), which is the duration of a plant retaining its appearance after being cut. By knowing the diameter of xylem vessels, we have information about the VL of cut flowers [14] and disease susceptibility in crops [15]. During plant breeding, farmers and horticulturists can select the plants with the desired characteristics and use those for further crossing and breeding [16]. In the case of optimising VL, the plants with thinner xylem vessels (read: smaller diameter, not thinner cell walls) should be selected and used for further breeding. However, these plants will grow slower.

In this thesis, I show the scientific background surrounding the AEs from plants, which reveals a field yet to be discovered. For example, the vulnerability curve mentioned before has been widely investigated. But what we do not know is for example how the characteristics of individual acoustic pulses are influenced by several factors such as water content and microclimate. In this thesis, I hope to find correlations between the characteristics of the AEs and the environment of the observed plants. This research is part of the 4TU Plantenna project, which aims at developing smart sensors for horti- and agriculture.

In chapter 2 the background of plants' water transport and their vascular physiology is given. This includes the phenomena cavitation and embolism. Here also a translation from AE to plant characteristics is shown. Next, in chapter 3 the thesis research objective is formulated with its related research questions. Relevant literature elaborates on these questions to form hypotheses. The method and setup of the experiments to test the hypotheses are shown in section 4. In section 5 the first steps of the data analysis are described. This explains the step between the raw data and the results we are interested in. These results are then shown in section 6. An interpretation of the results is given in the discussion of section 7. This includes recommendations for future experiments and research. Finally, in section 8 a conclusion is given.

In the appendix A, an overview of different properties and their relations demonstrated by literature can be found. In appendix B, clarifying pictures from literature are shown. Additional pictures and graphs from experiment 1 and 2 can be found in appendix C and D, respectively.

2   Background

In this section, the background information around AEs is given. This information is based on scientific articles and provides guidance in assumptions and relations for later in the rapport.

2.1   Transpiration, anatomy and water transport

For every photosynthetic reaction in plants, water is used. However, this constitutes less than 1% of the total water use. The rest is almost entirely needed for transpiration [17]. Some larger trees can consume up to 1180 L of water every day [18], but usually the water usage of trees with a height of around 21 m is between 10 and 200 L per day [19], or between 0.015 to 0.2 L per day for small plants such as crops and weeds [20].
Transpiration in plants has several functions [21]. It provides a cooling effect, just like sweating human beings and other mammals. Moreover, it changes the osmotic pressure of the cells. Furthermore, it enables the flow of nutrients and water through the plant. But the most important function is that it opens the stomata, which can be considered to be the pores adjacent to the atmosphere. This enables the diffusion of carbon dioxide into the plant, which is necessary for photosynthesis and therefore life on earth.

Seed-bearing plants can be divided into two types: gymnosperms (those with revealing seeds) and angiosperms (those with enclosed seeds). The cells that transport water are called *tracheids* in gymnosperms and *xylem vessels* in angiosperms. Due to their anatomy and prevalence in the agri- and horticultural sector, our focus will be on the latter. Xylem vessels consist of several cylinder-shaped xylem vessel elements stacked on top of each other, resulting in a long cylinder-shaped conduit (see figure 1). These vessel elements can exchange fluids through their pits. Water is transported upwards by the tension in the xylem water column due to transpiration.
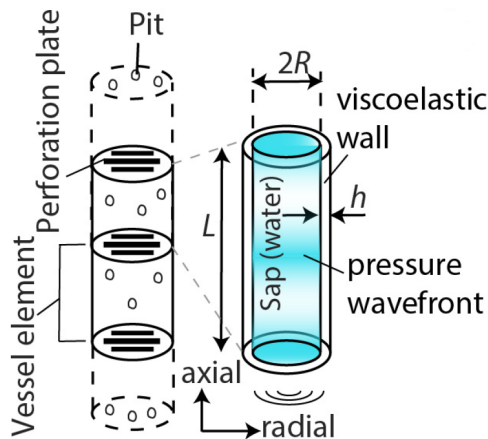
Figure 1: Cylindrical xylem vessel (schematic). From Dutta et al. [13]

2.1.1   Tension & water potential

Tension in xylems can be explained by the cohesion-tension theory. This theory dictates that due to the evaporation of water molecules, water is pulled upwards. This pulling or sucking of water should be large enough to compensate for gravity and friction. The transpirational pull, combined with capillary action and osmosis, can result in negative pressure down to -2 MPa at the leaf surface, enough to transport water up to 120 m above ground [22]. Water always moves from a system with a higher water potential to a system with a lower water potential. The water potential at the top of the plant is thus lower than the water potential at the bottom during transpiration.
Note that for gas, negative pressure is impossible since it cannot go below zero pressure. However, this theory does not hold for liquids where negative pressure is possible. It can be compared to tension in solids. With negative pressure in water, water molecules are pulling on each other and their surroundings.

When the pressure difference is too large, *cavitation* (which is the formation of bubbles in a liquid) can occur [1, 3, 17, 23, 24]. When a bubble enlarges until the whole vessel is filled with gas instead of liquid, it is called *embolism*, which is the obstruction of a conduit [2, 6, 25]. After a vessel is embolized, it prevents any passage of air or fluid, thus making the xylem dysfunctional [26]. It was found that when two-thirds of the functional transporting cells were embolized, the hydraulic conductance was reduced by 70% [5]. Vulnerability to cavitation is measured using P_{50}: the xylem pressure at 50% loss of hydraulic conductivity. More about the cavitation process is explained in section 2.2.

2.1.2 Trade-off: hydraulic conductance versus resistance to cavitation

The xylem vessels should have a low resistance to water flow to efficiently transport water. This is called hydraulic conductivity or hydraulic efficiency, indicated as K_h. Hydraulic conductivity can be indicated with water transport capacity (Φ in m^3/s) per pressure difference (ΔP in Pa). High hydraulic conductivity means that much water is transported with a small pressure difference. The hydraulic conductivity of a vessel increases with the fourth power of its diameter, following the Hagen-Poiseuille law (equation 1) [27].

$$\Delta P = \frac{8\eta L \Phi}{\pi r^4} \tag{1}$$

Here ΔP is the pressure difference, η the dynamic viscosity, L the length of the cylinder, Φ the volumetric flow rate and r the cylinder radius. So a larger vessel diameter results in lower resistance to water flow and thus efficient transport [28]. Considering equation 1, one would assume that smaller length also benefits hydraulic efficiency. However, since about 50% of the resistance arises at the pit membranes, the opposite is true (longer vessels result in fewer pit membranes) [2]. So to conclude, long and wide vessels are preferred for high hydraulic conductivity. Evolution has therefore driven plants towards this physiology [29]. According to Sevanto et al., drought may alter hydraulic conductance [30]. In other words: the relation between xylem diameter and hydraulic conductance is not constant but may depend on environmental parameters.

As stated in section 2.1.1, large negative pressure can result in cavitation and embolism which is disadvantageous for the plant. The larger the diameter of a plant, the larger the pit membrane area per vessel (A_P). A larger vessel surface area and thus larger pit membrane area per vessel results in a decreasing resistance to cavitation. In other words: a smaller diameter results in less cavitation. A trade-off is therefore found: with smaller xylem vessel diameters, less cavitation occurs which is beneficial for the plant, but the hydraulic conductance is decreased as well, which is disadvantageous for the plant.

2.2 Cavitation: an acoustic event

During cavitation, an ultrasound signal can be detected [4, 6, 8, 31], lasting for about $40\mu s$ (see figure 2a) [32]. This is the start of the embolism process, see figure 2b. It is found that each cavitation event produces one AE [3]. These sounds can be observed 10 cm from the source [12]. The nucleation of a bubble can release several tens of MPa [33]. However, note that insufficient model-based evidence exists to conclusively contribute the AEs to cavitation and embolism [34].

(a) The ultrasonic signal measured during cavitation in the time domain.

(b) The embolism of a xylem vessel.
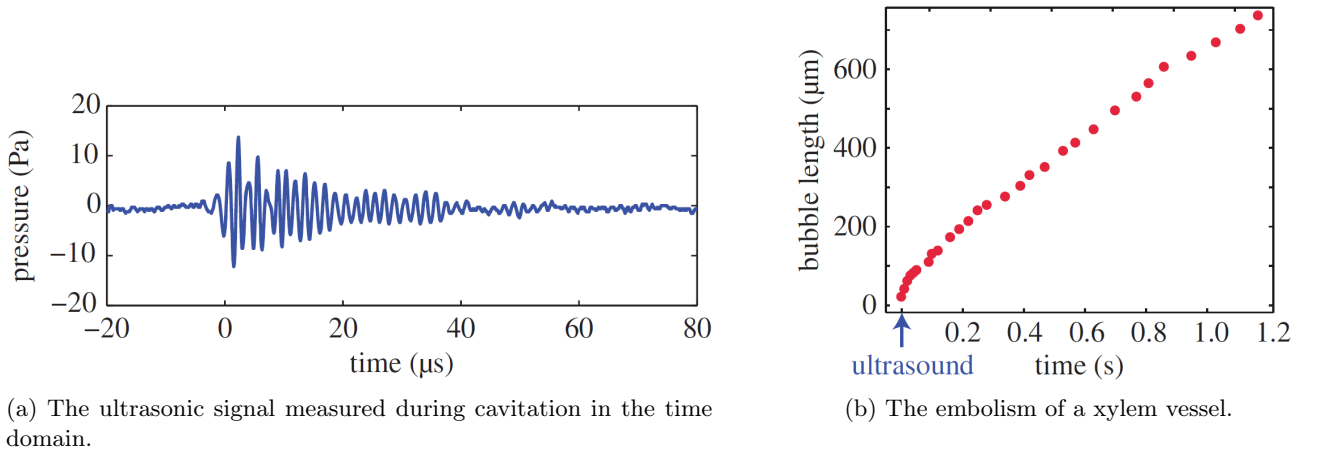
Figure 2: The cavitation and embolism process within a slice of wood. From Ponomarenko et al. [32]

As can be seen in the vulnerability curve from figure 3, the more water is lost, the more AEs occur [3]. This substantiates the above-mentioned assertion that each cavitation event produces one AE. It is interesting to see the S-shaped relation between water loss and the cumulative number of AEs.

2.2.1 Behaviour of bubbles

Several models about the dynamics of bubbles in finite spaces and their natural frequency have been investigated [35, 36, 37, 38, 39, 40]. However, we now know that is not solely the bubble that makes the sound, but mainly the relaxation of the cell wall [41, 42]. The detected signal originates from the sudden abrupt AE source, rather than the oscillating source [31]. Note that besides cavitation, other sources of AE have been demonstrated.

Figure 3: Vulnerability curve. Shown is the cumulative number of AEs versus the total water loss from stem segments dehydrated from various initial water potentials. The arrows indicate the estimated per cent of the total water contained in the severed tracheids at both ends of the stem segment. From Tyree et al. [3]

These are cell-wall shrinkage [43], crack formation [7], capillary action of free water (Haines jumps) [44], bark-tissue shrinkage [44] and nucleation and propagation of ice in the freezing xylem (similar to drought 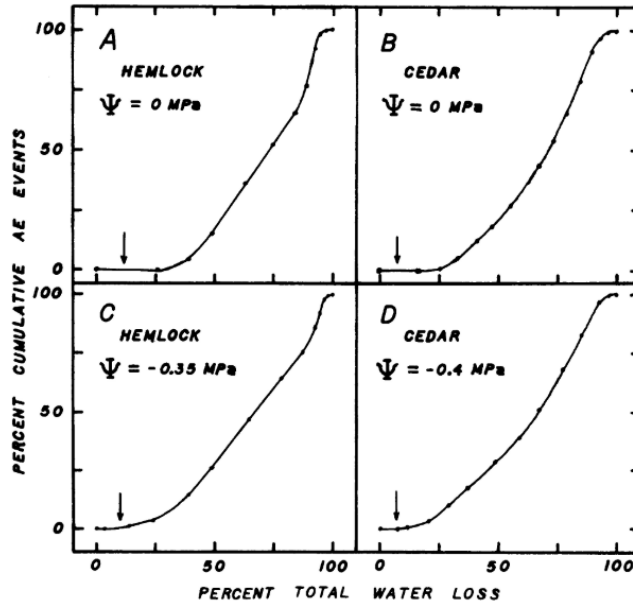stress) [45]. In a recent master thesis with 3D printed replicates of xylem vessels, Bieling found AEs that possibly originated from fluid front displacement, material expansion and water evaporation from surfaces and porous membranes [46].

2.3 Acoustic properties versus xylem anatomy

Now that we know about the origins of the AEs, we can dive deeper into the information the AEs entail. I will do so by linking the xylem vessel properties to characteristics of sound. The speed of sound for a certain medium is given by equation 2. Note that wave velocity and speed of sound are the same as phase velocity.

$$c = \sqrt{\frac{K_s}{\rho_l}} \tag{2}$$

Here c is the wave velocity of the medium, K_s the isentropic bulk modulus (i.e. resistance to compression) and ρ_l the density. For water, these properties are $c = 1480$ m/s, $\rho_l = 997$ kg/m^3 and $K_s = 2.2$ GPa.
The isentropic bulk modulus differs from the Youngs modulus, as the isentropic bulk modulus is a parameter to measure how volumetrically resistant to compression a substance is, whereas the Youngs modulus describes the response to lengthwise compression or stretching and shows thus the areal resistance. This relation is given in equation 3.

$$K_s = \frac{E}{3(1 - 2\nu)} \tag{3}$$

Here ν represents the Poisson ratio: the deformation of a material in the direction perpendicular to the direction of loading. As plant tissue includes fibres, the material is anisotropic, meaning that the properties of the material depend on the direction. This also means that the Poisson ratio has different values, depending on the direction. The value of the Poisson ratio is usually between 0 and 0.5. A large value for the Poisson ratio means that the deformation in the lateral direction is large with a tensile load in the longitudinal direction.
It can be deduced from equation 2 that when the density increases, the speed of sound always decreases. However, this is incorrect. As the bulk modulus is defined as equation 4, the influence of density in equation 2 for the speed of sound is not as straightforward.

$$K_s = \rho_l \frac{dP}{d\rho} \tag{4}$$

$dP/d\rho$ denotes the derivative of pressure with respect to density. For composite materials such as the cell wall, the bulk modulus (and therefore the speed of sound) is dependent on the material composition [47]. This can be

4

calculated by obtaining the weighted average of each component (see section 2.5). However, a more prevailing approach is to use the cross-sectional compressibility β, which can be calculated using equation 5. Consider the xylem vessel as a cylindrical Helmholtz resonator filled with water with radius R, length L, wall thickness h and Youngs modulus E (see figure 1).

$$\beta_{\text{xylem}} = \frac{2R}{hE} \tag{5}$$

To calculate the effective speed of sound v_{eff}, we have to implement the cross-sectional compressibility β in equation 2. This yields equation 6 [47, 48].

$$v_{\text{eff}} = \sqrt{\left(\frac{1}{c^2} + \rho_l \cdot \beta\right)^{-1}} \tag{6}$$

Equation 4 implies the liquid ρ_l is considered compressible. One might suggest that if so, the density ρ_l in equation 6 will change as well. Although this is true, its change is negligible compared to the change in cross-sectional compressibility since the compressibility of water is in the order of magnitude of 10^{-10} Pa^{-1} [49] and pressure does not go below -2 MPa [22].

The following equations are obtained from Dutta et al. [13]. If an acoustic pulse is determined, we can use the damping coefficient to calculate the diameter of the xylem vessel using equation 7. This diameter will further in the report be referred to as the acoustic diameter.

$$D = 2\sqrt{\frac{4\,\eta_l\,\tau_s}{\rho_l}} \tag{7}$$

Here η_l is the dynamic viscosity of water and τ_s the settling time of the envelope (i.e. the time needed for the amplitude to decrease by factor 'e'). The length of the xylem vessel can be calculated using the resonance frequency measured, see equation 8. Remember v_{eff} from equations 6 and 5.

$$L = \frac{v_{\text{eff}}}{2f_L} \quad \text{or} \quad f_L = \frac{v_{\text{eff}}}{2L} \tag{8}$$

In theory, a lower Youngs modulus would result in higher cross-sectional compressibility, lower effective speed of sound and thus lower frequency. Likewise, a smaller radius would result in a higher frequency. This is with the sidenote that this holds only if β is large enough compared to $1/c^2$ in equation 6.

Note that we ignore the vessel membranes, commonly referred to as microperforated panels (MPP). These are found to absorb some of the frequencies. In the study of Maa et al., it was found that the frequency range from 0 to 8 kHz was partially absorbed [50]. This was however for a rather large MPP compared to those in xylem vessels. Absorption will only partially absorb frequencies, so a clear signal should remain.

2.4 Other acoustic effects

2.4.1 Specific acoustic impedance

The specific acoustic impedance z can be calculated using equation 9. It is defined as "the ratio of the complex amplitude of sound pressure to that of a specified vector component of the associated particle velocity" [51]. I.e. the acoustic impedance is used to indicate how well sound is transmitted from one medium to another.

$$z = \rho\,c \tag{9}$$

Here z is the specific acoustic impedance of the medium, ρ is the density and c is the wave speed. Using equation 2 we can calculate that the specific acoustic impedance for water equals 1.48 MPa s/m. Note that the *specific* acoustic impedance z is not to be confused with the acoustic impedance Z. The latter takes the area of transmission into account and is thus size-dependent whereas the former is solely material specific: $Z \cdot A = z$ with A the unit area.

For composite materials, we cannot substitute c with v_{eff} from equation 6. We need to use the approach of using the parameters of each component and calculate the impedance as if these components are in series. The reflection ratio (which is the inverse of the transmission ratio) can be calculated using equation 10.

$$R = 1 - T = \frac{I_r}{I_0} = \frac{(Z_2 - Z_1)^2}{(Z_2 + Z_1)^2} \tag{10}$$

Here R is the reflection ratio, T is the transmission ratio, I_r is the intensity of the reflection, I_0 is the total intensity. Z_1 is the specific acoustic impedance of substance 1 and Z_2 for substance 2. The smaller the difference between Z_1 and Z_2, the smaller the reflection and therefore the larger the transmission ratio.

Because the frequency of a sound is defined as the number of waves per second, the frequency of sound does not change when entering a new medium. When the speed of sound in the new medium differs from the former, the wavelength is changed, but the frequency remains constant.

2.4.2 Acoustic dispersion

Acoustic dispersion can be compared to optical dispersion, which happens in a prism. In certain media, the speed of light differs for different frequencies. This holds for the speed of sound and acoustic frequencies as well. This would result in an altered sound pulse. However, this phenomenon does not change the frequencies or amplitude, it only changes their time of observation. Due to the relatively low frequency of sound, the magnitude of dispersion for most materials is less than 1% for frequencies between 1-10 MHz [52].

2.5 Mechanical properties of plant stems

The properties of plants that we investigate are summed up in appendix A table 2. Also the relation between several properties is depicted there (table 3).

Plants show biphasic behaviour [53]. This means that in the stress-strain curve, two Youngs moduli are observed. We can see this biphasic behaviour in figure 38a in appendix B, where the stress-strain curve of the hydrated sample has two main slopes. This can be interpreted as a composite material with stiff fibres embedded in a less stiff matrix [53]. I.e. this means that the stiffness of the plant stem depends on the strain of the stem itself. Hysteresis, which is connected to biphasic behaviour, is observed as well (figure 39a). Plastic deformation is shown as well since in the same research the Youngs modulus of the first loading-unloading process was about 80% as large as the following loading-unloading processes. Note that biphasic behaviour is different from viscoelasticity. Viscoelasticity means that the relationship between stress and strain is time-dependent. Plants show both biphasic and viscoelastic behaviour. This is nicely depicted in figures 38 and 39 in appendix B. This nonlinear behaviour in plants is the result of a complex structure of the cell wall. This wall consists of four main building blocks, namely cellulose, hemicellulose, lignin and pectin. The composition of these building blocks determines the mechanical properties of the cell [54].

The Youngs modulus of plant stems increases during dehydration, as can be seen in figure 38a [55]. This is contradictory to the results of Niklas (figure 38b) [56], which claims the Youngs Modulus of parenchyma cells in tubers decreases during dehydration. In the same line as Niklas, Fariñas et al. found that reduction of transpiration due to a reduction in temperature and light intensity increased turgor pressure, stiffness and increased resonant frequencies of leaves [57]. However, it is important to become familiar with the difference between turgor pressure and xylem vessel pressure. Turgor pressure is the positive pressure in the plant cells that allow the stiffness of plants. If this pressure decreases, the stiffness decreases as well, as we see in figure 38b. The pressure in the xylem vessels is negative, as explained in section 2.1.1. The xylem vessels consist of lignified walls (dead tissue) with water in the interstitial spaces. As water content decreases, the fibres on the lignified walls of the xylem vessels become more rigid and the Youngs Modulus increases [58]. This can be seen in figure 38a.

Due to tissue anisotropy, the modulus-water relations are quite complicated. The tensile Youngs Modulus may not be the same as the flexural Youngs modulus or compression Youngs modulus. As tensile Youngs modulus is most general and commonly used, this will be the focus of this research. In both figures 38a and 38b, the tensile modulus is depicted.

Moreover, plants exhibit viscoelastic behaviour. This means that a tensile Youngs modulus is not sufficient to describe its behaviour, since a time-dependent viscous component is missing. This component will result in hysteresis and creep, which is indicated in figures 38b and 39 in appendix B. However, the first part of the load-displacement curve, which is used to determine the tensile Youngs modulus, will not be greatly affected by this complex behaviour. Limiting the scope of the thesis, I will focus on the tensile Youngs modulus deduced from the initial load-displacement curve.

3 Research Objective and State of the Art

This research mainly builds upon the work of Dutta et al. [13], which relates the characteristics of AEs to the internal structure of plants. As the AEs are often the result of dehydration which is a time-dependent variable, a point measurement does not seem suitable. Therefore, this change in water content should be investigated. Changes in water content lead to changes in the material properties (such as Youngs modulus), and it may therefore also influence the characteristics of the AEs. The main question that arises is:

1. **How do the characteristics of the AEs change with decreasing water content?**

The acoustic signal has several characteristics to evaluate which are mainly frequency, amplitude, and settling time of the pulse. These should all be measured and analysed.

Other questions that arise are the following:

2. What are the effects of changes in light, temperature and humidity on the AEs?

3. How does the growth affect the AEs?

4. What can the AEs say about the vase life of flowers?

Since it was only recently discovered that the acoustic signal entails relevant information, almost no research is done on how the signal is affected by environmental changes. Prior to the research from Dutta et al. [13], the focus was on the number of AEs and its link to hydraulic vulnerability, rather than on the change of each cavitation pulse [3, 4, 5, 7, 8, 59]. Analysing each AE will extend the work of Dutta et al. and give a more clear insight into the plant's response to the environment.

Below, state-of-the-art about each of the research questions is given. This shows the current knowledge gap, underpins the research and aids in forming hypotheses.

3.1 How do the characteristics of the AEs change with varying water content?

As stated above, this research question follows stems from the lacking link between the water loss of the plant resulting in AEs, and the characteristics of those AEs.
Beall claims that as long as the moisture content of the fibres in wood is above the fibre saturation point (FSP), the velocity of acoustic waves is constant in the longitudinal grain direction [59]. Below the FSP, increasing moisture content resulted in a decrease in wave velocity [60]. The other way around holds: during dehydration the wave velocity is deemed to increase. It is not stated how this influences the vibration frequencies of the vessels. However, considering equation 8, a lower wave velocity would result in lower resonance frequency. This only holds in the given medium of that wave velocity.
In a recent student assignment conducted at the TU Delft, the relation between water loss and frequency using the Acousto-ultrasonic (AU) technique was investigated [61]. This technique is explained in chapter 4. This group concluded that water potential does not influence the frequency. They did notice however that when water potential decreases, the amplitude increases. However, this result is rather small. In figure 40 in appendix B, the acoustic signal from the plant *Hydrangea Macrophylla* is shown in the frequency domain for several percentages of water loss.
Oletic et al. also performed a frequency analysis of drying grapevines [40]. Figure 4 shows some interesting insights. Both low and high frequencies are more visible at the end of the drying process. To be precise: both low and high frequencies did not necessarily increase in amplitude, but rather in occurrence. Figure 4b corresponds to figure 3, but it is not extensive enough to make claims about the relationship between water potential and frequency. Nothing is said about the amplitude- or frequency shift during dehydration.

Decreasing water potential could also influence the dimensions of the xylem vessel elements. Considering equations 7 and 8, changes in the dimensions would result in changes in both frequency and settling time. Shrinkage of length and radius would theoretically result in pulses with higher frequency and smaller settling time respectively.
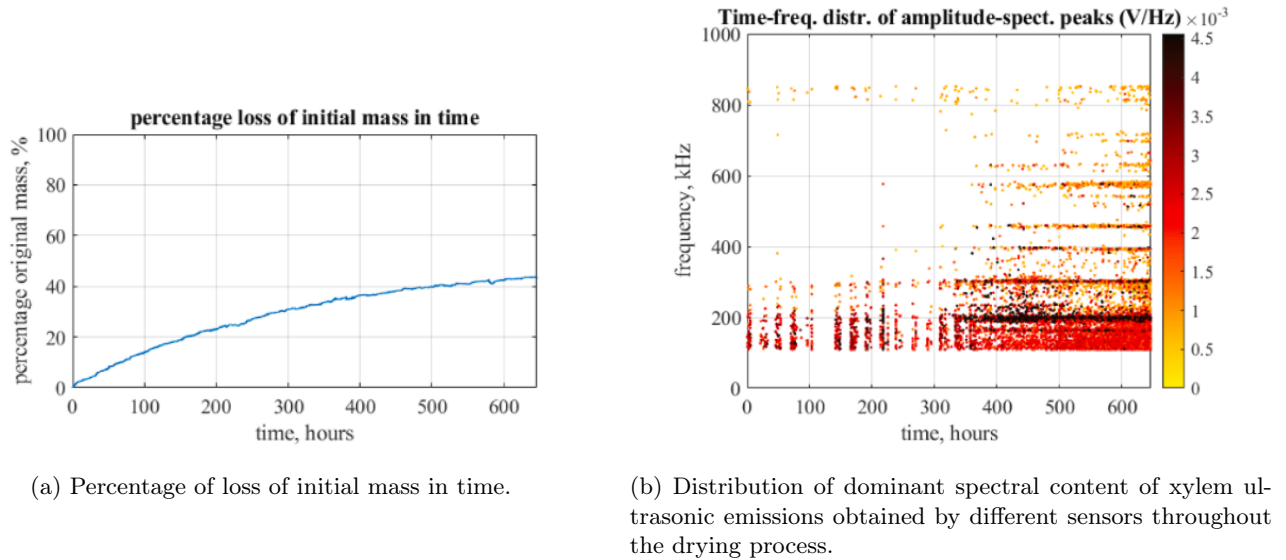
(a) Percentage of loss of initial mass in time.

(b) Distribution of dominant spectral content of xylem ultrasonic emissions obtained by different sensors throughout the drying process.

Figure 4: Long-term natural bench drying experiment of grapevine. From Oletic et al. [40].

3.2 What are the effects of changes in light, temperature and humidity on the AEs?

With this research question, I want to show the relationship between the AEs and the environment or microclimate of the plant. With microclimate, I mean the environmental factors that the plant experiences.

As can be seen in figure 5, the diurnal changes in temperature, light and humidity may affect the xylem diameter and therefore the settling time of the AEs. However, no quantitative link to these properties is given, solely the fluctuations during the day for a period of 7 to 132 days in different months.
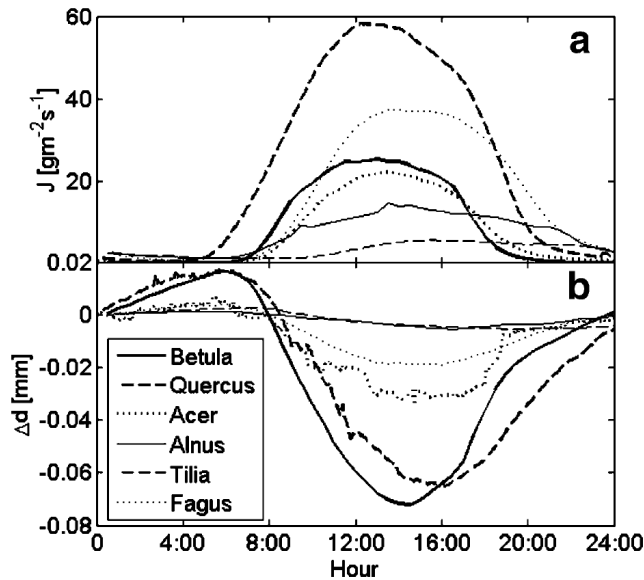

Figure 5: Daily average pattern of **a:** sap flow rate and **b:** xylem diameter variation. The different lines indicate 6 different deciduous tree species. From Sevanto et al. [30]

In the work of Mott et al., the effects of humidity on light-induced stomatal openings are investigated [62]. They explain that there is typically a delay between the illumination moment and the stomatal opening. This delay, called the *Spannungsphase*, varies between 15-60 minutes (figure 41 in appendix B). Many factors influence the opening of the stomata, such as solute concentration, salt, light intensity and light colour [63].
The diurnal patterns of increased light, temperature and humidity increase AE count [64]. Dostál and Sriwongras found that the temperature of the air was the most correlated to the rate of AEs, followed by humidity, atmospheric pressure and light intensity, in that order [65, 66]. They found this result by calculating the correlation coefficient R.

8

3.3 How does the growth affect the AEs?

It is shown that vulnerability to embolism is related to xylem vessel diameter and that the vessels are wider at the base than at the top (section 2.1.2). These two factors predict a limited maximum vegetation height. Vessel diameter is therefore an important indicator for the growth of the plant. The relation between vessel diameter D_V and stem length L_S is given with equation 11 [67]. This is supported by the work of Olson et al. [68]. When we relate this to equation 7, it is expected that during constant growth, the decay time would increase super-linearly. I.e. when we combine the equations 7 and 11, we get $L_S^{0.2} \propto D_V \propto \tau^{0.5}$ which translates to $\tau \propto L_S^{0.4}$. Figure 6 shows a similar function, where regression models predict basal vessel diameter $D_{V(0)}$ and apical vessel diameter $D_{V(N-1)}$ based on SL. This shows the scaling of $D_V \propto L_S^{0.23}$ [67].
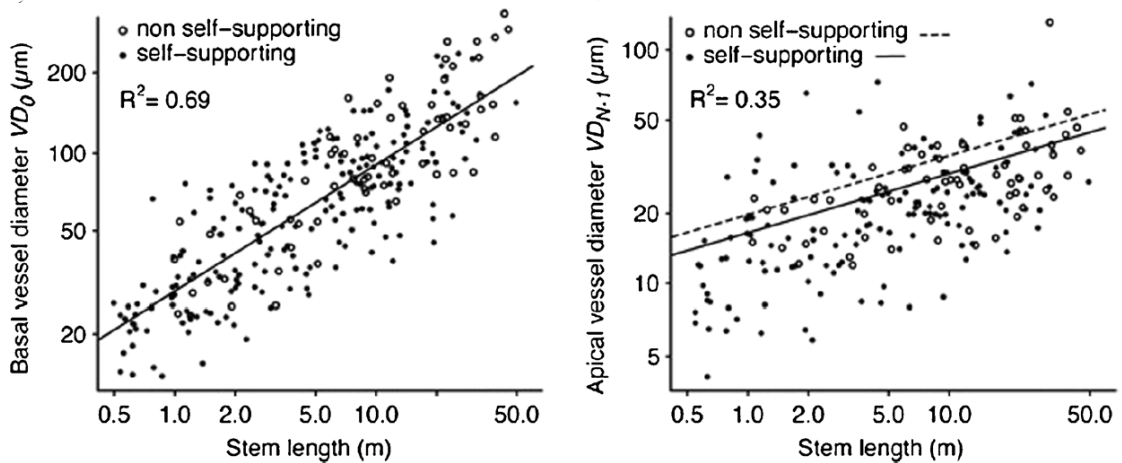
$$D_V \propto L_S^{0.2} \tag{11}$$

Figure 6: Scaling of xylem vessel diameter with stem length across angiosperm species and habits (points are mean values of species). **left:** Basal vessel diameter ($D_{V(0)}$) scales similarly with L_S between self- and non-self-supporting species. **right:** Twig apical vessel diameter ($D_{V(N-1)}$) scales with L_S across self- and non-self-supporting species, meaning that taller plants and longer lianas have predictably wider vessels not only at the stem base but also at the stem apex [67].

Given equation 8, we can calculate the length of the xylem vessel with the AE. As the plant grows, I expect the xylem vessel to grow along. This means that the frequency is hypothesized to decrease with water loss.

By artificially controlling the duration of light exposure, the length of Chrysanthemum flower stems can be controlled [69]. Nissim et al. found that overnight lighting resulted in inhibition to flowering for Chrysanthemums [70]. In figure 42 in appendix B we can see that the growth increases with overnight lighting as well.

3.4 What can the AEs say about the vase life of flowers?

Using the information given in the introduction, we know that a larger xylem vessel diameter decreases VL [14]. Because the basal part of the stem is cut and therefore exposed to air, embolism occurs in this part. These emboli should disappear during rehydration. Xylem vessels with small diameters are found to be better at removing the air-blockages compared to xylem vessels with large diameters. From equation 7 we know that a larger settling time τ_s implies a large vessel diameter. This suggests that a larger settling time in the acoustic signal will result in a decrease in VL.

As stated in section 2.1.2, a larger xylem vessel diameter reduces hydraulic conductance. In evolution, this hydraulic conductance is important because of competition. Markesteijn et al. found that indeed pioneers tended to have larger hydraulic conductance and smaller safety margins (read: larger diameter) than shade-tolerant species [29]. In the trade-off between hydraulic conductance and the ability to remove emboli, the latter is of greater importance considering VL.

In table 4 in appendix A the influence of many factors on the VL is depicted [71].

4 Measurements & Setup

Two types of ultrasonic technologies could be of use in this research area: naturally induced Acoustic Emissions (AEs) and Acousto-ultrasonics (AUs) [59]. Where AEs work without an actuator, AUs work with an active pulser used to inject stress waves into the sample. The sample attenuates some frequencies more than others, while all are observed. Our focus will be on the naturally induced AEs because this builds on previous research [13]. As I am measuring plants in-vivo, I will only measure the AEs in the radial direction.

The 4 research questions mentioned in the previous chapter will be answered using three separate experiments. The experiments will be categorized as follows:

- **Experiment 1: Greenhouse.** This experiment will answer the two research questions *How do the characteristics of the AEs change with varying water potential?* and *What are the effects of changes in light, temperature and humidity on the AEs?*

- **Experiment 2: Climate Chamber.** Here we will investigate two research questions: *How does the growth affect the AEs?* and *What can the AEs say about the vase life of flowers?*

4.1 Experiment 1: Greenhouse

This experiment was conducted in a greenhouse at the Wageningen University and Research facility in Bleiswijk. The reason to perform this experiment in a greenhouse is to simulate a natural environment, while simultaneously logging and controlling the varying parameters. Due to the limited capacity in the greenhouse and the dependency on harvesting time, this experiment was performed first. The duration was 22 days as I measured from November 1 until November 23 (not including November 23). For the research in the greenhouse, several properties are taken as variables whereas others are taken as constant. These properties will be elaborated on below.

4.1.1 Variables

The parameters that act as variables are the following:

- Water Content
- Acoustic Signal
    - Amplitude
    - Frequency
    - Settling Time
- Temperature
- Humidity
- Light Intensity

Under drought stress, the *water content* in the soil can be obtained by measuring the water potential in the soil. I used two types of water content sensors, the 5TM which measures water content in cubic meters per cubic meter, and the TEROS 21 which measures water potential in Pascal. Another method to measure water potential is the 'Pressure Bomb' [72, 73, 74]. This method is destructive and rather time-consuming. Therefore, the former method is chosen.

The *acoustic signal* can be measured using a microphone (Pettersson M500 USB Ultrasound Microphone). This microphone has a sampling frequency of 500 kHz and thus a maximum observable frequency of 250 kHz. Note that this microphone comes with a supplementary horn for amplifying the signal, but this horn will mostly magnify the 7 kHz frequency, so it is advised not to use this. Signals were observed if they exceeded a threshold value of -40dB and 5kHz for amplitude and frequency, respectively. The amplitude threshold was the lowest possible in the software and the 5 kHz was chosen to limit the amount of data while still being large enough to incorporate all acoustic events.

The greenhouse facility has sensors for logging the *temperature, humidity* and *light intensity*. These environmental parameters are logged every 5 minutes.

4.1.2 Constants

Some parameters influencing the observed signal that are tried to remain constant are summed up below.

- Plant species

- Position of the microphone from the ground

- Distance between plant and microphone

For plant species, the *Solanum Lycopersicum* (tomato plant) is chosen for 3 reasons. First, this plant is part of the Solanum genus, and it reacts quite fast to for example water deficit. Secondly, the plant has a short lifecycle, which means we can measure it multiple times a year. Finally, it has a large economic value, which makes applications more interesting for companies. Recently, a master's student in Wageningen conducted experiments to form a database of several plant species and their response to drought [75]. This research supported the theory proposed by Dutta et al. [13] to be valid for different species.
For the distance between the plant and the microphone, a module is created using 3D printing. This is elaborated below in section 4.1.3.

Several other factors could potentially influence the result, but are believed to be constant or have negligible impact. These are stated below.
Pressure is assumed to be constant since the atmospheric pressure will likely not shift much given the local climate. The *Dynamic Modulus* could interfere with the Youngs Modulus. However, this interference is only present at high frequencies that we will not use. *Acoustic dispersion* happens when sound travels through different media. This would influence the signal shape. However, as stated in section 2.4.2, the magnitude of dispersion is rather low. Since the speed of sound in plants and water are close to each other, this factor can be neglected. *Noise* in the frequency response is unavoidable. Careful analysis of the signal in both time- and frequency domain should be performed before taking values for settling time and frequency. *Air velocity* should be kept to a minimum. Since the experiment will take place in a greenhouse, no wind will be present. However, the opening of doors or people walking past the stem will create air velocity. This should be kept to a minimum. *Carbon dioxide and oxygen* are not constant. There are sensors provided by the greenhouse to measure CO_2 levels. The effects of these concentrations are deemed negligible by experts from the greenhouse and will therefore not be analysed further. *The stage of life and seasonality* of the plant could potentially influence the AE. The experiment will take place right after the harvest of the tomato fruits. The greenhouse will reduce the effect of the season. In experiment 2, the effect of growth will be investigated. *Nutrition* should be kept constant. *The size of the plant* and the number of leaves should be constant as well. Since the duration of the experiment is only a few weeks and it is after harvest time, the size of the plant will not change much.

4.1.3 Greenhouse setup

Two microphones are used to measure two different tomato plants. This was done to account for plant-to-plant variability in the results. The microphone is attached to the plant stem to make sure the distance between the microphone and stem remains constant. With the 3D printing technique, a plastic module is created using the agile approach. This module can hold the microphone and is mounted onto the plant stem using two tie-wraps, see figure 7. The distance between the microphone and plant is fixed at 1.0 mm. As the tension in the water column is more negative high above the ground and the number of air-seeding cells will be larger as well, the microphone is mounted high above the ground at roughly 1.80 m high. I had only one computer and the Batsound software allowed only one recording device to measure. Therefore, the two microphones were used in a time-interleaved manner. This means that every hour, microphone 1 measured for 20 minutes, then microphone 2 measured for 20 minutes, followed by a 20-minute break. Using a mouse-clicking program, this routine was automated. The 20-minute break was implemented to allow the mouse-clicking program to terminate a measurement, save the data and select a new measuring device.

(a) The beginning of experiment 1 when all leaves are still green.

(b) The end of experiment 1 when the plants are wilted and dried out.

Figure 7: Greenhouse setup for measuring AEs of the plant during dehydration (experiment 1). The black device is the ultrasound microphone and the grey clamping module holds it in its place.

4.2   Experiment 2: Climate chamber

I conducted this experiment using three different varieties of *Chrysanthemums*. These flowers are chosen because they grow straight up and their physiology and behaviour are well understood at the facility. The experiment is performed at a climate chamber at Deliflor in Maasdijk. The measurements took place from May 2 to May 30 (until May 30 10:00).

4.2.1   Variables

The parameters that act as variables in this experiment are the following:

- Acoustic Signal

    - Amplitude
    - Frequency
    - Settling Time
    - Duration

- Plant Height

- Plant species

For observing the water content and acoustic signal, the same equipment as in experiment 1 is used (see section 4.1). The plant height is observed during the experiment. This height is the distance from the soil to the top of the plant. As the leaves are growing at an angle, a small error in measuring cannot be avoided (figure 8a). Finally, the experiment is performed on three different species, each with a different vase life. For each variety, two plants are monitored, resulting in six plants total.
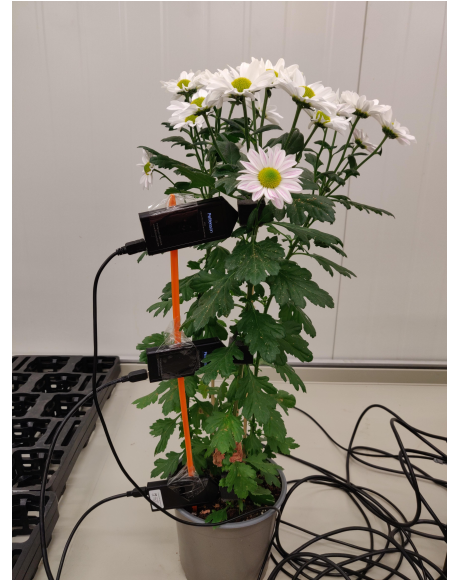
4.2.2   Constants

Other parameters are taken as constant. These are summed up below.

- Temperature

- Light Intensity

- Humidity

- CO_2
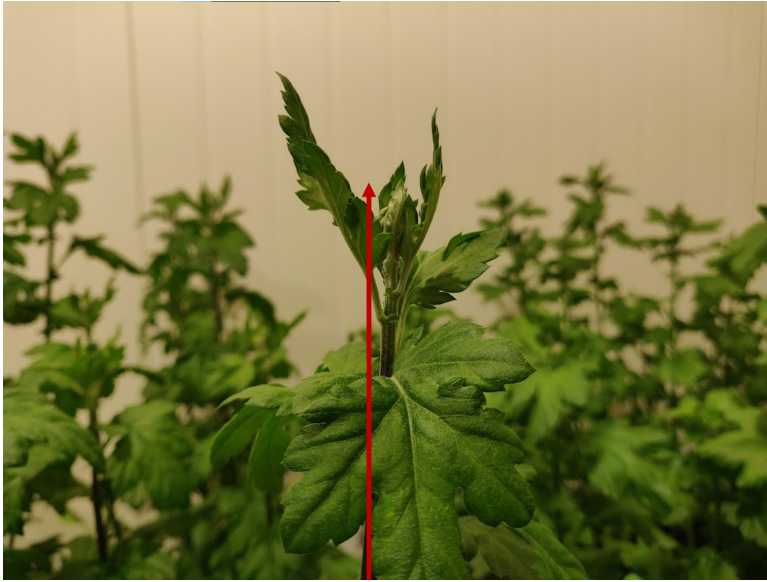
(a) The top of the plant is measured without the leaves on the side. The distance from the top of the plant to the soil is the plant length.

(b) Setup to determine the optimal location for the ultrasound sensor during the mock-up experiment.

Figure 8: Specifics for experiment 2 in the climate chamber at Deliflor.

- Soil water content
- Height of measuring relative to plant

The environmental parameters Temperature (18,0°C), Light Intensity (31 µmol m^{-2} s^{-1}), Humidity (60%) and CO_2 (300 ppm) are deemed constant. I assume these parameters as constant because this experiment is performed in a specially designed climate chamber with automatic feedback systems.

The light intensity is kept constant for three reasons. First, by having this as a constant, the AEs will not be influenced by fluctuations in the light intensity. The other two reasons have to do with the growth and flower development of the plant. As stated in section 3.3, the amount and duration of light are important for growth and flower development. For example, Deliflor produces flowers according to the following method: first, the flowers will have many hours of light every day, called the Long Day Period (LDP). This will promote the growth of the flower. After 10 days of LD, the plants move to the Short Day Period (SDP) for 40-45 days with fewer hours of light, which enables flowering. If plants continuously experience LD, they will keep growing indefinitely and not produce any flowers. In this experiment, I look solely at the growth of the plant. With continuous light, the plants will grow more rapidly (see figure 42 in appendix B). In addition, flowering may have an effect on the AEs. To eliminate this potential effect, it was decided to use continuous light.

The plants are watered 3 times per week. The option to have the roots of the plants continuously watered was not feasible, as this would result in rotting. The change in soil water content varied mostly by 10% between two irrigation moments, except for one time when this change was 32% due to a pause of 5 days between two irrigation moments.

At the beginning of the experiment, I did not yet know if and how the relative position of the microphone on the plant would influence the AEs and where most AEs happen. A small mock-up experiment was performed, using microphones at three different heights (figure 8b). I observed that the microphone in the middle location yielded the most AEs (8 AEs) compared to the lower (2 AEs) and higher (2 AEs) microphones. Therefore, I decided to mount the microphone to the plant at 50% of the plant height during the real experiment. The growth of the plant happens at the top. Since the microphone is mounted at a fixed location, it does not grow along with the plant. Therefore, it needs to be adjusted every few days to remain at the same position relative to the plant, which is at 50% height.

4.2.3 Setup

The experiment is conducted in a special climate chamber, where environmental properties are made constant. The equipment used to remain these properties constant was very loud. Therefore, isolation between the microphone and plant was required. By putting sound-isolating foam in between, the noise was damped as much as possible (figure 9a). To filter the unwanted sound sources further, a frequency threshold was set at 25 kHz. This limit was required to reduce false triggering of data acquisition due to acoustic sources other than

the plant. The duration was 26 days. After this duration, some plants were unable to bear their weight and broke down. The plants were measured with two computers. Computer A measured plants 1A, 2A and 3A and computer B measured plants 1B, 2B and 3B (figure 9).

(a) Isolation (grey) between microphone and plant to dampen external noise, held in its place by a 3D printed clamp.

(b) Plants in the climate chamber with ultrasound microphones. 2 Plants of 3 varieties are being measured.

Figure 9: Setup for experiment 2 in the climate chamber at Deliflor

Every Monday, Wednesday and Friday, the plants were irrigated. This was done by flooding the container the pots were in for roughly twenty minutes to make sure the soil had enough time to take up the water. Water could reach the soil through the bottom of the pots. After twenty minutes, the water was drained again.
The microphones were mounted on a stick at the desired height. Next, the horn of the microphone was pushed towards the plant stem, after which the foam was put around it to isolate the sound. Finally, a 3D printed clamp was put around it to make sure it stayed put.

(a) The beginning of experiment 2 when the plants are small.

(b) The end of experiment 2 when the plants are grown. Some plants have fallen due to their large weight. No flowering had occurred.

Figure 10: Development of the plants during experiment 2.

4.3 Supportive destructive measurements

To generate material properties of the different samples, multiple tests have been conducted. To obtain the density and dimensions, the samples were measured using a calliper and scale. The calliper had an accuracy of 0.1 mm and the scale had an accuracy of 0.5 mg.

4.3.1 Optical microscopy of xylem vessels

To determine the diameter of the xylem vessels, I put the samples under a microscope that used VHX-6000 communication software. Using this software, I took pictures and measured the diameters of the xylem vessels. An example of such a picture is seen in figure 11. I distinguished the xylem vessels from the phloem using figure 44 in appendix B, where we see that the phloem is located in the outer parts of the stem and the xylem vessels are more located in the inner part of the stem [76].
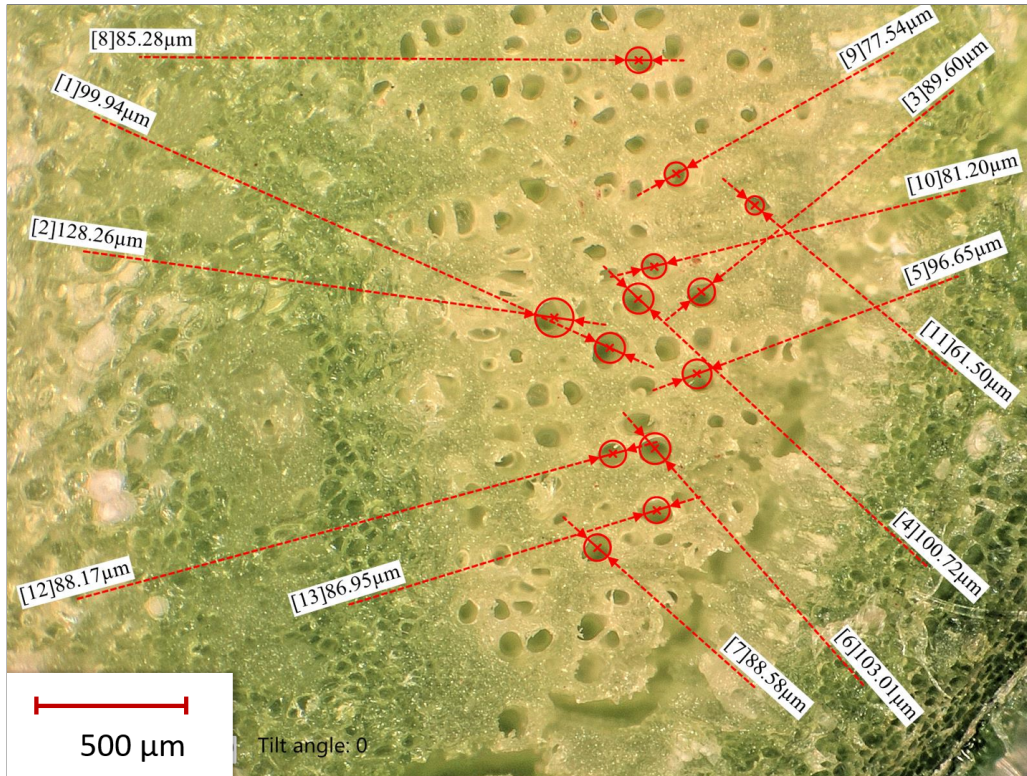
Figure 11: Microscope picture of the cross-section of the tomato plant stem from experiment 1, with the diameters of some xylem vessels depicted.

Some xylem vessels appear more elliptical instead of round. If that was the case, the long and short diameters are taken. With this, the area is calculated. With this area, I calculate the diameter as if it was a perfect circle. By following this method, I account for errors that would shift the measured diameter.

4.3.2 Weight and cross-section

To obtain the density, two samples were weighted and the area of the cross-section and length were measured. As both plants had their irregularities, the main error in the density determination was in the area estimation. As sample A had an internal hole, the effective area is calculated by fitting a circle for the outer- and inner diameter and subtracting the corresponding areas (figure 12a).

(a) Sample of the tomato plant from experiment 1.

(b) Sample of the chrysanthemum from experiment 2.

Figure 12: Microscope picture of the cross-section of a tomato and chrysanthemum stem.
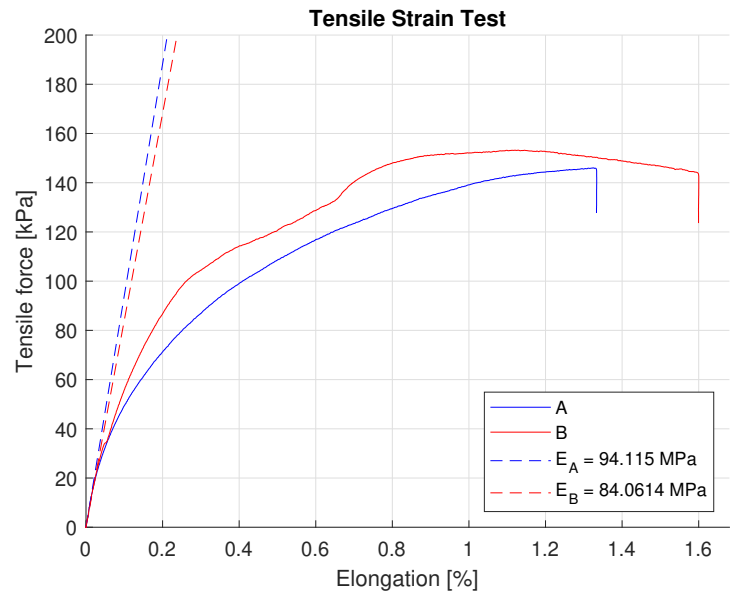
4.3.3 Tensile test

A tensile test with uniaxial tensile loading is performed to obtain the Youngs modulus E. Using a tensile test bench, the elongation of a sample as a function of force can be calculated with equation 12.

$$E = \frac{\sigma}{\epsilon} = \frac{F/A}{dl/l} \tag{12}$$

here the stress σ is the force F per unit area A and the strain ϵ is the extension dl per unit length l. Once area A and unit length l are measured and known, we simply take the derivative from figure 13b to get the factor F/dl.

(a) A sample of the tomato plant is put in a tensile test bench to determine the Youngs modulus.

(b) Tensile force as a function of the elongation of the sample. The dotted line is a linear fit for low straining. The slope indicates the Youngs modulus.

Figure 13: Tensile test to determine the Youngs modulus of a tomato plant stem sample from experiment 1. The same test is performed for the chrysanthemums in experiment 2 (figure 55)

5   Data Processing Method

In this section, the filtering, categorising and discrimination of data are explained. We need to do this before we can interpret the data for the results in the next section. To wit, when a signal comes from someone walking by, we need to exclude it from our data set.

The recordings are analysed using Matlab [77]. I have categorized the data in several steps (figure 14). This is initially done with the raw data from experiment 1 because this experiment was performed first.

As the microphone got triggered when there was an AE from the plant, but also when a loud sound was present in the greenhouse as well, a clear distinction between these different sources has to be made.
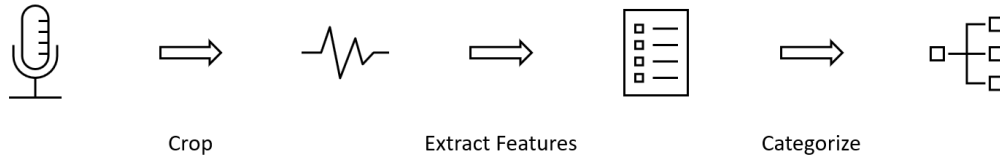
Figure 14: Using a microphone, sound files are created. These are first snipped and cropped so only the relevant peak remains. From this peak, several features are extracted, such as decay time and time duration. Using these features, we can categorize different sounds.

I will now explain these parts step by step.

5.1   Cropping the signal

The software that comes with the Pettersson ultrasound microphone is called Batsound. This has a function that is only triggered and saves the recording when certain amplitude and frequency thresholds are exceeded. By using this function, data is only generated per sound pulse instead of continuously. This results in a first filter (based on amplitude and frequency) and in an enormous reduction in data, which makes it easier to analyse. Each recording has a pre-recording of 0.2 seconds and remains for at least 0.5 seconds after the threshold exceeding, resulting in recordings of at least 0.7 seconds.

From literature, we know that the acoustically emitted sound by plants is in the form of a pulse with a peak [13, 58]. These peaks contain the relevant information, whereas the rest of the file is mainly noise. To eliminate signals that have a low peak-to-noise ratio and are therefore less useful, I set the requirement that the peak should have at least five times the magnitude of the noise amplitude. This yielded a reduction of 28% of the data files. This requirement was not set in experiment 2. As stated above, the recordings were at least 0.7 seconds long. Most pulses were much shorter than 0.7 seconds. This results in recordings where the peak is only a small part of the recording, whereas the rest of the recording is usually just background noise. An example of such a signal is depicted in figure 15a. As can be seen, the peak is around 0.2 seconds.

To determine the decay time, we will crop the signal around the pulse (figure 15b).
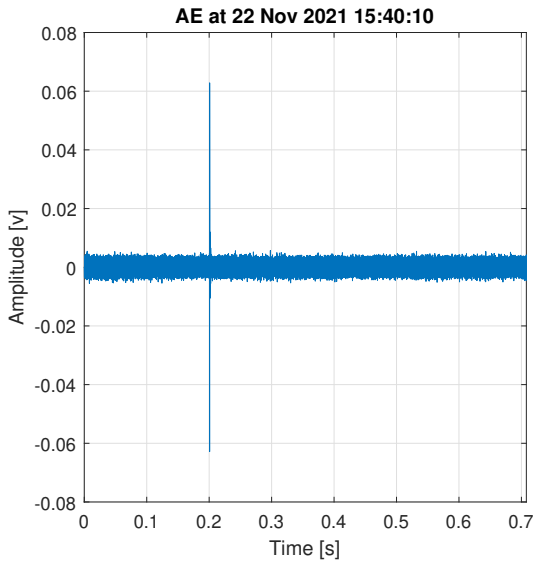
(a) Original Signal of an AE in the time domain
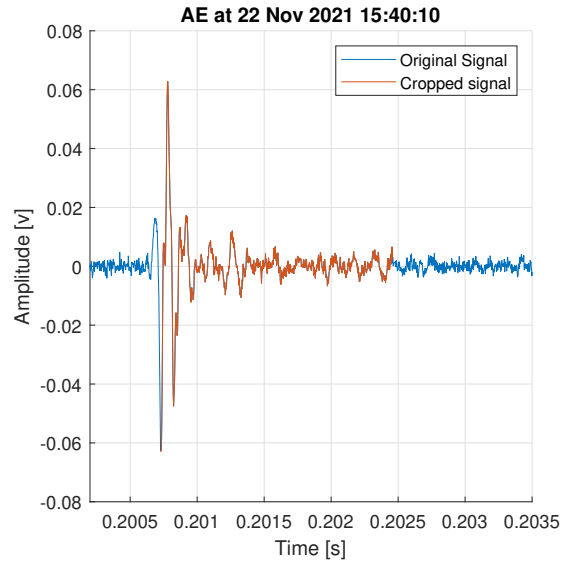
(b) Cropped Signal of an AE in the time domain.

Figure 15: Example of an AE in the time domain from a tomato plan during the greenhouse experiment.

To determine where to crop the signal, we used the stepresponse function `stepinfo` with steady-state value `yfinal` 0 and settling time threshold of 115% of the noise amplitude. The noise amplitude is found by taking the maximum value from the signal between 0 and 0.15 seconds. This gives a 15% margin that the signal can be above its predetermined noise level without being seen as part of the peak. There is a trade-off with this margin value. If this margin value is too large, the peak is often too short to determine the actual decay time. If this margin value is too small, it often detects a point later in the signal above this value, making the whole signal part of the peak. This results in a large error in the pulse duration and in the determination of the decay time. Some trial and error resulted in 15% being a viable margin value. In figure 16 an example of the `stepinfo` command is shown. In this example, the steady-state value `yfinal` is 1, whereas this value is 0 in the used code. In this thesis, the pulse duration dt is the time between the `finalTime` and `PeakTime`. I have changed the Matlab command `SettlingTime` to `finalTime` (bottom right of figure 16) to avoid confusion with the settling time used throughout the thesis.
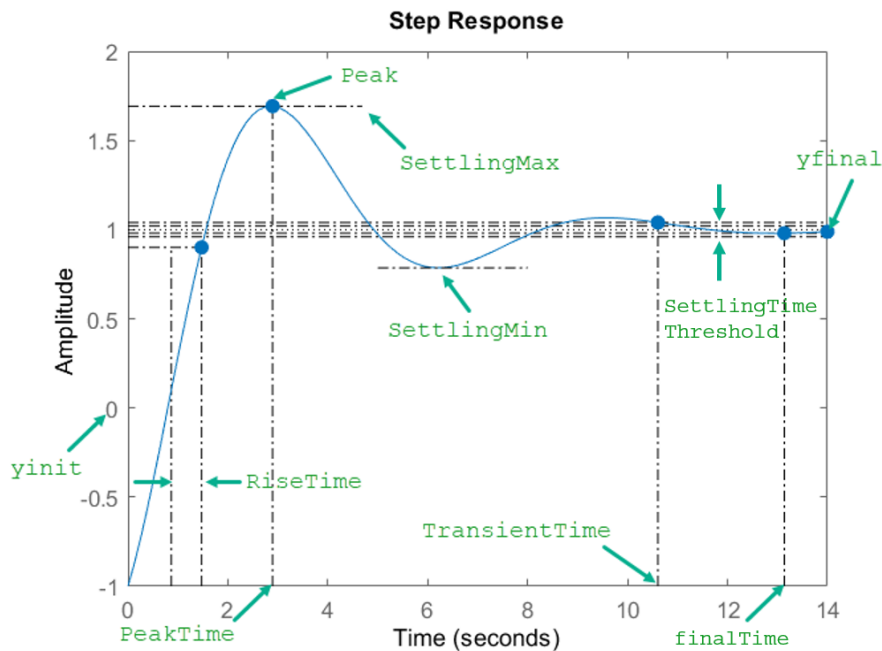
Figure 16: Matlab function `stepinfo` with its characteristics. A steady-state value of 0 (instead of 1 in the picture) is chosen for the data processing method. The graph is taken from the Mathworks website and is adjusted.

18

Since sometimes there are 2 or more pulses within one recording, these should be separated as well. This is done using a 'valley' threshold. An explanatory diagram is depicted in figure 17, where the cropping to the pulse is shown.
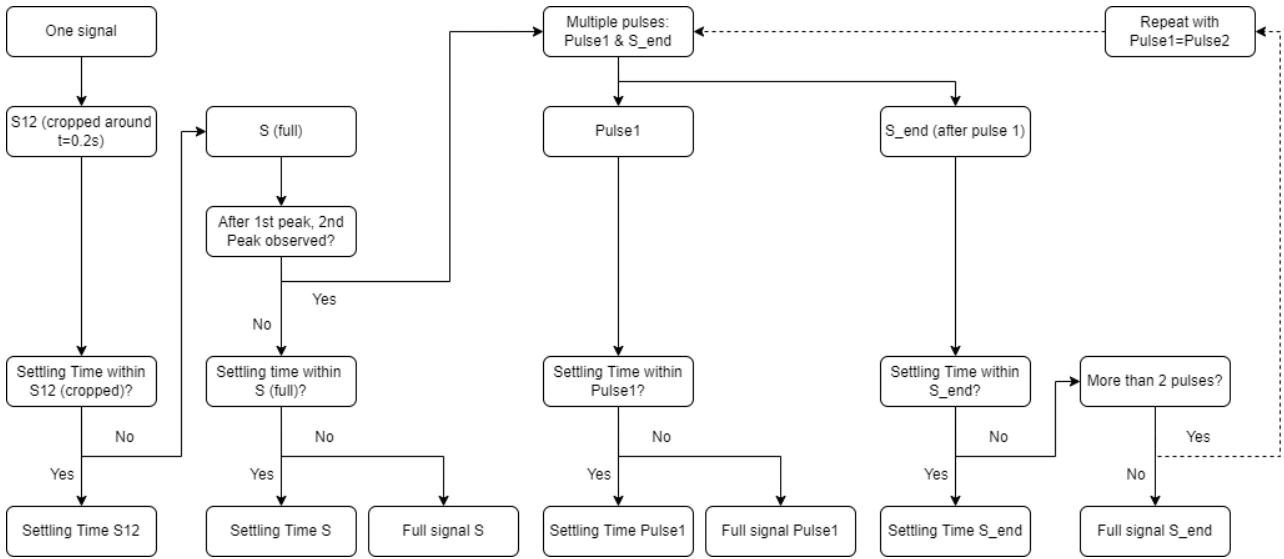

Figure 17: Flowchart for cropping the acoustic signal

5.2 Extract features

When we have found the actual pulse, we can deduce information. The information each signal entails is translated into features: single values that are used to reduce the amount of information. The international standard features for each signal that are incorporated are:

- Amplitude [V] or [dB]

- Settling Time [s]

- Frequency [Hz]

The *amplitude* is the maximum value of the signal in the time domain. This is measured in volt and can be translated to decibels. This relationship is $y_{db} = 20 \log_{10}(y_V)$. The *settling time* is found by first finding the peaks, next plotting the envelope of these peaks and finally fitting an exponentially decreasing function over this envelope. This can be seen in figure 18. By using a fast Fourier transform of the pulse with Matlab command `fft` we can find the peak *frequency*.
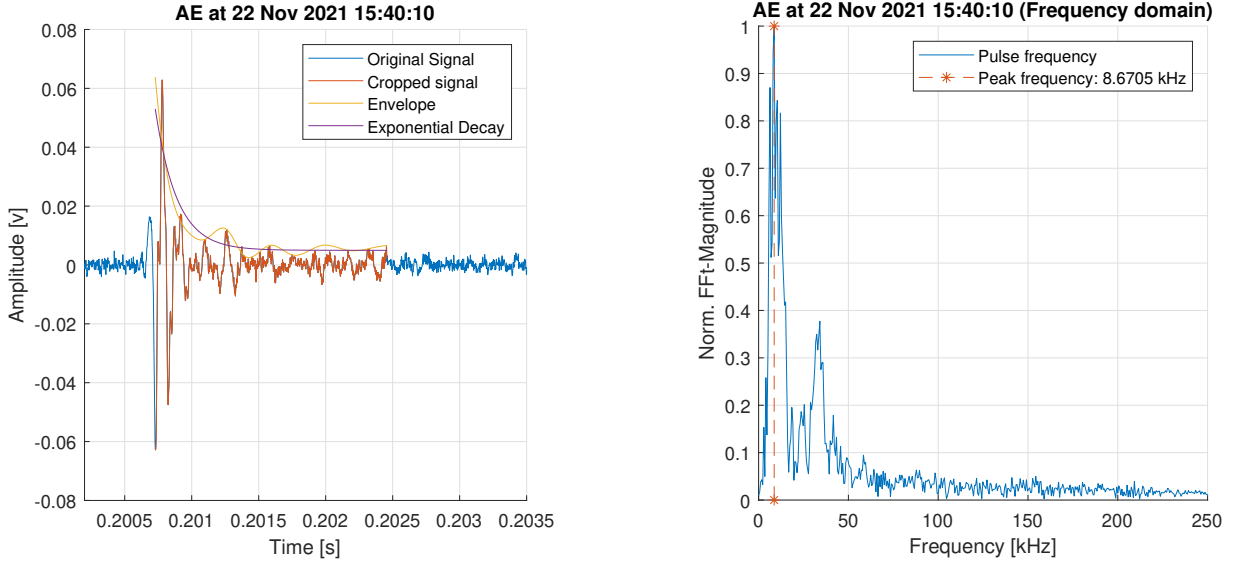
(a) Cropped AE signal in the time domain with fitted envelope and exponential decay.

(b) Corresponding Fourier Transform in the frequency domain from cropped AE signal (normalized)

Figure 18: Example of AE in the time- and frequency domain with corresponding fits from a tomato plan during the greenhouse experiment.

Other features are described in the work of Sause [78]. These features are used by other authors [44, 79] as supplementary parameters to describe the signals. A table of these features is shown in table 43 in appendix B. These features are also investigated for categorization. The most important feature of these is the pulse duration dt.

The cropping and extraction of features resulted in a calculation time of roughly 1 second per sound file. With the 10,410 sound files from experiment 1, the running time was about 170 minutes to extract all features.

5.3 Categorize

By mapping different features of each signal, we can distinguish between different clusters. We used the list of features from Sause [78] for pattern recognition.

The first and most logical parameter to check is the square root of the settling time because this feature is linearly proportional to the hypothetical diameter of the xylem vessel (equation 7). Solely based on this parameter, already 3 clusters can be distinguished, as can be seen in figure 19. Here the settling time has already been calculated to the acoustic diameter (with the dynamic viscosity and density taken as constant). The cluster with the lowest acoustic diameter seems to correspond to the diameters measured with a microscope.
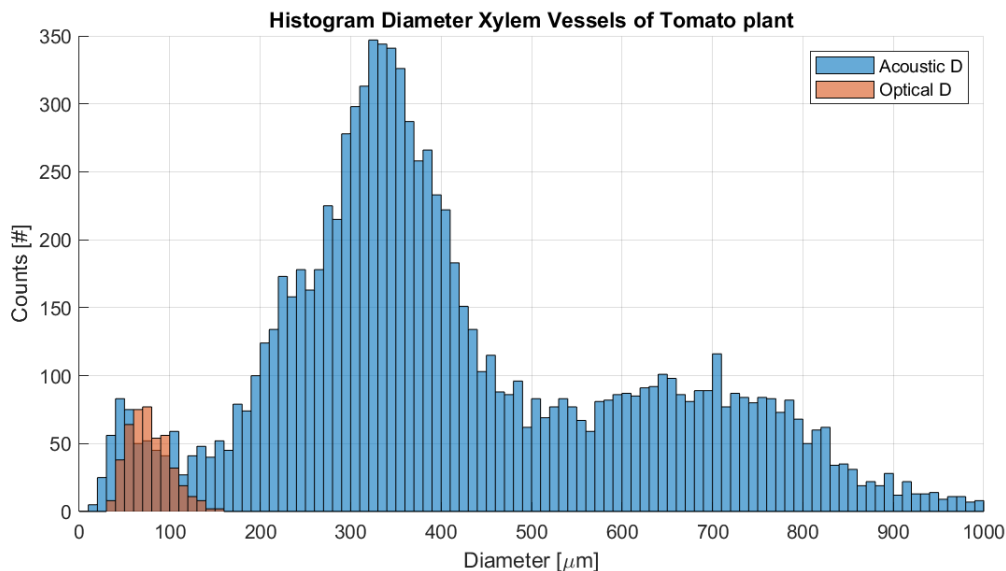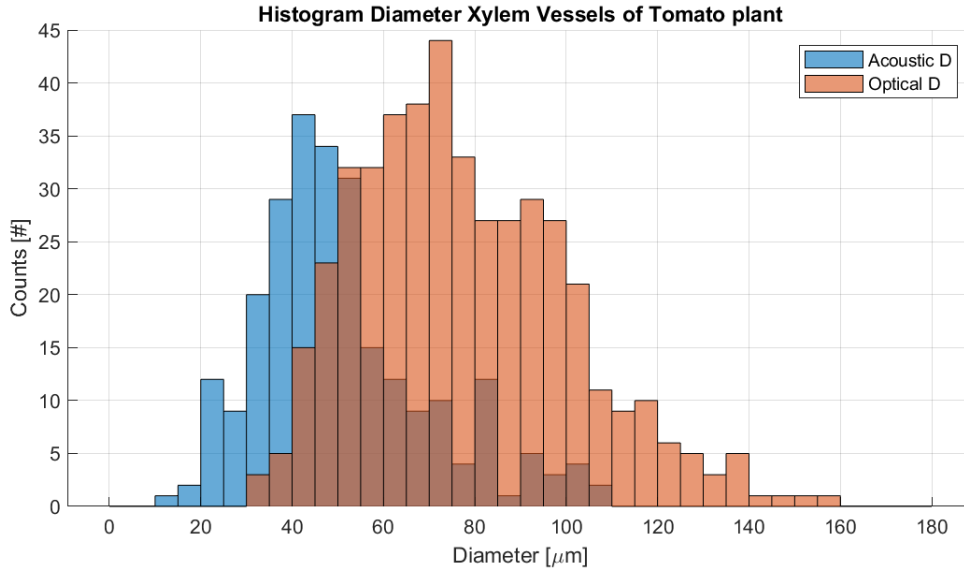
Figure 19: Histogram of hypothetical acoustic xylem vessel diameters calculated using settling time from all signals (blue) and optical xylem vessel diameters of two samples using a microscope (orange) from a tomato plant from experiment 1.

When taking a second feature into account, I found that the best second feature for distinction is the pulse duration. This resulted in the 2D histogram in figure 20a. Here we can see the 3 different clusters more clearly. A third separation feature was also investigated, but this did not improve the separation significantly and is therefore not used.

Clustering algorithm

For clustering or categorizing the different types of plant signals, three types of algorithms are mentioned in the literature.

Khait et al. used a Support Vector Machine (SVM) [80]. The SVM takes multiple data sets and separates them in the best possible way [81]. Khait et al. used an SVM classifier with a scattering network that achieved about 70% accuracy for each pair. Scattering networks are "a class of designed convolutional neural networks with fixed weights" [82].

De Baerdemaeker et al. used a Linear Discriminant Analysis (LDA) to categorise the AEs. The LDA used by de Baerdemaeker et al. is based on amplitude, counts, duration, signal strength, absolute energy and partial power in the range of 100-200KHz.

Vergeynst et al. [44] used an Automated Clustering Algorithm (ACA) to distinguish different clusters of signal sources. This looks at different parameters and tries to group data based on those parameters. It was found that based on frequency features the clusters were best grouped.

Following an approach similar to that used by Vergeynst et al. [44], we used a density-based clustering algorithm to distinguish different clusters. This method was chosen, as this proved to give a clear separation between groups. With some manual trial and error for input values, the density-based clustering algorithm `dbscan` was used to automatically separate these three signal clusters, which can be seen in figure 20b. The cluster in purple on the left bottom will be used for further analysis because the acoustic diameter corresponds to the optical diameter. I will refer to this cluster as type I. The signal shown in figures 15 and 18 is a type I signal. Examples of type II and type III signals are shown in appendix C in figure 45. We can see that their decay time and duration are much longer. Note that the duration of the pulse of type II and type III is much longer compared to the type I signal.
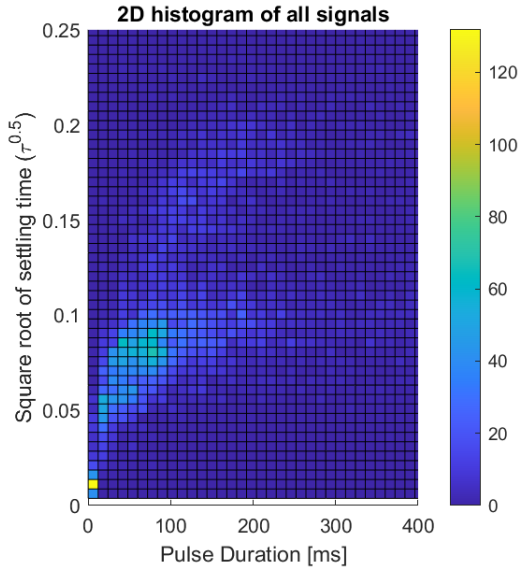
(a) 2D histogram of signals with the counts indicated with colour. Only signals with a peak amplitude that is 5 times the noise level are included.
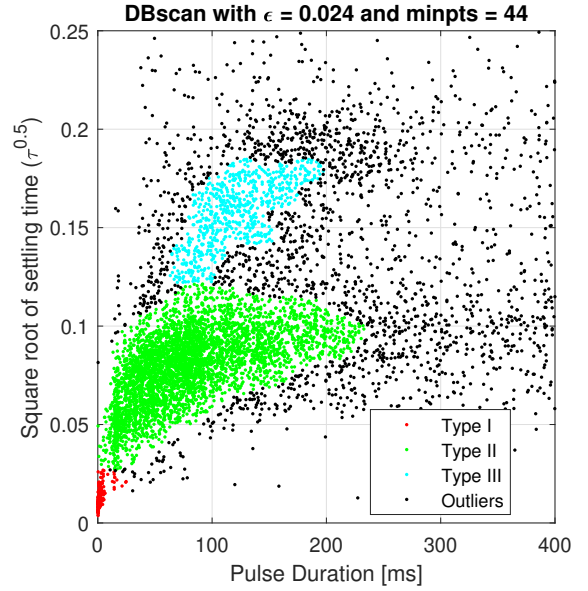
(b) The distinction between three clusters using density based-clustering algorithm `dbscan` with pulse duration and settling time as input variables. Black dots are the outliers.

Figure 20: Clustering different types of signals based on the pulse duration (x-axis) and the square root of the decay time (y-axis) from a tomato plant from experiment 1. The total number of pulses in both graphs is 6777.

Since the cluster on the bottom left (type I) has a calculated diameter corresponding to the diameter measured with a microscope, I will use these type I signals for further analysis in section 6 and refer to these type I signals as AEs. From all 10,410 observed signals, 252 are type I AEs. When comparing the diameter from this cluster to the diameter of the xylem vessel measured with a microscope, they do overlap, with the side note that the diameter of the calculated diameter from AEs (blue) is somewhat smaller compared to the diameter measured with a microscope (orange) (figure 21).

Figure 21: Histogram of acoustic xylem vessel diameters calculated using settling time from the type I AEs (blue) and optical xylem vessel diameters of both stem samples using a microscope (orange) of both tomato plants from experiment 1.

5.4 Validation

We have found a way to distinguish type I signals from type II and type III, but we still need to verify that the type I signals are indeed coming from the plant. Ultimately, we have based the fact that these signals

correspond to what we expect, on the fact that they correspond.

When we take a look at figure 3 from section 2.2, we know that the cumulative number of pulses initially increases super-linear. When we look at the three pulse types during dehydration, we would expect this super-linear increase for the type I signals, but not for the type II and type III signals. This is plotted in figure 22.
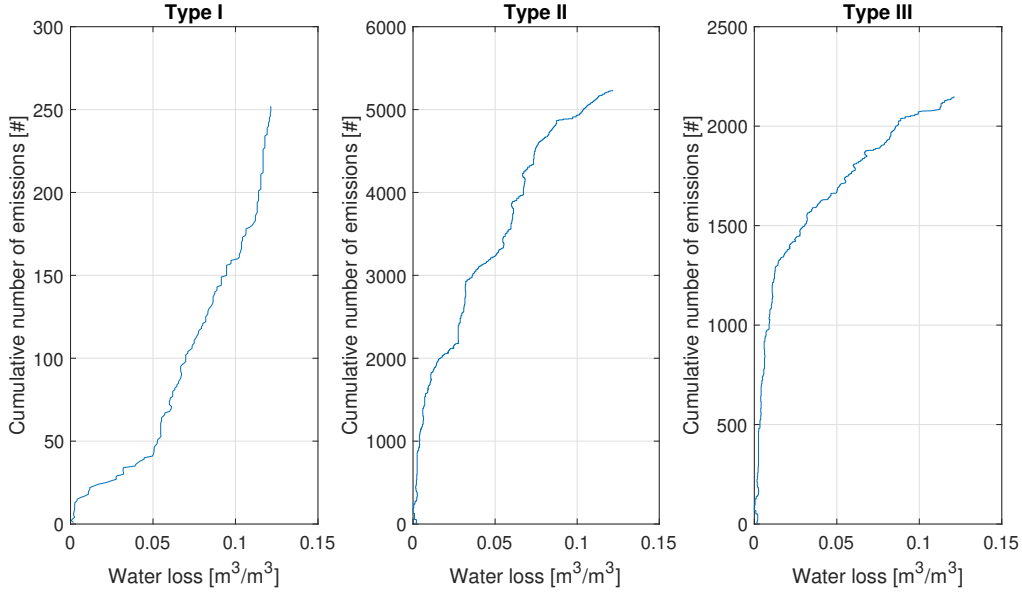

Figure 22: Cumulative number of AEs as a function of water loss for the three different types of signals (clusters from picture 20b). The cumulative rate is plotted chronologically. The type I signals (left) have an acoustic diameter corresponding to the optical diameter (figure 21).

As can be seen in figure 22, indeed the cumulative number of signals from the cavitation cluster increases super-linear during dehydration, whereas the other clusters increase sub-linear as a function of water loss. This validates our assumption that type I signals from figure 20b indeed represent AEs from the plant. Note that the water content decreased super-linear, as can be seen in figure 24. In other words, the water loss was low most of the time. This results in the sub-linear increase of type II and type II signals. The cumulative rates of emissions for type II and type III signals would increase linearly if plotted as a function of time.

Extrapolation to experiment 2

As this analysis is done with the raw data from experiment 1 in the greenhouse, it could not necessarily apply to the raw data from experiment 2 in the climate chamber, due to the differences in environment, setup and the measured plant species. When we compare figure 20b to figure 23a, we can see that with some different input variables for the algorithm, type I signals are still distinguishable from other signals. In figure 53 we can see two examples of signals from this experiment.

The xylem vessel diameter from the AEs (calculated with equation 7) can be compared to those measured under a microscope. This can be seen in figure 23b. We can immediately see that the acoustic diameters for the type I AEs overlap, but on average the acoustic diameter is larger than the optical diameter measured under a microscope.
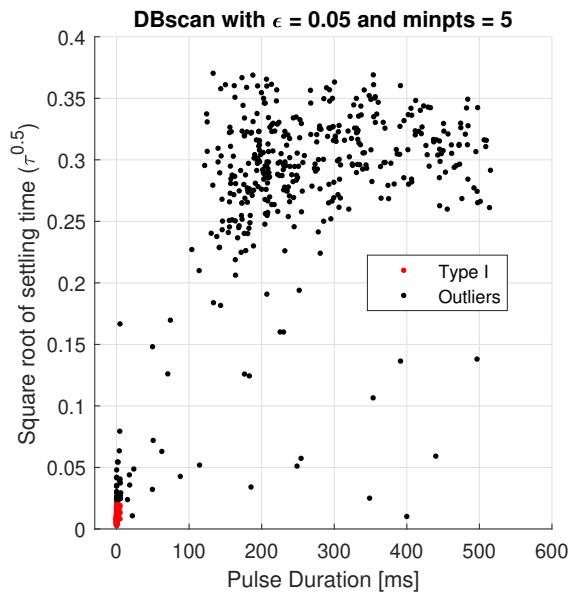
(a) The distinction of type I signals (red) using density-based clustering algorithm `dbscan` and with black the outliers.
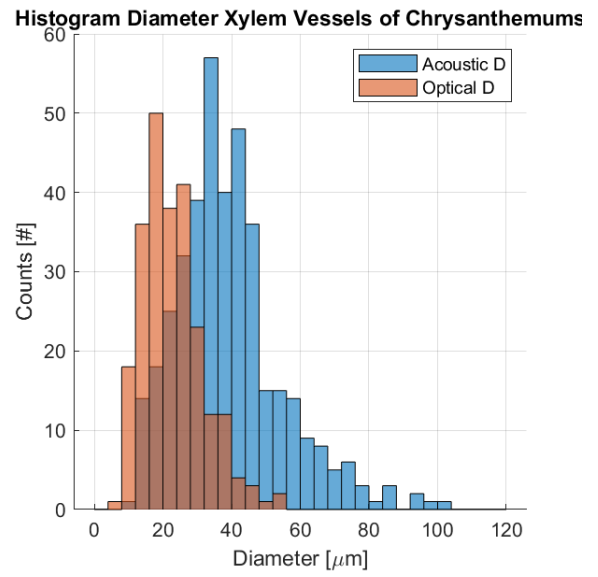
(b) Histogram of calculated xylem vessel diameter from Chrysanthemum plant using the AEs of type I (blue) and measured xylem vessel diameter of 6 samples using a microscope

Figure 23: Data analysis for extracting type I signals for experiment 2 in the climate chamber

6 Results

The results will be divided into two parts: Experiment 1: greenhouse (6.1) and Experiment 2: climate chamber (6.2). Only the type I signals (described in section 5) will be considered, as these are expected to be AEs from the plants.

6.1 Experiment 1: Greenhouse

In the first experiment in the greenhouse in Bleiswijk, the sensor has measured for 22 days during the dehydration of tomato plants. This section will cover three aspects of research: rate of emission (6.1.1), the influence of light, temperature and humidity (6.1.2) and finally the changes in characteristics of the AEs during dehydration (6.1.3). But first, the material properties will be shown.

Material properties

The cross-sectional area of the samples is needed to determine the Youngs Modulus, as this is calculated using equation 12 where A represents the cross-sectional area. From figure 12a we can see an example of this cross-section. For plant A this yielded a cross-sectional area $A_A = 94 \pm 9 \cdot 10^{-6}$ m^2 and for plant B $A_B = 104 \pm 9 \cdot 10^{-6}$ m^2.

The Youngs Modulus from the tomato plant sample is deduced from figure 13b and gives $E = 94 \pm 11$ MPa for sample A and $E = 84 \pm 11$ MPa for sample B. The error comes from both the error in the cross-sectional area and the error in the determination of the slope in figure 13b.

The length of sample A was 59.25 mm and for sample B this was 45.20 mm. Their corresponding weights were 5.70 g and 3.71 g for samples A and B respectively. This yields a density of 1020 ± 100 and 790 ± 80 kg/m^3 for samples A and B respectively. The error in density comes from the dominant error in the cross-sectional area. This density is used to translate the settling time to acoustic diameter (equation 7).

6.1.1 Rate of emission

The cumulative number of AEs is plotted in figure 24. Especially around November 19, one can detect a step-wise increase in the number of AEs. We can interpret that as follows: where the slope is more horizontal, the rate of AEs is low and where the slope is more vertical, the rate of AEs is high.
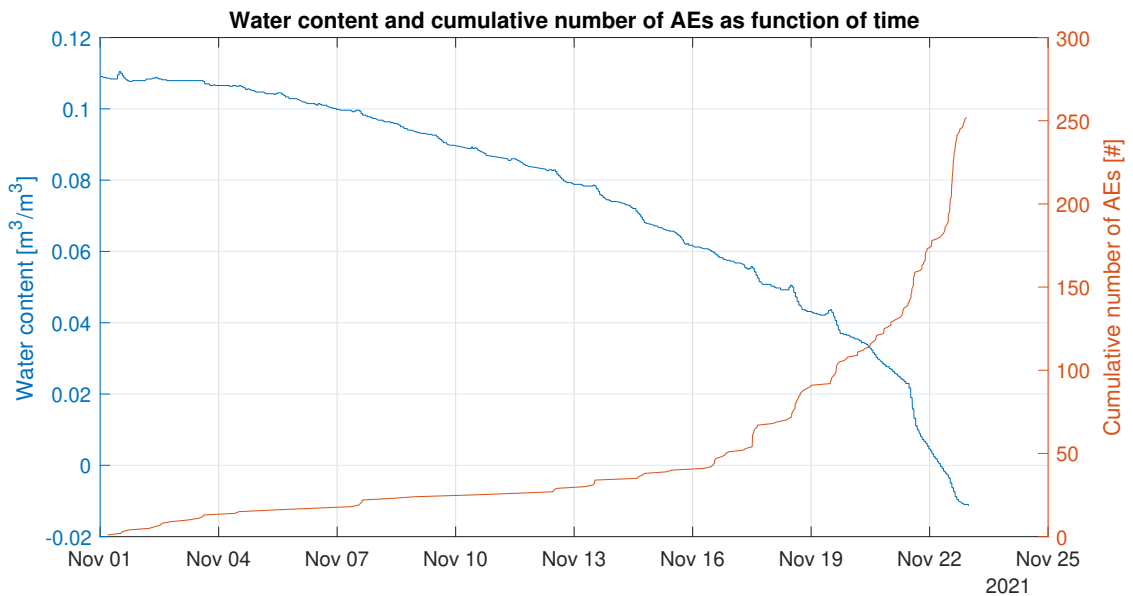

Figure 24: Water content (blue) and cumulative number of AEs from the tomato plants (orange) during experiment 1.

From figure 22, we can see that the rate of emission increases as a function of water loss. When we fit the power function $y = a \cdot x^b$ with $a = 7471$ and $b = 1.65$, we get an R-square value of 0.985 (figure 25). Since $b > 1$, this indeed implies a super-linear increase.
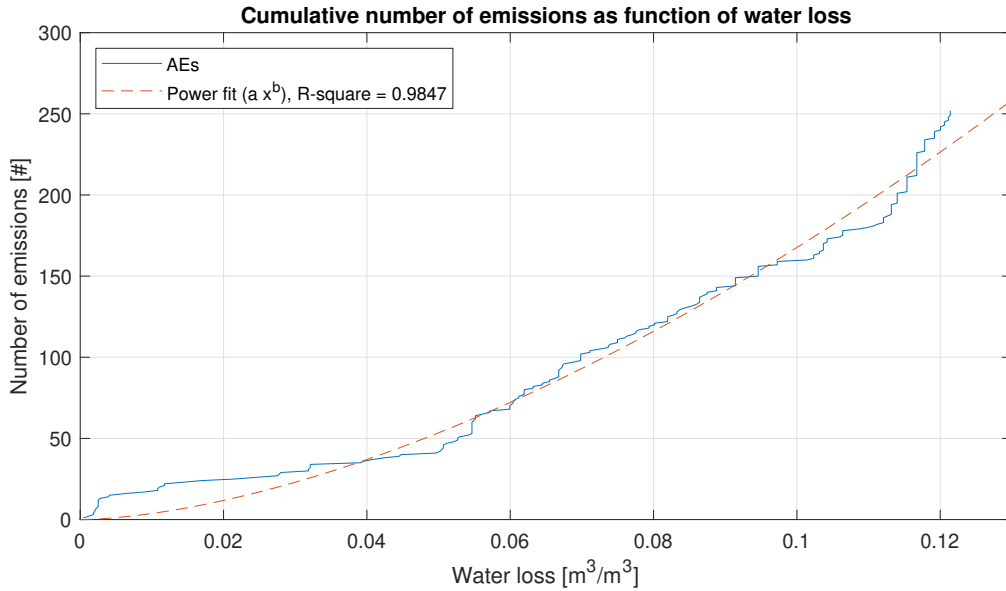
Figure 25: Cumulative number of AEs as a function of water content with power fit (a= 7471; b = 1.65) during experiment 1.

6.1.2 Light, temperature & humidity

During the experiment, the water content of the soil, temperature, humidity, light intensity and time were all measured. CO2 concentration was also measured, but not investigated in this thesis. In figure 46 in appendix C, the values for light, temperature and humidity during the experiment are shown. However, the diurnal patterns are more interesting to consider. We should be careful how to plot these values if we want to relate them to the AEs. As the experiment developed, the season changes. Therefore, the diurnal patterns of light, temperature and humidity change as well.

As most AEs happened at the end of the experiment, the environmental parameters at the beginning of the experiment are less relevant compared to these parameters later in the experiment. In figure 26 I have plotted the average temperature, light and humidity for 24 hours starting November 16th, as more than 80% of the AEs occurred after this date. In figure 47a in appendix C, also the relation between the counts of AEs and light, temperature and humidity, taken as average for the whole duration of the experiment, is shown.
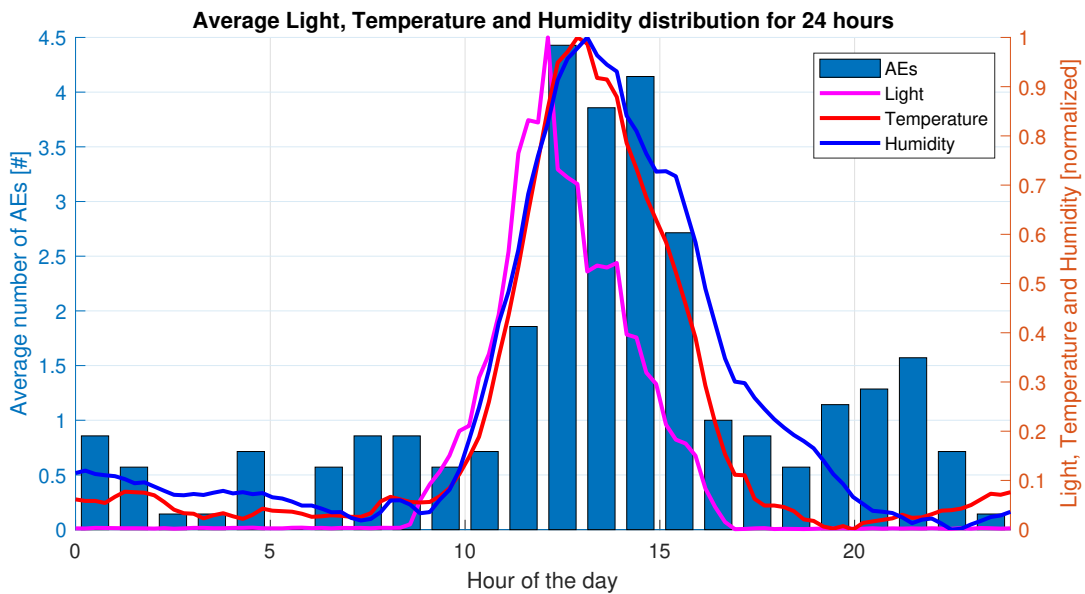
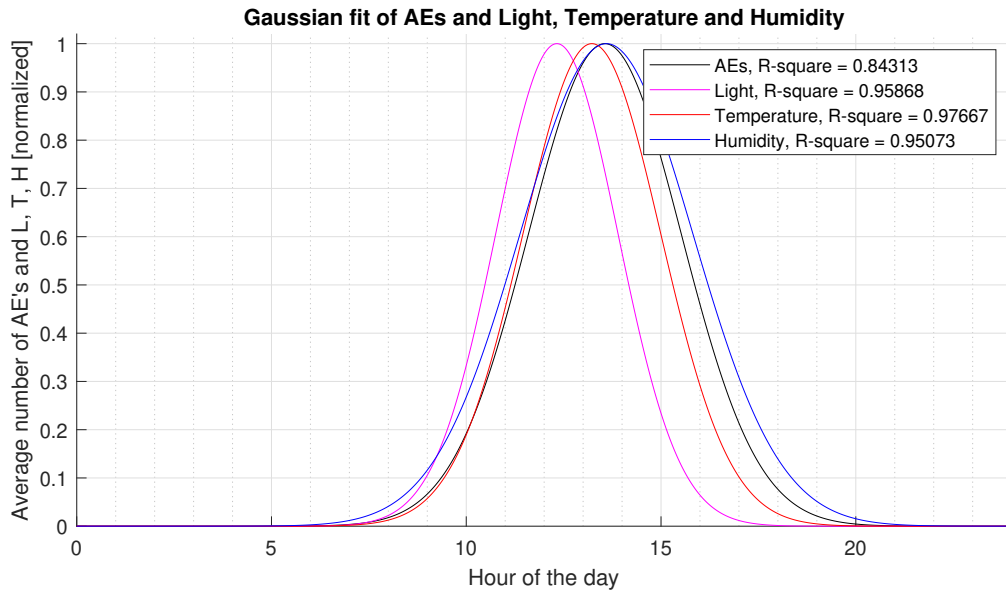Figure 26: Relations between the daily average number of AEs and temperature, light intensity and humidity during the day taken from 16-22 November. For light, temperature and humidity, the average value for every 15 minutes is taken and normalized.

A certain delay between for example the increase in light intensity and the increase in the rate of AEs can be spotted. To make figure 26 more quantitative, I have plotted the Gaussian fit of each parameter in figure 27.

I will use the AE count curve (black in the plot) as the benchmark to calculate the delay of other parameters. When we consider the increasing period in the morning when all normalized values are at 0.5, we can see that light precedes the AE count by 45 minutes. This advance is 15 minutes for humidity and 5 minutes for temperature. For their peak values, light precedes the AE count with 75 minutes, temperature with 20 minutes and humidity has its peak at the same time. In the afternoon when all parameters are at 0.5 again, we can see that light precedes the AE count with 105 minutes, temperature with 35 minutes and the humidity succeeds the AE count after 15 minutes.

The correlation coefficients R between AE count and light, temperature and humidity are 0.79, 0.93 and 0.91 respectively. These coefficients have been calculated using the Matlab command `corrcoef` and they indicate the statistical relationship between two variables.

Figure 27: Relations between the number of Acoustic Emissions and temperature, light intensity and humidity during the day from 16-22 November. The Gaussian fit of values from figure 26. The peak values for light, temperature, humidity and AE count are at 12:20, 13:15, 13:35 and 13:35 respectively (rounded to 5 minutes).

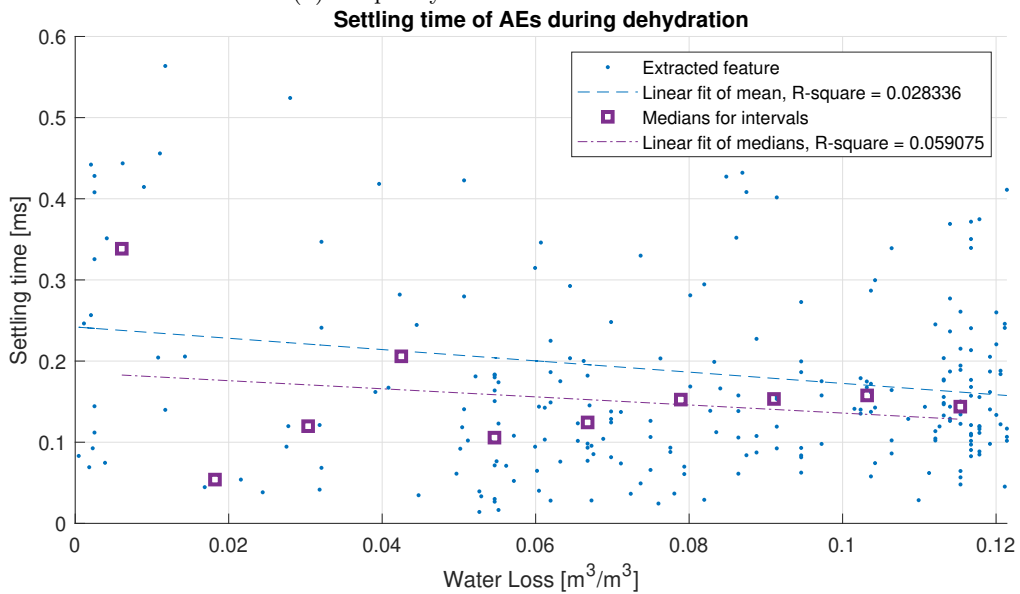### 6.1.3 Change in acoustic signal during dehydration

The change in signal characteristics as a function of water loss is plotted in figure 28. The signal features depicted are amplitude, frequency and settling time.
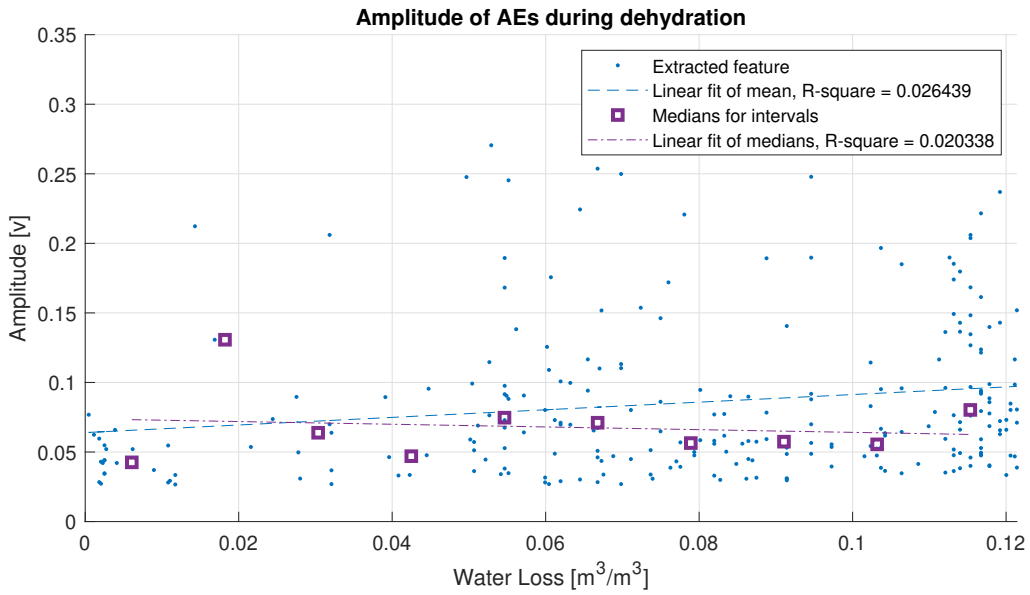
(a) Amplitude as a function of water loss.
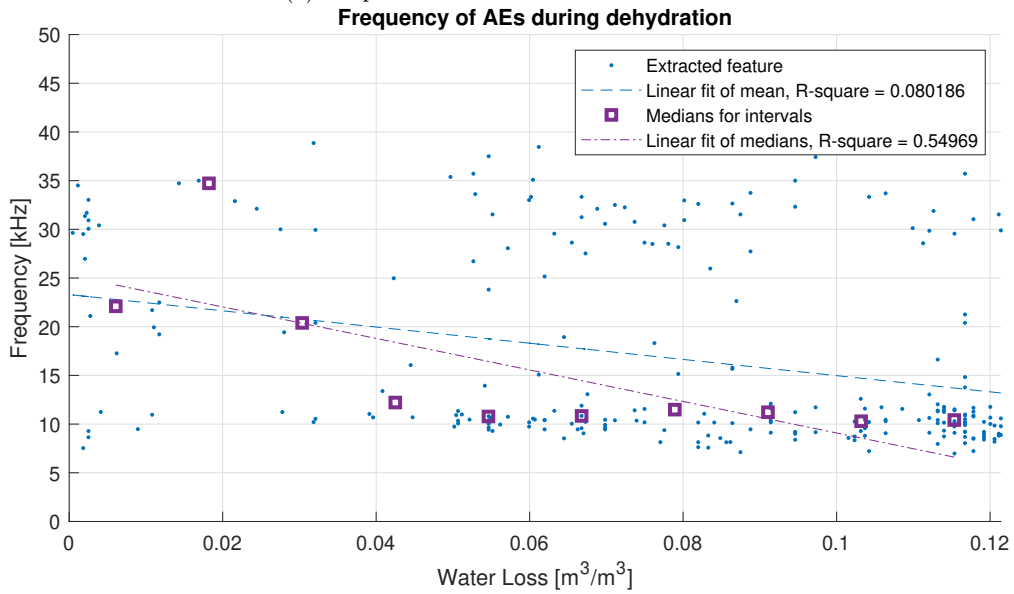
(b) Frequency as a function of water loss

(c) Settling time as a function of water loss

Figure 28: The change of three key parameters of the AEs during dehydration of experiment 1.

As can be seen in figure 28a, the amplitude of the signals increases during dehydration. Figure 28b shows a decrease in frequency during dehydration, but this should be nuanced. This graph will be elaborated on below in section 6.1.3. From figure 28c we can see a clear decrease in decay time.

Frequency mode separation

To further dive into the detailed time- and frequency behaviour, we separate the frequency modes. I have done so by dividing the signals into two groups: frequency modes above 20 kHz (high-frequency group in red) and below 20 kHz (low-frequency group in blue), see figure 29. We can see that both do not necessarily change, except for the fact that the amount of low-frequency signals increases. However, note that the 20 kHz threshold is quite arbitrary and therefore might influence this change. The high-frequency signals remain at 30 kHz.
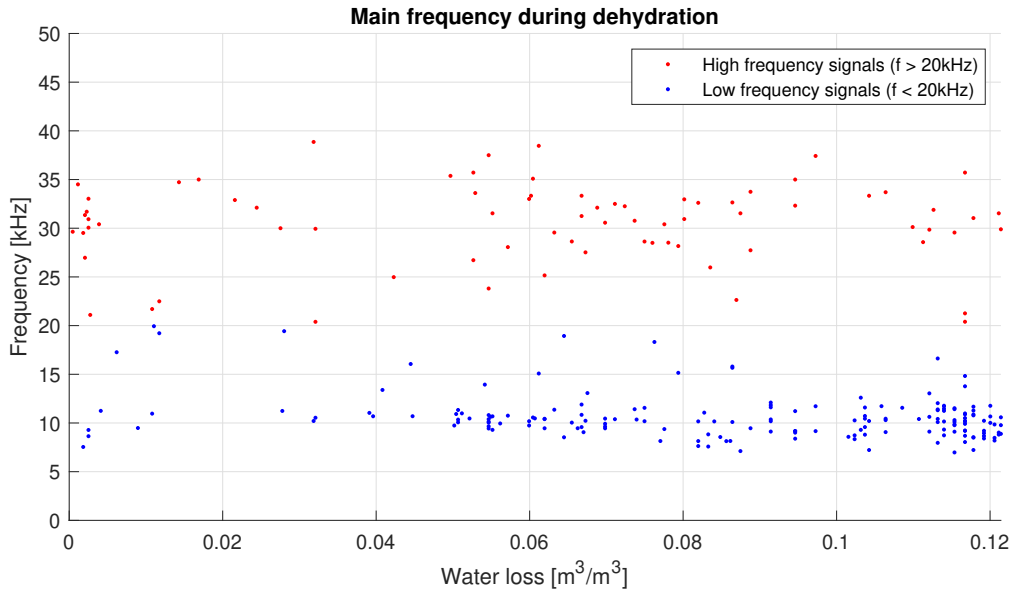

Figure 29: Frequency as a function of water loss during experiment 1, divided at 20 kHz in high- and low-frequency groups.

These are separated based on their maximum frequency value, calculated using a fast Fourier transform. Two examples of AEs from different groups are depicted in figure 30.
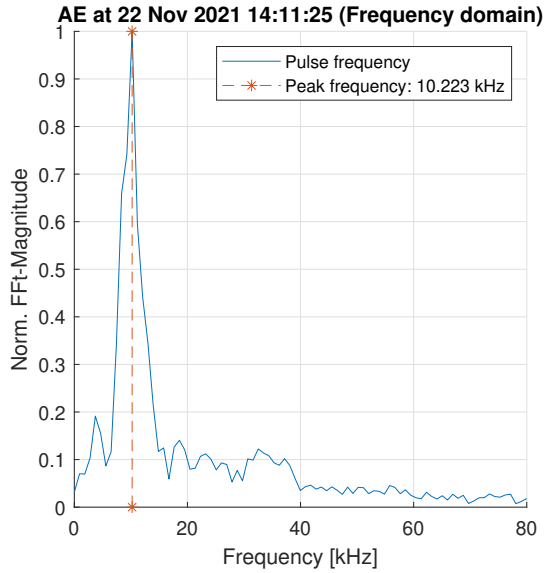
(a) Frequency domain of pulse from the low-frequency group. Mainly a peak at 10 kHz can be seen.
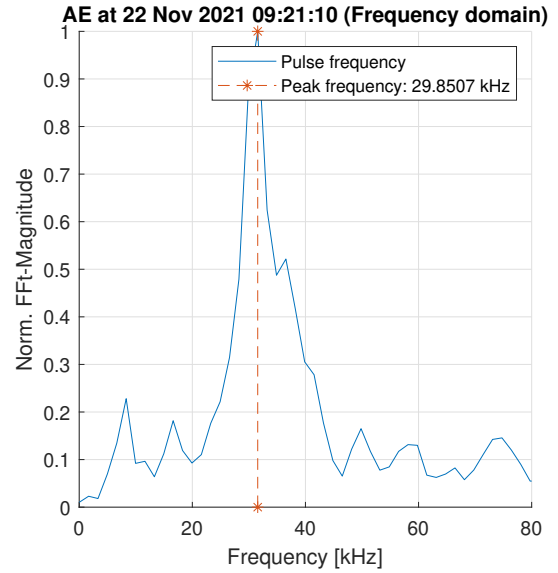
(b) Frequency domain of pulse from the high-frequency group. Mainly a peak at 30 kHz can be seen. At frequencies below the main peak, peaks at integer multiples of 8 kHz can be detected.

Figure 30: Example of low-frequency signal (left) and high-frequency signal (right) in the frequency domain (normalized) cropped to 80kHz.

When we separate these frequency groups, we can see how these two groups change during dehydration. For the low-frequency group, a decrease from an initial 11 kHz to a final 10 kHz can be spotted.
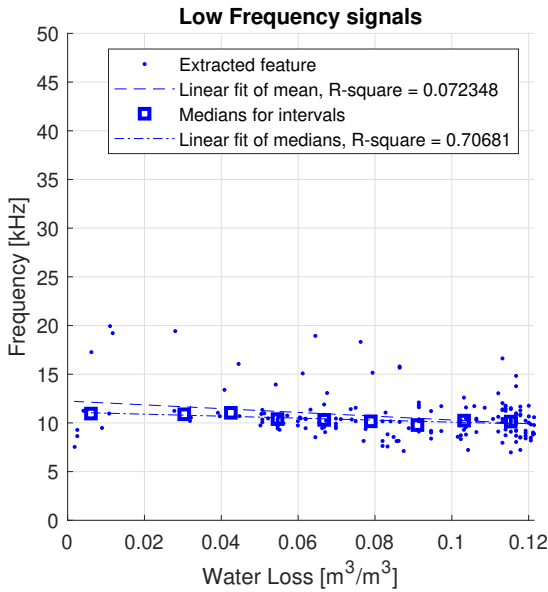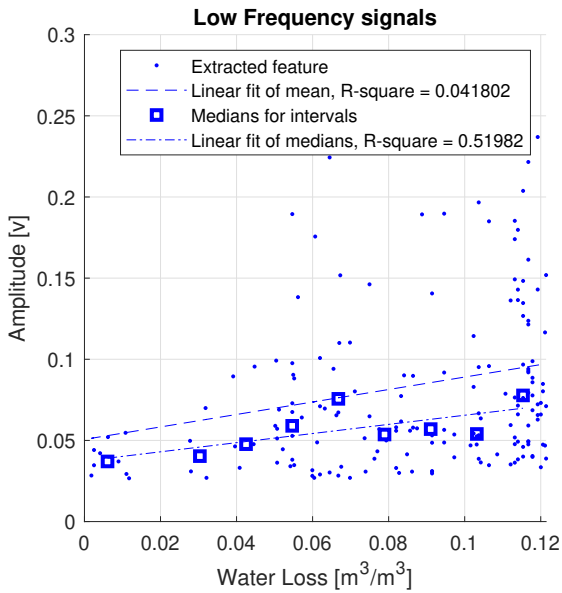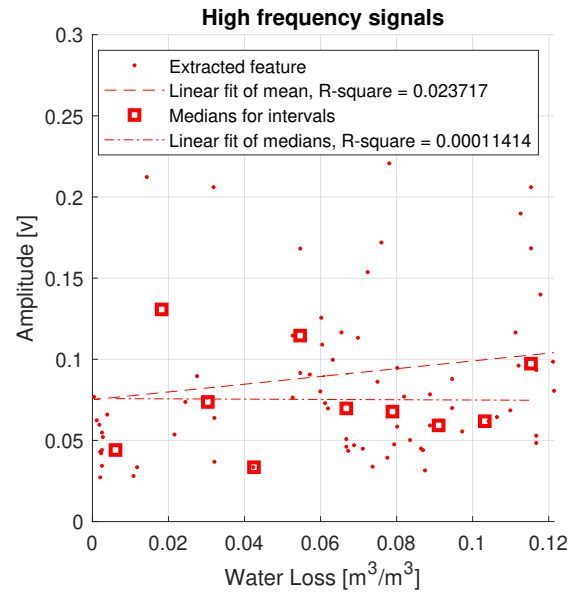

(a) Frequency of low-frequency signals
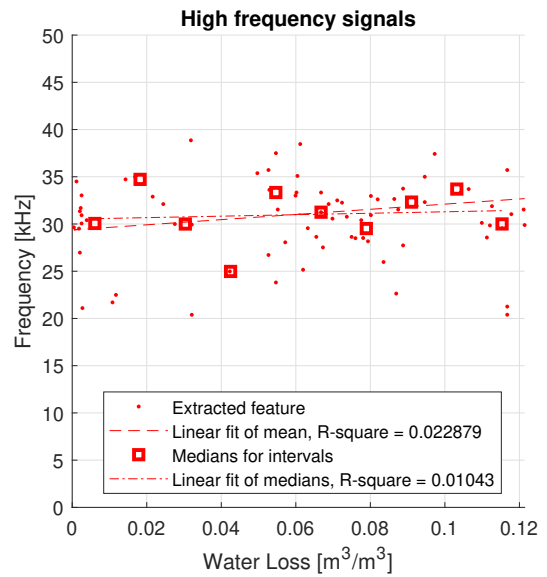
(b) Frequency of high-frequency signals

Figure 31: Frequency as a function of water loss for high- and low-frequency signals during experiment 1, separated at 20 kHz. The dots indicate each data point and the squares are the medians over a given interval. The dashed line indicates the linear fit of all data points. The dotted line indicates the linear fit of the medians.

The amplitude of the AEs increases during dehydration, both for low- and high-frequency AEs (figure 32). Especially the low rate of AEs at low water loss makes the accuracy for the medians quite low, resulting in a very small R-square value.
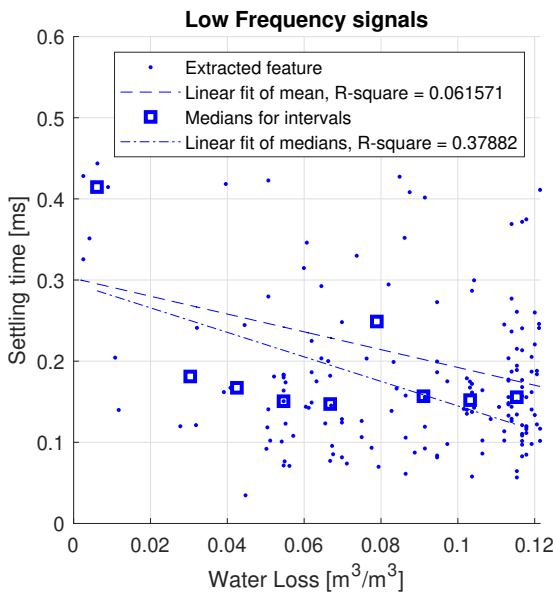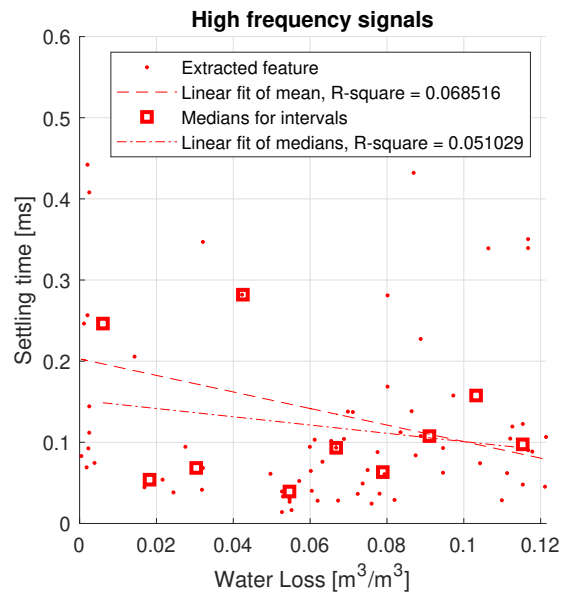
(a) Amplitude of low-frequency signals

(b) Amplitude of high-frequency signals

Figure 32: Amplitude as a function of water loss for high- and low-frequency signals during experiment 1. The dots indicate each data point and the squares are the medians over a given interval. The dashed line indicates the linear fit of all data points. The dotted line indicates the linear fit of the medians.

For the settling time, we can see a decrease as a function of water loss for the AEs. This is also visible for both low- and high-frequency AEs.
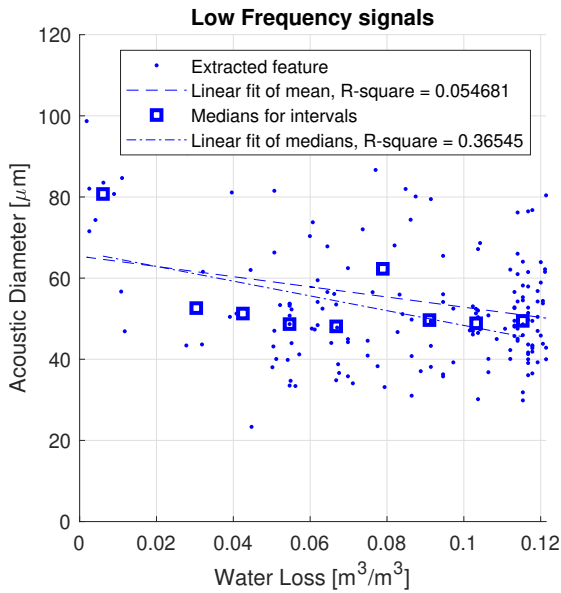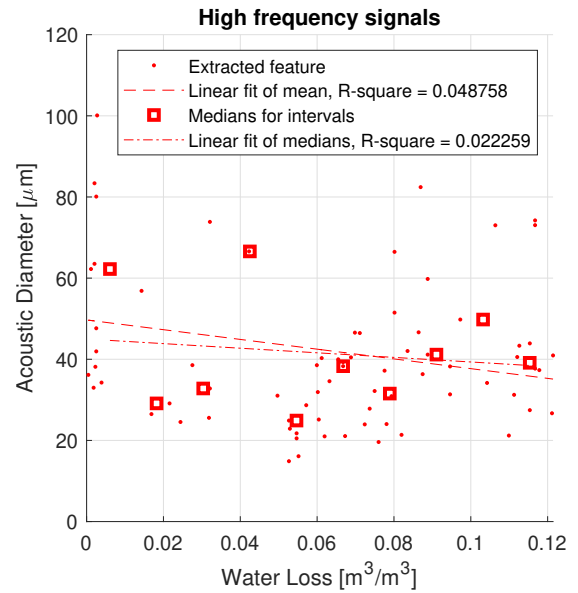

(a) Settling time for low-frequency signals

(b) Settling time for high-frequency signals

Figure 33: Settling time as a function of water loss for high- and low-frequency signals during experiment 1. The dots indicate each data point and the squares are the medians over a given interval. The dashed line indicates the linear fit of all data points. The dotted line indicates the linear fit of the medians.

We can use figure 33 together with equation 7 to see how the xylem vessel diameter changes during dehydration. This yields figure 34.

(a) Acoustic diameter for low-frequency signals   (b) Acoustic diameter for high-frequency signals

Figure 34: Acoustic Diameter calculated from settling time as a function of water loss for high- and low-frequency signals during experiment 1. The dots indicate each data point and the squares are the medians over a given interval. The dashed line indicates the linear fit of all data points. The dotted line indicates the linear fit of the medians.

6.1.4 The difference between plants A and B

No difference in signal change for plants A and B is found. The graphs showing the change for the two samples (plant A and plant B) of frequency (figure 48), amplitude (figure 49) and settling time (figure 50) during dehydration are shown in appendix C. In these graphs, the distinction between high- and low-frequency remains. The relations shown in figures 32 and 33 do not significantly alter when we separate plant A from plant B. The main difference between the plants was the number of AEs, which was 78 for plant A and 174 for plant B. When we separate plant A and B into low- and high frequency signals, this results in 139 low- and 34 high-frequency signals for plant A and 37 low- and 42 high-frequency signals for plant B.

6.2 Experiment 2: Climate Chamber

In the second experiment in the climate chamber, I measured AEs for 28 days of plant growth. The experiment was terminated because plants were growing beyond their weight-bearing capacity as shown in figure 10b.

6.2.1 Differences between the varieties

As stated in section 4.2.2, the continuous light resulted in the non-stop growth of the plants. In figure 35 the heights of the two plants per variety are depicted. It can be seen that variety 1 grows slower compared to varieties 2 and 3. On May 6, the light intensity was increased, which can be seen in the steeper slope of the growth from that day onwards.
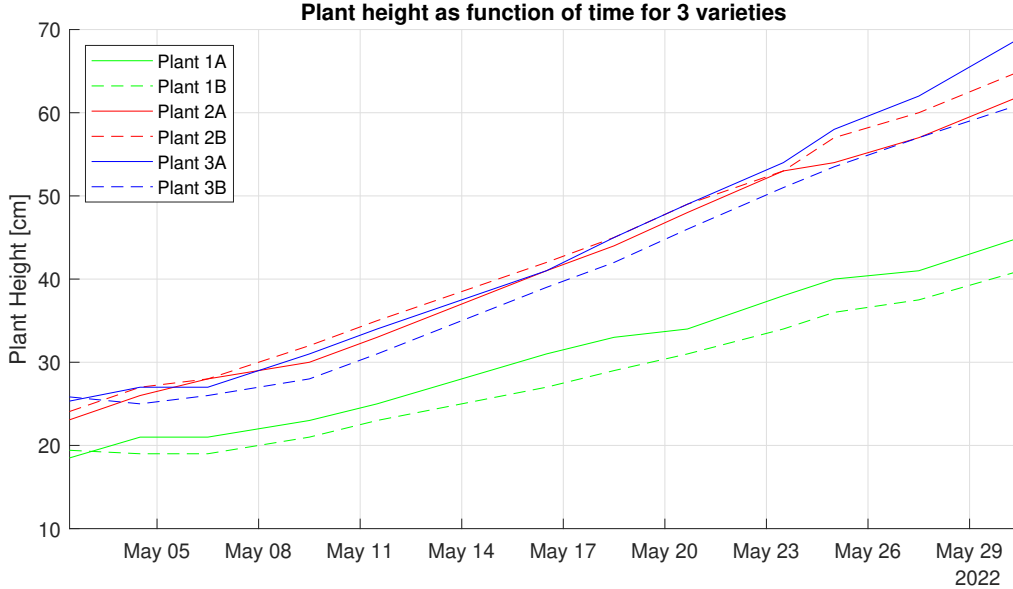

Figure 35: Growth of 6 Chrysanthemums in the same conditions for the total duration of experiment 2.

Other differences between the varieties are the vase life, which is 20 days for variety 3 and 11 days for variety 1 and 2. This is an objective predetermined value. As the actual vase life of flowers depends on many properties such as light and water supply, the VL value depicted here is just used to categorize varieties. Furthermore, the calculated Youngs modulus for varieties 1 2 and 3 were 590, 980 and 700 MPa respectively. These values are derived from the tensile test. The graphs are shown in figure 55 in appendix D. Note that these Youngs Moduli are much higher than the Youngs modulus of the tomato plant from figure 13 where this value was around 90 MPa. The density of the samples for the three varieties is also shown. In many cases, the error in density is related to the error in the Youngs modulus, as both errors are partially due to the error in the calculated cross-sectional area.

Plant variety	VL (days)	L_{stem} (cm)	E (MPa)	D_{xylem} (μm)	ρ (kg/m^3)
1	11	45 ± 1	590 ± 70	24 ± 12	825 ± 65
2	11	66 ± 1	980 ± 60	20 ± 16	760 ± 5
3	20	69 ± 4	700 ± 200	20 ± 20	720 ± 95

Table 1: Material properties of three plant species of Chrysanthemums. VL = Vase Life, L_{stem} = length of the plant at the end of the experiment measured from ground to top, E = Youngs modulus from figure 55, D_{xylem} = mean optical xylem vessel diameter, ρ = density of sample. The margins indicate the variance between different samples. The uncertainties shown are due to a dominant variance.

6.2.2 Rate of AEs

In this experiment, the microphone is relocated twice to have it at 50% plant height. This results in 3 stages: before replacement 1, between replacement 1 and 2, and after replacement 2. As can be seen below in figure 36, the cumulative number of AEs differs greatly between the plants. In figure 36 it seems as if the first replacement of the microphone reduced the number of AEs after that moment for plant 3B.
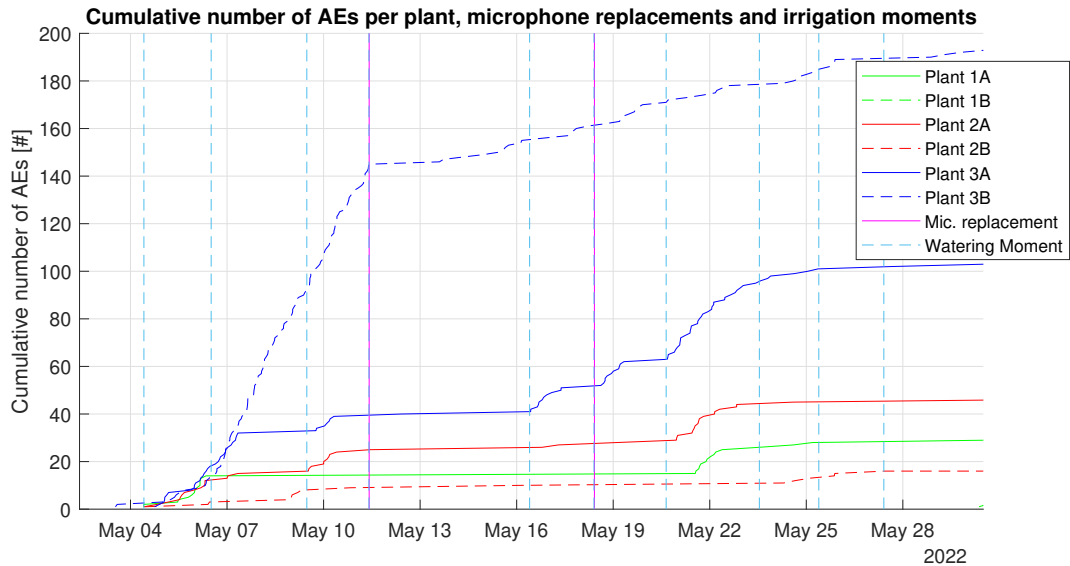
Figure 36: Cumulative number of AEs for both plants of 3 varieties during experiment 2. The vertical blue dashed lines indicate the moments of irrigation and the vertical purple lines indicate the moment of microphone repositioning. Note that only 2 AEs from plant 1B were observed (on May 30).

When we take a closer look at all plants measured with computer A (plants 1A, 2A and 3A), a step-wise increase can be detected. If we consider the moment of irrigation (figure 36), we can see that in most cases the number of AEs stops 24 hours after irrigation. This can be accounted to malfunctioning equipment. Every 2 to 3 days I would irrigate the plants, and see if the computer was still recording. Often computer A was frozen or crashing and had to be reset. We can validate this using figure 56 in appendix D where only outlier signals are depicted. We see that indeed after 24 hours, no signals are recorded (except after irrigation moments 1, 7 and 8). This means that for 45% of the time during the experiment, computer A was not recording.

6.2.3 Change in signal during growth

Initially, when we plot the three main characteristics of the AEs as a function of plant height, no relation is found (figure 57 for frequency, 58 for amplitude and 59 for settling time in appendix D). However, let's consider the fact that the microphone is replaced twice. If we only look at the first period (May 4th to May 11th), we can see a relation between the frequency and growth (figure 37) for plant 3B. Plant 3B is also the plant with most AEs. We can also deduce from figure 36 that between replacements 1 and 2 of the microphone, almost no AEs occur. In the latest stage, this rate is once again increased. Plotting the characteristics from May 18th onwards does not yield any promising results. The graph is shown in figure 60 in appendix D.
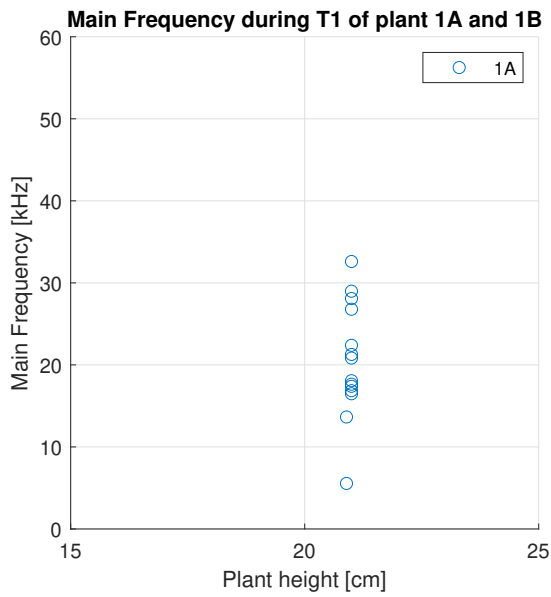
(a) Main frequency during the first measurement stage of plants 1A (1B did not yield any AEs in the first stage)
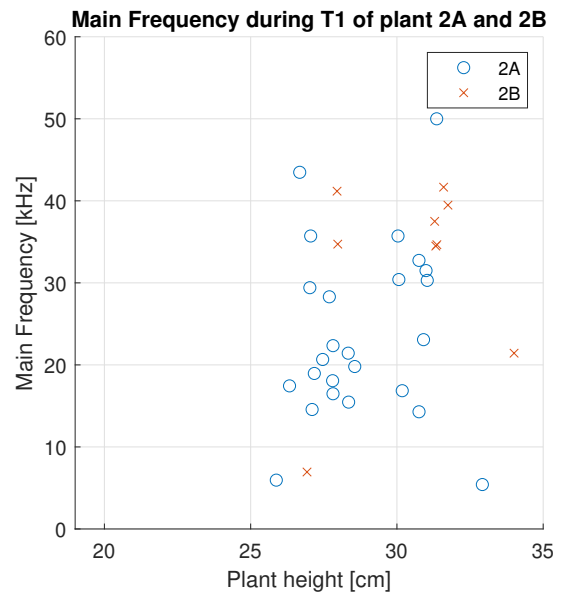
(b) Main frequency during the first measurement stage of plants 2A and 2B
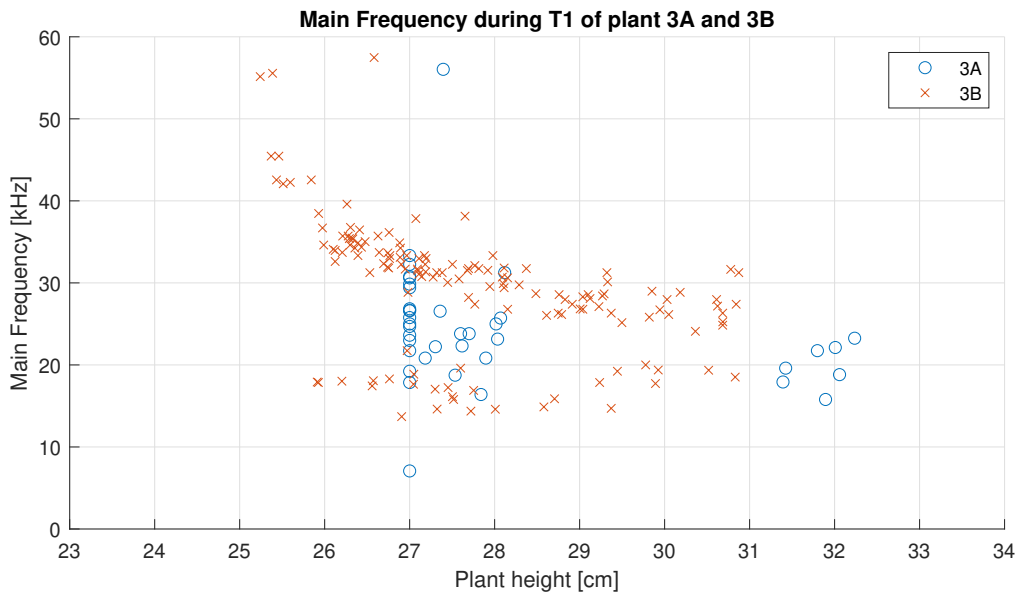
(c) Main frequency during the first measurement stage of plants 3A and 3B

Figure 37: Frequency as a function of time in the first stage of experiment 2 (before microphone replacement 1) for plants 1, 2 and 3.

7 Discussion

In this section, I will first discuss some general parts of this research. Next, I will review the data processing method and two experiments. The data processing method is discussed in section 7.2. The results for experiment 1 are discussed in section 7.3 and for experiment 2 in section 7.4. Finally, recommendations for future studies and experiments are given in section 7.5.

7.1 General

Before I discuss the different parts of the research in-depth, there are some general points of interest to note.

7.1.1 Type I signals

The relation between the settling time of the acoustic signal and xylem vessel diameter was the main tool to relate any signal to cavitation-related AEs from the xylem vessels. Therefore, I used this as the main driver to separate expected xylem-related AEs (the type I signals) from other signals. With the assumption that the data processing method is valid and the type I signals are indeed AEs related to the bubble formation from the xylem vessels, the rest of the thesis is written.
However, we should note that there is insufficient evidence to claim that the type I signals are indeed from cavitation-related events. As explained in section 2.2.1, there are different sources for acoustic signals coming from the plant. It could be the case that the type I signals are not cavitation-related signals, but that they are the result of e.g. capillary action of free water. Still, considering figure 22, I have reason to believe that the used method is valid for considering the type I pulses as cavitation-related AEs from the xylem vessels.

The type II and type III signals from experiment 1 are not observed in experiment 2. That is to say: the density based clustering algorithm did not detect any clusters that would correspond to type II and type III signals. When we consider figure 23a, we can manually see a certain group around $\sqrt{\tau} \approx 0.3$, but these data points are not dense enough to form a cluster based on the input values of the algorithm. This absence of type II and type III signals in experiment 2 can be attributed to several aspects, see the section 7.1.2 below. For further elaboration of type II and type III signals, see discussion section 7.2.4.

7.1.2 Differences between greenhouse experiment and climate chamber experiment

Of course, the main differences between the experiments are the facts that I measured different plants (tomato and chrysanthemums) and I performed different experiments: in the greenhouse experiment I let the tomato plants dry out, and in the climate chamber I mapped the growth of the plants in a constant environment. There are however other points of interest to consider.

One point of interest is the difference in setup between the greenhouse experiment and the climate chamber experiment. For the former, a clamping module was used to attach the microphone to the plant. For the latter, the microphone is mounted to a stick in the ground and attached to the plant stem using isolating foam. Between this foam, the horn is placed to make sure the isolating foam does not go between the microphone and plant stem. This horn may influence in two ways. First, the distance between the microphone and the plant stem is larger due to the size of the horn compared to this distance with the clamping module. In the greenhouse, the distance was 1.0 mm, and in the climate chamber, this distance is 9.0 mm. Secondly, this horn may result in shifts in the acoustic characteristics of the AEs. For example, amplitude- or frequency attenuation may happen due to the horn.
Furthermore, the isolating foam reduces the number of noise signals significantly. The total amount of signals in the greenhouse experiment was 10,410 whereas the total amount of signals in the climate chamber was 1,813. It must be mentioned that with one computer in the greenhouse experiment and two computers in the climate chamber experiment, the measuring capacity in the climate chamber was twice as large. However, a comparison between signals that are not type I may not be fair, as the surrounding noises are very different due to the difference in atmosphere.

7.1.3 A limited number of data points

The total number of useful data points is limiting. For the greenhouse experiment, the number of AEs was 252 and for the climate chamber experiment, this number was 393. We do have enough data points to make some assumptions, but more data would be beneficial to make relations clear and claim correlations with more confidence. The variance in the graphs support this statement.

The number of samples is limited as well. In the greenhouse, I tested on 2 plants and in the climate chamber, I tested on 2 plants for 3 varieties. With only 2 plants per variety, claims about correlations are not very strong, as one plant might react differently to changes than others. Especially considering the climate chamber experiment, where the difference per variety was something to look for, this limits the results. As the number of AEs per microphone and plant differs greatly, more samples would be beneficial. Furthermore, as we are measuring living organisms that respond to more than just temperature humidity and light intensity, the measurements are prone to error. Increasing sample size will improve accuracy and will reduce the effects of outliers.

In this thesis, the limitation of the sample size was due to a limited amount of computers. To measure with one microphone at 100% capacity, you need one computer per microphone. For the greenhouse experiment, one computer was used for 2 microphones which resulted in a measuring capacity of 40% per microphone (20% was used to switch between microphones). For the climate chamber experiment, 2 computers were used for 6 microphones, resulting in a capacity of 30% per microphone (10% per computer was used to switch microphones). By capacity I mean the percentage of time that the microphone was measuring.

7.1.4 Material properties

To obtain the material properties, samples were weighed and measured to obtain the density, a tensile test was performed for the Youngs Modulus and samples were examined under a microscope to get the optical xylem vessel diameter.

The microscope test to obtain the optical xylem vessel diameter was for both experiments performed at the end of the experiment, as this is a destructive test. This also means that if the diameter changes during the experiment, the optical test from figure 11 is not representative of the diameter throughout the experiment. Given figure 34, we see that the acoustic diameter decreases over time. If indeed the diameter decreases over time, the optical diameter during the experiment would have been larger than at the end when the optical test is performed. This would make the difference between the acoustic and optical diameter from figure 21 even larger. The decrease in acoustic diameter is debated in section 7.3.3.

Moreover, there is uncertainty in the measured optical diameter (figure 11). The optical xylem vessels were measured randomly, but this means there is a human bias: I only measured those xylem vessels that were well visible. Therefore, the very small xylem vessels that are hard to distinguish are perhaps not accounted for. If I were to account for this, the mean of the optical diameter in figure 21 would shift to the left. This would reduce the difference. Furthermore, the xylem vessels from the tomato plant were quite distinguishable from the phloem. However, this distinction was less clear for the chrysanthemums (figure 12). For the chrysanthemums, I possibly also measured the optical diameter of the phloem with the microscope.

7.1.5 Time as a secondary variable

In experiment 1 the main variable for change in AEs was water loss. In experiment 2 this was growth. Both these parameters were used to map changes in the acoustic characteristics of the AEs observed. We should note that both experiments have been conducted in a time-passing manner. That is to say, we could also plot the changes in characteristics as a function of time, and similar correlations would be seen. It cannot be ruled out that the plant behaviour and response to both water loss and growth may be influenced by the duration of the experiment. To put it in other words: the relation between the increase in amplitude and increase in water loss in figure 32 may become smaller or larger when the dehydration process would happen in just 2 days, instead of the 21 days of the experiment. This line of reasoning holds for all relations found. As plants are complex organisms with many processes inside, their response to environmental changes or their changes due to growth may be influenced by time.

7.2 Data processing method

The method described in section 5 was used to obtain features which were also used to select the type I signals. This method has a few drawbacks. These are elaborated below.

7.2.1 Cropping the signal

There are three main aspects to mention about cropping the signal. First, as stated in section 5.1, a 15% threshold value on top of the noise amplitude for the steady state is taken. This value is chosen based on some trial and error and therefore it is arbitrary. A margin too large resulted in a too narrow peak. This resulted in few data points to fit the exponential decay. A margin too small often resulted in the fact that the signal never got below the margin. This resulted in a fit that is based on many irrelevant data points.

Second, if the noise in the 0.2 s before the peak is large, the pulse duration is very small. Moreover, if the noise prior to the peak is very small but the noise after the peak is quite large, the settling time is very large as well. Even one small peak in the 0.2 s before or after the actual pulse peak influences the pulse duration immensely.

Not only is the pulse duration affected, but the settling time that is fitted over the length of the pulse is affected as well.

Finally, when there are two pulses in one file, the second pulse is ignored by the algorithm, which influences the pulse duration. In the flowchart of figure 17, this is taken into account. However, perhaps some secondary peaks are still evaluated as being noise, therefore influencing the pulse duration.

7.2.2 Extracting features from the pulse

From the frequency domain of the pulse, only the main frequency is taken. This means that if the frequency domain has multiple peaks, many are ignored. From the two signals in figure 30, the main peaks are quite obvious. However, there are also pulses where the peaks in the frequency domain were broader and only taking one value as the main frequency is less straightforward. Furthermore, the sensitivity function of the microphone is not incorporated. The sensitivity function indicates how well certain frequencies are observed. This sensitivity function may differ per microphone or in general, may measure certain frequencies better than others. For example, the sensitivity at 20 kHz may be very low. This would mean that frequencies with 20 kHz as the main frequency would have a lower amplitude and for all frequencies in general that in the frequency domain, 20 kHz would have a lower magnitude.

When the pulse duration is determined, the exponential decay is automatically fitted. Needless to say, some fits are better than others. As this fit is performed automatically, not all fits are evaluated. It might therefore be the case that some fits do not follow the decay as it would when done manually. This affects the extracted settling time and therefore the calculated acoustic diameter.

7.2.3 Categorizing

In figures 20b and 23a I found a separation between type I signals and other signals. Even though a clear distinction is found between the type I signals and other signals, there are still limitations. As the extracted features are sometimes not well extracted from the data file, this could put certain type I AEs in type II, type III or outlier clusters. This holds the other way around, perhaps many signals are assigned type II, type III or outliers and are therefore excluded, even though they were cavitation-related AEs from the xylem vessels.

Moreover, the density-based clustering algorithm sets a boundary automatically but is still based on arbitrary input values. Changes in these input values would move the boundaries, thereby including or excluding certain data points.

7.2.4 Type II, type III and outliers

In figure 20b we can see two clusters beside the type I cluster. In figure 23a there is no cluster other than type I. In chapter 6, we only analyzed the type I signals, as these are assumed to be linked to the xylem vessels. But perhaps the signals from the other clusters are interesting as well. Since the origins of the other signals are unknown, we can only speculate. There could be several reasons for this, three of which I will discuss. Figure 45 in appendix C shows the time- and frequency domain of an example of type I, II and III AE.

The phloem vessels are somewhat similar to the xylem vessels. They are also vascular tissues in the form of long tubes that transport nutrients and water in the plant. There are some differences though: the phloem has bidirectional movement whereas the xylem has unidirectional transport. Another difference is that the xylem vessel consists of dead tissue, whereas the phloem consists of living tissue. These phloem vessels may also emit AEs, which then may have different characteristics compared to the xylem AEs. If for example, the diameter of the phloem cylinders is larger than the xylem vessels with all other parameters from equation 7 the same, a larger settling time is expected. Furthermore, the parameters could differ in the phloem. E.g. a smaller dynamic viscosity in the phloem (with a diameter similar to the xylem vessels) would yield a larger settling time. The same reasoning holds for a larger density.

Besides the xylem and phloem, the plant has many processes going on inside. As stated in section 2.2.1, there are many sources of AEs from plants. This list of sources can even be expanded with sources such as snapping plant stems, wilting leaves or cracking and separation of tissue.

Of course, many noises happen in greenhouses. I observed that if someone walked by and made a whistling sound, the microphone was triggered. Other equipment such as machinery and trolleys, or even rustling leaves or insects might have triggered the microphone. These signals might form the type II or type III signals.

7.3 Experiment 1: Greenhouse

This section will have a similar setup as the results from section ??, where I will first discuss the rate of emission (7.3.1), next the environmental parameters (light, temperature, humidity) 7.3.2 and finally the change in characteristics of the AEs during dehydration (7.3.3).

7.3.1 Rate of emission

When we look at figure 24, we can see a super-linear increase in the rate of emissions as a function of time. When we plot the rate of emission as a function of water content, as is done in figure 25, we can still see a super-linear increase. This shows that the rate of emissions corresponds to what we expect from literature (figure 3), where the initial increase is also super-linear. Unfortunately, the experiment had to be terminated after 22 days, so the successive decrease in the rate of emissions from figure 3 was not observed.

Two soil sensors were used in this experiment, one for each plant. These sensors gave quite different values for water content. I expected this to be due to an error in the calibration value. In a recent supplementary experiment, the sensors were implemented in the same slab, see figure 51a in appendix C. Here we can see that the four sensors give indeed quite different values for water content. To see if the error is due to reference or sensitivity, I have plotted the values with normalization (figure 51c) and without normalization (figure 51b). The graph without normalization gives a lower RMSE. This indicates that the difference between values for water content can be solved by solely shifting the values. This also explains why the water content in figure 22 goes below zero. As I used water loss instead of water content throughout the thesis, this issue is accounted for.

7.3.2 Temperature, light, humidity

Most AEs were emitted with large values for temperature, light and humidity as can be seen in figure 26. This was expected, as light results in photosynthesis and high temperature results in more evaporation, both increasing the tension in the xylem vessels. However, also during the nocturnal period, some AEs occur. During the night, water still evaporates from the leaves and soil, increasing the tension in the xylem vessels. Moreover, more factors than just water loss, light, temperature and humidity might influence the emission of AEs.
For the total duration of the experiment, a second peak for the light intensity in figure 47a (appendix C) is seen as well. This might have to do with shadow due to the non-optimal positioning of the light intensity sensor. This second peak is less visible after November 16, as can be seen in figure 26 where only the average values for light, temperature and humidity are plotted after this date. In this period, the angle of the sun may have been slightly different compared to the total duration of the experiment.

Next to the greenhouse experiment, another experiment was pursued to see which of the environmental parameters would be dominant for the change in acoustic characteristics or the rate of AEs. The setup of this experiment is depicted in appendix C in figure 52. The light was simulated using a grow LED light source. However, with this setup, no AEs were observed. The light intensity during this experiment was 4 µmol m^{-2} s^{-1}, which is much smaller than the greenhouse experiment (light intensity reaching sometimes 400 µmol m^{-2} s^{-1}) or climate chamber experiment (light intensity was 31 µmol m^{-2} s^{-1}). This suggests a certain threshold value for light intensity is needed for AEs to occur. However, this remains speculative.

Changes in characteristics due to light, temperature and humidity In the work of Mott et al., they found changes in the xylem diameter with an immediate change in light intensity from 0 to 1000 μmol/m^2/s. This would be visible in the settling time of the AEs. However, no such trend is observed.

Delay A delay between the light intensity on the one hand, and temperature and humidity on the other hand, can be spotted in figures 26 and 27. As temperature and transpiration increase as a result of sunlight, this was expected. The increase and decrease in the rate of AEs from figure 27 have an inaccuracy of ±30 minutes. Moreover, the R-square value for the Gaussian fit of the AE rate is lower than the R-square value for the other parameters plotted in figure 27. With this information in mind, we should consider the delay in the peak value (the centre of the Gaussian) for all parameters. The difference in the peak for the number of AEs compared to light translates to an overall delay of 75 minutes. From section 3.2 we know that the response of stomatal opening to sudden light increase is 15-60 minutes. This suggests there is some delay between the stomatal opening and the increase in the rate of AEs. A more time-accurate experiment could enhance these results.

The correlation coefficients indicate the statistical relationship between two variables. For this experiment, I calculated the coefficients to see how well the different parameters of light, temperature and humidity relate to the AE count. The correlation coefficients between the AE count and light, temperature and humidity correspond to the relation found by Sriwongras et al. as stated in section 3.2 [66]. The correlation coefficient between the count of AEs and temperature was largest with $R = 0.93$, followed by humidity ($R = 0.91$) and light ($R = 0.79$). We should note that the correlation coefficients do not necessarily indicate the interlinkage between the AEs and the environmental parameters. For example, the correlation coefficient between light and temperature is only 0.9 in the experiment. But we know that the temperature increase is due to the increase in light intensity of the sun. The delay between the parameters results in a decrease in the correlation coefficient. A low correlation coefficient should therefore not be an indicator of a bad correlation.

Impact of the season On November 1st, the sunrise was at 07:35 and sunset was at 17:10, whereas on November 22nd, sunrise was at 08:10 and sunset at 16:40. This means that the duration of large temperature-, light- and humidity values became 11% less during the experiment, which can be seen as more narrow peaks in figure 46 in appendix C. As most AEs are emitted diurnally (figure 26), this may have reduced the increased rate of emissions and therefore the effect of water loss. Furthermore, the maximum light intensity during the experiment was 450 µmol m^{-2} s^{-1}. In summer, this value often reaches 1500 µmol m^{-2} s^{-1} as was shown in a different experiment. Also, temperatures in November are lower than in the summer months, which results in slow dehydration due to slow evaporation.

7.3.3   Change in acoustic signals due to water loss

From figure 28, we can see changes in all three parameters of the signal during dehydration. A linear fit through all data points and a linear fit through the medians are plotted. This is not done because this fit had the highest R-square value, but mainly to determine if the relationship was positive or negative. The linear fit through all data points will be used for further discussion. We should further note the fact that there is no difference observed between plants A and B for the change in acoustic characteristics. The fact that these AE characteristics changed similarly due to dehydration, supports the relations found.

Frequency When we initially plot the frequency during dehydration (figure 28b), it seemed as if the frequency decreases significantly. However, when we take a look at figure 29, we see that the AEs can be divided into two groups: high-frequency AEs around 30 kHz and low-frequency AEs around 10 kHz. Mostly the low-frequency AEs increase in number, which explains the above-mentioned decrease. It is unclear why especially these two frequencies are visible. If one would relate this to different modes, one would also expect a group AEs around 20 kHz if we assume integer modes. When we observe figure 30b, we can indeed see a peak a bit below 20 kHz. Somehow, the 20 kHz peak is rarely the main peak. This could be accounted to a loss in the data. When we consider figure 30b, we can see mainly a peak at 30kHz. However, for other pulses, a peak almost as high as the 30kHz peak was found at 20kHz. This data is neglected because only one main frequency is considered.

When considering the frequency of the AEs, it is important to know how the xylem vessels vibrate. As the xylem vessels act as liquid-filled cylinders, their frequency modes are a combination of flexural vibrations of the solid cylinder, the acoustic pressure of the liquid inside the cylinder, the perforation plates and the orifices of the pit membranes. These sources were investigated in the work of Bieling [46]. As the main frequency is a combination of these sources, it is possible that the 10 kHz signals and 30 kHz signals have a different main driver behind the vibration.
We can also relate the frequency of AEs as a function of drought (figure 29) to literature (figure 4b from Oletic [40]). Even though the observed frequencies from Oletic are much higher, a similar trend is visible concerning the rate of emission.

Amplitude In figure 28a we can see that the average amplitude of the signal increases from 0.065 V to 0.100 V during dehydration, which is an increase of 54%. When we separate the low- and high-frequency signals, we can see that for the low-frequency signals, this increase in amplitude is 90% and for the high-frequency signals, the increase in amplitude is 40% (figure 32). This agrees with the claim from the TU Delft bachelor group (section 3.1) that the amplitude increases during dehydration.

This result may be explained by the fact that the density or Youngs Modulus of xylem vessels increase during dehydration (explained in section 2.5). An increasing stiffness would result in a better transfer from the cavitation source to the microphone. That is to say, stiffer material has less damping for the impulse, resulting in an increased amplitude. Let's consider the following scenario, where the sound from the water in the xylem vessel travels through plant tissue to the air. We can estimate the specific acoustic impedance of the tissue by using equation 9. We substitute the isentropic bulk modulus with the Youngs Modulus from figure 13 and take the density from section 4.3.2. This yields a specific acoustic impedance of $z_{\text{tissue}} = 0.3$ MPa s/m. This value is closer to that of air ($z_{\text{air}} = 340$ Pa s/m) than to water ($z_{\text{water}} = 1.5$ MPa s/m). Using equation 10, it follows that an increase in specific acoustic impedance of the tissue would result in a larger transmission ratio and thus larger observed amplitude. This improvement of transmission with an increase of z_{tissue} holds until a value of roughly 0.75 MPa s/m, as beyond this value for z_{tissue} the transmission ratio decreases again.
We have substituted the Youngs Modulus for the Bulk Modulus in equation 9. We can only do this if we assume a Poisson ratio of $\nu = 0.33$. With $\nu = 0.33$, equation 4 gives $K_s = E$. A lower value for the Poisson ratio would result in a smaller value for the isentropic bulk modulus and therefore smaller value for the specific acoustic impedance. The value for $\nu = 0.33$ is assumed for simplicity, but is similar to for example the Poisson ratio of a tulip stem where $\nu = 0.37$ [83]. Even with some error, the reasoning remains valid, as long as the initial specific acoustic impedance is still below 0.75 MPA s/m.

The decrease in z_{tissue} can be due to a decrease in both stiffness and density as we can deduce from equation 9. As stated in section 3.1, Beall claims that during dehydration the wave velocity increases. With equation 9, this would increase the acoustic impedance. This ties in with the part mentioned above. Further research is needed to attribute the increase in amplitude to (one of) the two parameters.

Settling time We can see a decrease in settling time during dehydration in figure 28c and even more so in figure 33. We can argue that the dynamic viscosity, density and/or diameter of the xylem vessel from equation 7 change as a result of water loss. For dynamic viscosity, this would mean an increase in its value, for density and diameter this would mean a decrease in their respective values. Assuming water is incompressible, the density used in equation 7 is not likely to have changed during water loss. However, change in diameter quite possible. The hypothetical decrease in xylem vessel diameter could mean two things: the xylem vessels shrink during dehydration or xylem vessels with a larger diameter emit AEs sooner than vessels with a smaller diameter. One could argue that if indeed shrinkage happens, the length of the xylem vessels would shrink as well. Given equation 8, this would then increase the frequency. In figure 29, no such trend is observed. This shrinkage is thus a less likely explanation. A more likely explanation is that the larger xylem vessels cavitate with relatively low water loss, whereas the smaller xylem vessels cavitate later with more water loss. This is also supported by section 2.1.2, where I claim that xylem vessels with smaller diameters in general have increased resistance to cavitation.

7.4 Experiment 2: Climate Chamber

In this section, I will first comment on several aspects of the setup. After this, I will discuss the rate of emission. Next, I will discuss the change in AE characteristics as a function of growth. Finally, I will comment on the relation between vase life and AE characteristics.

7.4.1 Effect of the setup

In this experiment, the plants received constant light of 31 µmol m^{-2} s^{-1}. This constant light resulted in constant growth, as we can see in figure 35. Constant light, temperature and humidity were chosen to limit the impact of the change of these parameters on the AEs. Normally, plants experience nocturnal periods with no light. The nocturnal periods affect the plant metabolism and give the plants time to stop photosynthesis. These nocturnal periods are also important for the flowering process. As stated in the literature, overnight lighting would result in inhibition of flowering [70]. This was indeed observed during the experiment. The inhibition of flowering resulted in fewer variables during the experiment. This does beg the question of how flowering would affect the results. From a practical point of view, this is something to consider. Moreover, we cannot rule out that the nocturnal periods of no light have other effects on the AEs.
Furthermore, the isolating foam shown in figure 9a did have a small influence on the appearance of the plant. As I replaced the microphone and isolating foam, a small colour change was observed. At the location where the foam had been, the stem had a lighter green colour compared to the rest of the stem (figure 61 in appendix D). We can dedicate this to a decrease in Chlorophyll (green pigments that allow photosynthesis). As the stem is blocked from light, no photosynthesis happens. According to experts, this has almost no impact on the plant, as the colour change was minimal and most photosynthesis happens in the leaves and not the plant stem.

7.4.2 Rate of emission

As can be seen in figure 36, the number of AEs differs greatly between the six plants. Plant 3B yielded the most AEs with 193 in total, whereas plant 1B only yielded 2 AEs. This difference in the rate of emission can be attributed to the plant or the setup. I will give four potential explanations for the large difference in the observed number of AEs for the different plants.
First, the rate of AEs might be very plant-dependent. Some plants might emit many AEs whereas other plants, even from the same variety, do not emit any AEs. This is endorsed by the fact that the plants were hydrated during the experiment. As the rate of AEs increases during dehydration, the number of AEs during hydrated periods is quite arbitrary.
A second possible reason is that the AEs may be very local and thus the location of measurement is of great interest. For example, perhaps most AEs are emitted right at the leaf nodes. If one of the microphones is placed at such a location, it would receive more signals than the other microphones.
The third explanation has to do with the setup. In the setup, the microphone may be positioned in a non-ideal way. For example, the isolating foam may dampen AEs that are further away or get in between the stem and microphone. In figure 36 we can see that indeed after the first microphone replacement, the rate of emissions for plant 3B decreases. This may be the result of the non-ideal positioning of the microphone. However, note that the change in the rate of AE after the first microphone replacement for plant 3B can also be attributed

to the aforementioned reason of local AEs. When we consider figure 56 (appendix D) where all outlier signals are depicted, we can see that the number of outlier signals for plant 3B is rather small, whereas for plant 1B this number is quite large. This inverse relation of outlier signals compared with type I signals suggests two things. The first is that the algorithm determines many signals outliers instead of type I signals. After a thorough investigation, I found that this was rarely the case. Most outlier signals had a frequency of 5 kHz and a rather large settling time (figure 54 in appendix D). These signals are correctly excluded from the type I cluster. Another explanation for why the number of type I signals seems to be inversely related to the number of outlier signals is as follows. If the microphone is not ideally positioned, the damping from the foam may have been insufficient. This way, loud sounds from the climate chamber may have interfered, thereby drowning out the AEs from the plant.

Finally, the frequency threshold of 25 kHz was set to limit the number of unwanted sound sources. As we can see in figure 37c, the signals from plant 3B stop around this threshold. If the natural frequency of the plants is below the 25 kHz threshold, the signals are never recorded.

With figure 56 in appendix D, we can see that all microphones are working, because many signals not type I are still measured. The fact that plant 1B only had 2 AEs cannot be accounted to a malfunctioning microphone. There is more to plant 1B. To see if the microphone was working, I flicked plant 1B twice with my fingers to generate AEs. This yielded the two AEs from plant 1B in the experiment. This means that these AEs did not occur by themselves.

7.4.3 Change in AE characteristics during growth

For the first stage of the experiment (May 4th to May 11th), we can see a clear relationship between the frequency of the AEs and the growth of plant 3B (figure 37c). From equation 8 we know that the frequency of the signal is inversely linearly related to the length of the xylem vessels (if the effective speed of sound is constant). When we plot the frequency as a function of plant height in the first stage for plant 3B, we can indeed see a decrease. The decrease however looks sub-linear. This implies that the xylem vessel length grows slower than the plant stem. For the other plants measured, this relationship is not visible.

We can see that this decrease in frequency stops when the plant is 31 cm. When we consider figures 35 and 36, we can see that the microphone is replaced on May 11th when the plant is at 31 cm. Both the replacement of the microphone or the fact that the signals reached the 25 kHz threshold may explain why the aforementioned relationship is not visible after this moment.

In section 3.3 I hypothesized that we could see a difference in the settling time during the growth of the plant in the form of $\tau \propto L_S^{0.4}$. However, figure 59 does not show such or any relation. Other relations between the characteristics of the AEs and growth are also not found.

7.4.4 Vase Life

The VL of the three species were 11 days, 11 days and 20 days for the green, red and blue species respectively. The mean xylem vessels were 24µm, 20µm and 20µm. This result does not support the hypothesis that a smaller vessel diameter translates to a larger VL. The plant with the larger VL (Plant 3) stands out in the number of AEs, but as stated before, this can be accounted to many things. We can thus not say anything about the vase life of the different varieties based on the AEs.

7.5 Recommendations for future experiments

Both experiments would benefit from more data to generate a conclusion with more confidence. By using an exciter, the signals can be summoned on demand. This yields a more evenly distributed number of signals and improves the accuracy of relations found. However, one must be careful by relating these induced signals from an exciter to natural AEs. As the source may be the same, the cause is not. This extends to the fact that an exciter might influence the plant itself. Perhaps the excitation of plant tissue results in cracks or other deformations that are disadvantageous for the plant itself. If that happens to be the case, the applications are severely limited.

The accuracy can also be improved by using more microphones and more importantly more laptops. During the experiment, the microphones did not measure at full capacity, because the microphones have been recording in an alternating fashion. With more computers, the microphones could record continuously, increasing the effective recording time to 100% per microphone.

The data processing method could also be improved, which would lead to more useful data. The algorithm in general is not yet optimized. By implementing more gates and reviewing more examples, the algorithm will get more precise, more accurate and perhaps even detect more type I pulses. Moreover, the method was designed based on the results from experiment 1 and used for experiment 2 as well. Due to the difference in setup,

environment and plant species, the algorithm may work less well with these changes. A more thorough review of example pulses is probable to improve the results in both accuracy and precision.

We are still in the dark about the position of the microphone. The mock-up experiment, which was designed to determine the location of the microphone, yielded only a few signals. Therefore we cannot say with certainty where on the stem we yield the most AEs. Even more importantly, perhaps the location on the stem influences the characteristics of the observed signal as well. From the climate chamber experiment, we can deduce that the position of the microphone relative to the plant is important, as the relation of frequency as a function of growth was not visible after the first repositioning of the microphone of plant 3B (figure 37). Moreover, the difference in the rate of emission between different samples in both experiments supports this recommendation. Measuring for a long period on the same plant with multiple microphones would give us insights into the relevance of microphone placement.

As the first experiment was performed in November, dehydration took multiple weeks. In the summer period, this dehydration is much faster. This may result in different relations between the water loss in the soil and the response from the plant. Considering the application as a water demand sensor, the rapidness in response from the plant to drought and irrigation is crucial. If we only observe changes in the signal when the plant is already wilting, this application is not very suitable. If an experiment is performed in summer, the changes in temperature, light and humidity are expected to be larger as well. We should aim at relating the changes in these parameters to changes in the AE characteristics in a quantitative and qualitative way. In the current thesis, only the delay between the parameters and the rate of emission is investigated. As the rate of AEs was quite low, a change in characteristics due to e.g. increasing light was not investigated. This would however be interesting to pursue.

In this research, I have only experimented with two types of plants: tomatoes and chrysanthemums and only looked at two research questions per plant. It is therefore advised to find out to what extent the correlations found in this research are valid for other plant species.

8 Conclusion

In this thesis, the acoustic emissions from plants were investigated. This was done by performing two experiments. In the greenhouse experiment, we have seen how these AEs changed with varying environmental parameters, which are the water content of the soil, light intensity, temperature and humidity. In the climate chamber experiment, the changes in AE characteristics were observed and related to plant variety and growth. Before the relations between the AEs and the aforementioned variables were mapped, an algorithm was created to separate signals of the plant from other signals. After a thorough investigation of several features of the signal, the pulse duration and square root of the settling time formed the basis of this algorithm. With these normalized values, a density-based clustering algorithm detected different clusters of signals. The signals in one of those clusters were determined type I signals and were assumed to be related to the bubble formation in the xylem vessels. We have two reasons to believe that type I signals are from the xylem vessels. First, the acoustic diameter of the type I signals overlapped with the optical diameter of the samples measured. Second, the vulnerability curve of type I signals corresponded to literature, where the number of AEs increased super-linearly as a function of water loss. This curve was sub-linear for the other signals. With the type I signals, the rest of the thesis was written.

It was found that the amplitude of the AEs increased during dehydration and the settling time of the AEs decreased during dehydration. This change was magnified when the signals were divided into high- and low-frequency clusters, with high-frequency signals being above 20 kHz and low-frequency signals below 20 kHz. Especially the low-frequency signals increased in rate of emission during dehydration. This answers the main research question, which read *How do the characteristics of the AEs change with decreasing water content?* For the increase in the amplitude of the AEs, one explanation was proposed. I suggested that the driving principle behind the increase in amplitude was a change in the acoustic impedance of the solid tissue. An increase in acoustic impedance would arise from an increase in Youngs modulus of the solid tissue. With the solid tissue acting as an intermediate between water and air, the transmission ratio for sound would increase if the acoustic impedance of the solid increases. The decrease in settling time of the AEs was possibly due to the assumption that the xylem vessels with larger diameters (and thus larger settling time) embolize with relatively low water loss compared to the xylem vessels with smaller diameters.

The second research question was *What are the effects of changes in light, temperature and humidity on the AEs?* As expected, the number of AEs was largest at high values for light, temperature and humidity. The rate of emission was mostly correlated with the temperature. A novel finding is that the delay between the rate of AEs and the parameters light, temperature and humidity has been determined. I calculated that light preceded the AE count by 75 minutes, temperature preceded the AE count by 20 minutes and humidity did not precede nor follow the AE count.

For the third research question, I investigated *How does the growth affect the AEs?* When the frequency of the AEs was plotted as a function of growth, we can see a sub-linear decrease. The hypothesized increase in settling time was not observed.

Finally, the last research question read *What can the AEs say about the vase life of flowers?* A lack of data points prevented me from describing a relation between vase life and AE characteristics.

For future research three main recommendations were given. First, instead of waiting for AEs from the plant, an exciter should be implemented. This will result in on-demand AE acquisition. Not only will this improve the number of data points and therefore the accuracy, it will also improve the insights into the speed of response to for example change in light intensity. For this research, a comparison to naturally induced AEs should be made to see if the behaviour is similar. A second recommendation was to investigate the location of measurement. From both experiments, I found a large difference in the rate of emission. Moreover, from the climate chamber experiment, a large difference in signal behaviour was seen after repositioning the microphone, indicating that the position is very relevant for the observed AEs. Finally, the greenhouse experiment should be replicated during summer. This will show the impact of changes in light, temperature and humidity on the qualitative characteristics of the AEs.

By knowing how the AE characteristics change with water loss, we can use this information to automatically detect irrigation needs. More specifically, we can select a certain AE characteristic (e.g. amplitude) and define a threshold value. Once the plant emits AEs that exceeds this threshold value, a signal is sent to an actuator that results in irrigation.

References

[1] J. A. Milburn, "Cavitation in ricinus by acoustic detection: induction in excised leaves by various factors," *Planta*, vol. 110, no. 3, pp. 253–265, 1973.

[2] M. H. Zimmermann, "Pathology of the xylem," in *Xylem Structure and the Ascent of Sap.* Springer, 1983, pp. 107–125.

[3] M. T. Tyree, M. A. Dixon, E. L. Tyree, and R. Johnson, "Ultrasonic Acoustic Emissions from the Sapwood of Cedar and Hemlock," *Plant Physiology*, vol. 75, no. 4, pp. 988–992, 1984.

[4] A. Sandford and J. Grace, "The measurement and interpretation of ultrasound from woody stems," *Journal of Experimental Botany*, vol. 36, no. 2, pp. 298–311, 1985.

[5] M. Borghetti, A. Raschi, and J. Grace, "Ultrasound emission after cycles of water stress in picea abies," *Tree Physiology*, vol. 5, no. 2, pp. 229–237, 1989.

[6] G. E. Jackson and J. Grace, "Field measurements of xylem cavitation: Are acoustic emissions useful?" *Journal of Experimental Botany*, vol. 47, no. 304, pp. 1643–1650, 1996.

[7] S. Rosner, "Acoustic detection of cavitation events in water con-ducting elements of norway spruce sapwood," *Journal of acoustic emission*, vol. 22, p. 110, 2004.

[8] M. Nolf, B. Beikircher, S. Rosner, A. Nolf, and S. Mayr, "Xylem cavitation resistance can be estimated based on time-dependent rate of acoustic emissions," *New Phytologist*, vol. 208, no. 2, pp. 625–632, 2015.

[9] A. V. Klaveren, "Green digitalization," Greentech, 14-06-2022.

[10] T. J. de Jong, "Adaption in the horticulture," HortiHeroes, 23-06-2022.

[11] E. van Laerhoven, "Technological innovation in the horticulture," RoboCrops, 19-05-2022.

[12] I. Khait, R. Sharon, R. Perelman, A. Boonman, Y. Yovel, and L. Hadany, "Plants emit remotely detectable ultrasounds that can reveal plant stress," *bioRxiv*, p. 507590, 2019.

[13] S. Dutta, E. Kaiser, P. Steeneken, and G. Verbiest, "Listening to ultrasound from plants reveals xylem vessel anatomy," *Research Square*, 2021. [Online]. Available: https://www.researchsquare.com/article/rs-452046/latest?utm_source=researcher_app&utm_medium=referral&utm_campaign=RESR_MRKT_Researcher_inbound

[14] W. van Ieperen, J. Nijsse, K. Keijzer, T. Scheenen, H. Van As, and U. van Meeteren, "Processes and xylem anatomical properties involved in rehydration dynamics of cut flowers," in *VII International Symposium on Postharvest Physiology of Ornamental Plants 543*, 1999, pp. 199–205.

[15] J. Pouzoulet, E. Scudiero, M. Schiavon, and P. E. Rolshausen, "Xylem vessel diameter affects the compartmentalization of the vascular pathogen phaeomoniella chlamydospora in grapevine," *Frontiers in plant science*, vol. 8, p. 1442, 2017.

[16] J. Schutijser. (2021) Nieuwe groentes tegen verspilling: bloemkooltjes en broccoli met dunne stelen. [Online]. Available: https://www.nos.nl/l/m/2399523

[17] M. D. Venturas, J. S. Sperry, and U. G. Hacke, "Plant xylem hydraulics: What we understand, current research, and future challenges," *Journal of Integrative Plant Biology*, vol. 59, no. 6, pp. 356–389, 2017.

[18] C. F. Jordan and J. R. Kline, "Transpiration of trees in a tropical rainforest," *Journal of Applied Ecology*, pp. 853–860, 1977.

[19] S. D. Wullschleger, F. Meinzer, and R. Vertessy, "A review of whole-plant water use studies in tree," *Tree physiology*, vol. 18, no. 8-9, pp. 499–512, 1998.

[20] J. Pivec, V. Brant *et al.*, "The actual consumption of water by selected cultivated and weed species of plants and the actual values of evapotranspiration of the stands as determined under field conditions," *Soil and Water Research*, vol. 4, no. 2, pp. 39–48, 2009.

[21] H. R. Brown, "The theory of the rise of sap in trees: some historical and conceptual remarks," *Physics in Perspective*, vol. 15, no. 3, pp. 320–358, 2013.

[22] G. W. Koch, S. C. Sillett, G. M. Jennings, and S. D. Davis, "The limits to tree height," *Nature*, vol. 428, no. 6985, pp. 851–854, 2004.

[23] M. Fukuhara and S. D. Gupta, "Plant Tissue Culture Engineering," *Plant Tissue Culture Engineering*, no. January, 2006.

[24] O. Vincent, P. Marmottant, S. R. Gonzalez-Avila, K. Ando, and C.-D. Ohl, "The fast dynamics of cavitation bubbles within water confined in elastic solids," *Soft Matter*, vol. 10, no. 10, pp. 1455–1461, 2014.

[25] D. Newbanks, A. Bosch, and M. H. Zimmermann, "Evidence for Xylem Dysfunction by Embolization in Dutch Elm Disease," *Phytopathology*, no. January, pp. 1060–1063, 1983.

[26] S. J. Lee, J. Park, and J. Ryu, "Hydrodynamic study on the "stop-and-acceleration" pattern of refilling flow at perforation plates by using a xylem-inspired channel," *Frontiers in plant science*, vol. 9, p. 1931, 2019.

[27] M. T. Tyree and M. Zimmermann, "Conducting units: Tracheids and vessels," in *Xylem structure and the ascent of sap*.   Springer, 2002, pp. 1–25.

[28] U. G. Hacke, J. S. Sperry, J. K. Wheeler, and L. Castro, "Scaling of angiosperm xylem structure with safety and efficiency," *Tree Physiology*, vol. 26, no. 6, pp. 689–701, 2006.

[29] L. Markesteijn, L. Poorter, H. Paz, L. Sack, and F. Bongers, "Ecological differentiation in xylem cavitation resistance is associated with stem and leaf structural traits," *Plant, Cell & Environment*, vol. 34, no. 1, pp. 137–148, 2011.

[30] S. Sevanto, E. Nikinmaa, A. Riikonen, M. Daley, J. C. Pettijohn, T. N. Mikkelsen, N. Phillips, and N. M. Holbrook, "Linking xylem diameter variations with sap flow measurements," *Plant and Soil*, vol. 305, no. 1, pp. 77–90, 2008.

[31] L. L. Vergeynst, M. G. Sause, M. A. Hamstad, and K. Steppe, "Deciphering acoustic emission signals in drought stressed branches: The missing link between source and sensor," *Frontiers in Plant Science*, vol. 6, no. JULY, pp. 1–11, 2015.

[32] A. Ponomarenko, O. Vincent, A. Pietriga, H. Cochard, E. Badel, and P. Marmottant, "Ultrasonic emissions reveal individual cavitation bubbles in water-stressed wood," *Journal of the Royal Society Interface*, vol. 11, no. 99, pp. 1–7, 2014.

[33] O. Vincent, P. Marmottant, P. A. Quinto-Su, and C.-D. Ohl, "Birth and growth of cavitation bubbles within water under tension confined in a simple synthetic tree," *Physical Review Letters*, vol. 108, no. 18, p. 184502, 2012.

[34] N. J. De Baerdemaeker, M. Stock, J. Van den Bulcke, B. De Baets, L. Van Hoorebeke, and K. Steppe, "X-ray microtomography and linear discriminant analysis enable detection of embolism-related acoustic emissions," *Plant methods*, vol. 15, no. 1, pp. 1–18, 2019.

[35] J. B. Keller and M. Miksis, "Bubble oscillations of large amplitude," *The Journal of the Acoustical Society of America*, vol. 68, no. 2, pp. 628–633, 1980.

[36] F. Caupin and E. Herbert, "Cavitation in water: a review," *Comptes Rendus Physique*, vol. 7, no. 9-10, pp. 1000–1017, 2006.

[37] Y. A. Ilinskii, E. A. Zabolotskaya, T. A. Hay, and M. F. Hamilton, "Models of cylindrical bubble pulsation," *The Journal of the Acoustical Society of America*, vol. 132, no. 3, pp. 1346–1357, 2012.

[38] A. A. Doinikov, B. Dollet, and P. Marmottant, "Model for the growth and the oscillation of a cavitation bubble in a spherical liquid-filled cavity enclosed in an elastic medium," *Physical Review E*, vol. 97, no. 1, p. 013108, 2018.

[39] S. Wöckel, U. Steinmann, and H. Arndt, "Low frequency guided wave transmission in water pipe systems," *Procedia Engineering*, vol. 120, pp. 1257–1260, 2015. [Online]. Available: http://dx.doi.org/10.1016/j.proeng.2015.08.843

[40] D. Oletic, S. Rosner, M. Zovko, and V. Bilas, "Time-frequency features of grapevine's xylem acoustic emissions for detection of drought stress," *Computers and Electronics in Agriculture*, vol. 178, p. 105797, 2020.

[41] R. Laschimke, M. Burger, and H. Vallen, "Acoustic emission analysis and experiments with physical model systems reveal a peculiar nature of the xylem tension," *Journal of plant physiology*, vol. 163, no. 10, pp. 996–1007, 2006.

[42] L. De Roo, L. L. Vergeynst, N. J. De Baerdemaeker, and K. Steppe, "Acoustic emissions to measure drought-induced cavitation in plants," *Applied Sciences (Switzerland)*, vol. 6, no. 3, 2016.

[43] L. Vergeynst, M. G. Sause, and K. Steppe, "Acoustic emission signal detection in drought-stressed trees: beyond counting hits," in *31st conference of the European Working Group on Acoustic Emission (EWGAE)*, 2014.

[44] L. L. Vergeynst, M. G. Sause, N. J. De Baerdemaeker, L. De Roo, and K. Steppe, "Clustering reveals cavitation-related acoustic emission signals from dehydrating branches," *Tree physiology*, vol. 36, no. 6, pp. 786–796, 2016.

[45] G. Charrier, M. Pramsohler, K. Charra-Vaskou, M. Saudreau, T. Améglio, G. Neuner, and S. Mayr, "Ultrasonic emissions during ice nucleation and propagation in plant xylem," *New Phytologist*, vol. 207, no. 3, pp. 570–578, 2015.

[46] T. Bieling. Bio-inspired 3D printing of artificial xylem vessels to study ultrasound emission from plants. *Internal document*.

[47] M. S. Ghidaoui, M. Zhao, D. A. McInnis, and D. H. Axworthy, "A review of water hammer theory and practice," *Appl. Mech. Rev.*, vol. 58, no. 1, pp. 49–76, 2005.

[48] A. S. Tijsseling, "Exact solution of linear hyperbolic four-equation system in axial liquid-pipe vibration," *Journal of Fluids and Structures*, vol. 18, no. 2, pp. 179–196, 2003.

[49] R. A. Fine and F. J. Millero, "Compressibility of water as a function of temperature and pressure," *The Journal of Chemical Physics*, vol. 59, no. 10, pp. 5529–5536, 1973.

[50] D.-Y. Maa, "Potential of microperforated panel absorber," *the Journal of the Acoustical Society of America*, vol. 104, no. 5, pp. 2861–2866, 1998.

[51] F. Fahy, "7 - sound absorption and sound absorbers," in *Foundations of Engineering Acoustics*, F. Fahy, Ed. London: Academic Press, 2001, pp. 140–180. [Online]. Available: https://www.sciencedirect.com/science/article/pii/B9780122476655500084

[52] P. He, "Measurement of acoustic dispersion using both transmitted and reflected pulses," *The journal of the acoustical society of America*, vol. 107, no. 2, pp. 801–807, 2000.

[53] K. J. Niklas, "MECHANICAL BEHAVIOUR OF PLANT TISSUES : COMPOSITE MATERIALS OR STRUCTURES ?" *The Journal of Experimental Biology*, vol. 3272, pp. 3269–3272, 1999.

[54] L. J. Gibson, "The hierarchical structure and mechanics of plant materials," *Journal of the Royal Society Interface*, vol. 9, no. 76, pp. 2749–2766, 2012.

[55] D. Boldrin, A. K. Leung, and A. G. Bengough, "Effects of root dehydration on biomechanical properties of woody roots of ulex europaeus," *Plant and Soil*, vol. 431, no. 1, pp. 347–369, 2018.

[56] K. J. Niklas, "Dependency of the tensile modulus on transverse dimensions, water potential, and cell number of pith parenchyma," *American Journal of Botany*, vol. 75, no. 9, pp. 1286–1292, 1988.

[57] M. D. Fariñas, D. S. Knapik, J. J. P. Pina, E. G. Pelegrin, and T. E. G. Álvarez-Arenas, "Monitoring plant response to environmental stimuli by ultrasonic sensing of the leaves," *Ultrasound in medicine & biology*, vol. 40, no. 9, pp. 2183–2194, 2014.

[58] S. "Dutta, Z. Chen, E. Kaiser, P. M. Matamoros, P. Steeneken, and G. Verbiest, "Ultrasound pulse emission spectroscopy method to characterize xylem vessels in plant stems," Preprint, 2022, https://doi.org/10.21203/rs.3.rs-452046/v3.

[59] F. Beall, "Overview of the use of ultrasonic technologies in research on wood properties," *Wood Science and Technology*, vol. 36, no. 3, pp. 197–212, 2002.

[60] A. Minamisawa, A. Ozawa, H. Sakai, and K. Takagi, "Moisture effects on the ultrasonic velocities in woods," in *IEEE Symposium on Ultrasonics*. IEEE, 1990, pp. 1105–1108.

[61] J. Berkelbach, D. Vuik, and M. Wolbers, "Ultrasound sensor module for plant-health monitoring," 2021, *Internal document*.

[62] K. A. Mott, J. C. Shope, and T. N. Buckley, "Effects of humidity on light-induced stomatal opening: evidence for hydraulic coupling among stomata," *Journal of Experimental Botany*, vol. 50, no. 336, pp. 1207–1213, 1999.

[63] M. R. G. Roelfsema and R. Hedrich, "In the light of stomatal opening: new insights into 'the watergate'," *New Phytologist*, vol. 167, no. 3, pp. 665–691, 2005.

[64] M. Černỳ, P. Mazal, J. Čermák, L. Nohal *et al.*, "Potencials of sap flow evaluation by means of acoustic emission measurements," *Acta universitatis agriculturae et silviculturae Mendelianae Brunensis*, vol. 59, no. 2011, pp. 105–110, 2011.

[65] P. Dostál, P. Sriwongras, V. Trojan *et al.*, "Detection of acoustic emission characteristics of plant according to water stress condition," *Acta Universitatis Agriculturae et Silviculturae Mendelianae Brunensis*, vol. 64, no. 5, pp. 1465–1471, 2016.

[66] P. Sriwongras, P. Dostál, V. Trojan *et al.*, "The measurement of acoustic emission signals from stem of maize under controlled environment," *Acta Universitatis Agriculturae et Silviculturae Mendelianae Brunensis*, vol. 64, no. 2, pp. 535–541, 2016.

[67] J. A. Rosell, M. E. Olson, and T. Anfodillo, "Scaling of xylem vessel diameter with plant size: causes, predictions, and outstanding questions," *Current Forestry Reports*, vol. 3, no. 1, pp. 46–59, 2017.

[68] M. Olson, J. A. Rosell, C. Martínez-Pérez, C. León-Gómez, A. Fajardo, S. Isnard, M. A. Cervantes-Alcayde, A. Echeverria, V. A. Figueroa-Abundiz, A. Segovia-Rivas *et al.*, "Xylem vessel-diameter–shoot-length scaling: ecological significance of porosity types and other traits," *Ecological monographs*, vol. 90, no. 3, p. e01410, 2020.

[69] T. Hisamatsu, K. Sumitomo, and H. Shimizu, "End-of-day far-red treatment enhances responsiveness to gibberellins and promotes stem extension in chrysanthemum," *The Journal of Horticultural Science and Biotechnology*, vol. 83, no. 6, pp. 695–700, 2008.

[70] A. Nissim-Levi, M. Kitron, Y. Nishri, R. Ovadia, I. Forer, and M. Oren-Shamir, "Effects of blue and red led lights on growth and flowering of chrysanthemum morifolium," *Scientia horticulturae*, vol. 254, pp. 77–83, 2019.

[71] D. Fanourakis, R. Pieruschka, A. Savvides, A. J. Macnish, V. Sarlikioti, and E. J. Woltering, "Sources of vase life variation in cut roses: a review," *Postharvest Biology and Technology*, vol. 78, pp. 1–15, 2013.

[72] R. H. Waring and B. D. Cleary, "Plant moisture stress: evaluation by pressure bomb," *Science*, vol. 155, no. 3767, pp. 1248–1254, 1967.

[73] M. Tyree and H. Hammel, "The measurement of the turgor pressure and the water relations of plants by the pressure-bomb technique," *Journal of experimental Botany*, vol. 23, no. 1, pp. 267–282, 1972.

[74] C. Wei, E. Steudle, M. T. Tyree, and P. Lintilhac, "The essentials of direct xylem pressure measurement," *Plant, Cell & Environment*, vol. 24, no. 5, pp. 549–555, 2001.

[75] Z. Chen, "Relations between Xylem Radii and Ultrasound Emission Patterns from Stems of Plants in Multiple Species: An Experimental Study," 2021, *Internal document*.

[76] A. Pršová, "Light on phloem transport (an mri approach)," Ph.D. dissertation, Wageningen University and Research, 2016.

[77] MATLAB, *version 9.7.0.1216025 (R2019b)*. Natick, Massachusetts: The MathWorks Inc., 2019.

[78] M. Sause, *Identification of failure mechanisms in hybrid materials utilizing pattern recognition techniques applied to acoustic emission signals*. mbv, Mensch-und-Buch-Verlag, 2010.

[79] M. G. Sause, A. Gribov, A. R. Unwin, and S. Horn, "Pattern recognition approach to identify natural clusters of acoustic emission signals," *Pattern Recognition Letters*, vol. 33, no. 1, pp. 17–23, 2012.

[80] I. Khait, O. Lewin-Epstein, R. Sharon, K. Saban, R. Perelman, A. Boonman, Y. Yovel, and L. Hadany, "Plants emit informative airborne sounds under stress," *bioRxiv*, pp. 1–23, 2018.

[81] M. A. Acevedo, C. J. Corrada-Bravo, H. Corrada-Bravo, L. J. Villanueva-Rivera, and T. M. Aide, "Automated classification of bird and amphibian calls using machine learning: A comparison of methods," *Ecological Informatics*, vol. 4, no. 4, pp. 206–214, 2009.

[82] E. Oyallon, S. Zagoruyko, G. Huang, N. Komodakis, S. Lacoste-Julien, M. Blaschko, and E. Belilovsky, "Scattering networks for hybrid representation learning," *IEEE transactions on pattern analysis and machine intelligence*, vol. 41, no. 9, pp. 2208–2221, 2018.

[83] Z. Hejnowicz and A. Sievers, "Tissue stresses in organs of herbaceous plants: I. poisson ratios of tissues and their role in determination of the stresses," *Journal of Experimental Botany*, pp. 1035–1043, 1995.

[84] A. L. Jacobsen, L. Agenbag, K. J. Esler, R. B. Pratt, F. W. Ewers, and S. D. Davis, "Xylem density, biomechanics and anatomical traits correlate with water stress in 17 evergreen shrub species of the Mediterranean-type climate region of South Africa," *Journal of Ecology*, vol. 95, no. 1, pp. 171–183, 2007.

[85] K. J. Niklas, "Tissue density specific plant mechanical properties," p. 7, 1993.

[86] M. Holmes and V. C. Mow, "The nonlinear characteristics of soft gels and hydrated connective tissues in ultrafiltration," *Journal of biomechanics*, vol. 23, no. 11, pp. 1145–1156, 1990.

[87] D. U. Shah, T. P. Reynolds, and M. H. Ramage, "The strength of plants: Theory and experimental methods to measure the mechanical properties of stems," *Journal of Experimental Botany*, vol. 68, no. 16, pp. 4497–4516, 2017.

[88] A. Prusova, F. J. Vergeldt, J. M. Philippi, and H. V. As, "Effect of light on phloem transport in tomato plants," 2014. [Online]. Available: https://www.wur.nl/en/newsarticle/poster-price-alena-prusova.htm

A Parameters of plants

Property	Symbol	Unit
Vulnerability to cavitation	P_{50}	MPa
Hydraulic conductivity	K_h	m^3/s Pa
Youngs modulus	E	GPa
Breaking stress	σ	MPa
Thickness of cell wall	h	m
Diameter of the cylindrical xylem vessel element	D_{xylem}	m
Length of the cylindrical xylem vessel element	L_{xylem}	m
Permeability	ϕ	-
Water potential	Ψ	KPa or %
Volumetric flow rate	Φ	mm^3/s
Dynamic viscosity	η	Pa s
Percentage Loss of hydraulic Conductivity	PLC	%
Photosynthetic Photon Flux	PPF	mmol/m^{2}s
Vase Life	VL	Months
Density	ρ	kg/m^3
Longitudinal Strain	ϵ	%
Tensile stress	σ	MPa
Frequency	f	Hz
Amplitude	A	V or Db
Rise time of pulse	τ_r	s
Settling time of pulse	τ	s
Humidity	ρ_v	g/m^3
Transpiration	R_{transp}	mg/m^{-2}s^{-1}

Table 2: Properties of plants, xylem vessel elements of plants and the environment

Property 1	Relation	Property 2	Source
D_{xylem}	-	VL	[14]
D_{xylem}	+	Disease susceptibility	[15]
D_{xylem}	+	Vulnarability to cavitation	[2]
$(t/b)^2$	-	Vulnerability to cavitation	[84]
Ψ	+	PLC	[17]
D_{xylem}	+	K_h^4	[27, 84]
D_{xylem}	+	P_{50}	[28]
PLC	+	Number of embolisations	[5]
E	+	σ^2	[85]
P	-	ϕ	[86]
E	-	Ψ	[55]
E	+	Ψ	[56]
PPF	-	$f_{\text{resonance}}$	[57]
E	+	σ^2	[85]
ΔP	-	ϕ	[86]
τ_s	+	D_{xylem}	[13]
τ_s	+	η	[13]
f	-	L_{xylem}	[13]
ρ	-	E	[13]
ϵ	+	E	[13]
R_{transp}	+	PPF	[57]
R_{transp}	+	T	[57]
R_{transp}	-	ρ_v	[57]

Table 3: Qualitative dependency of several plant properties

Factor	Change	Effect on VL
Air humidity	$\geq 85\%$	$\downarrow$
B. cinera spore density	$\uparrow$	$\downarrow$
B. cinera latent infections	$\uparrow$	$\downarrow$
Photoperiod	$(\leq 20)\uparrow$	x
	24 h	$\downarrow$
Light intensity	$\uparrow$	x/$\uparrow$
Light quality	$\neq$ sources, directional quality	x
Air temperature	$(< 21°C)\uparrow$	$\uparrow$
	$(> 24°C)\uparrow$	$\downarrow$
Root temperature	$(12 \leq T < 22°C)\uparrow$	$\downarrow$
Carbon dioxide	$\uparrow$	x/$\uparrow$
Air velocity	$\uparrow$	$\uparrow$
Nutrition	$(2 < EC < 5\text{mS cm}^{-1})\uparrow$	x
Season	Winter	$\downarrow$

Table 4: Effect of environmental conditions during growth on the vase life (VL) of cut roses [71]

B Additional figures from literature
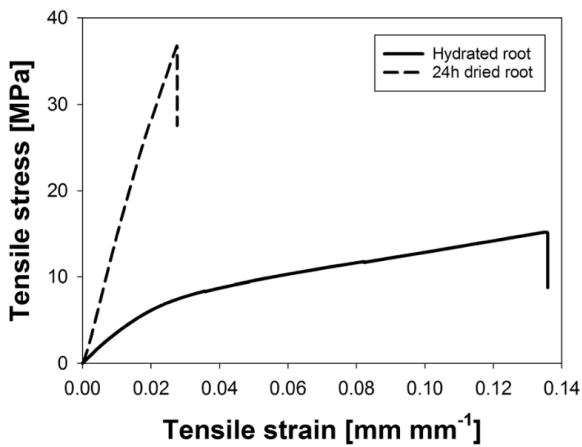
(a) Tensile stress versus tensile strain curves for a hydrated root sample and a root sample air-dried for 24 h of *Ulex europaeus* with xylem vessels. As the the packing density of fibres on the lignified xylem vessel walls increases during dehydration, the Youngs Modulus increases as well. From Boldrin et al. [55]
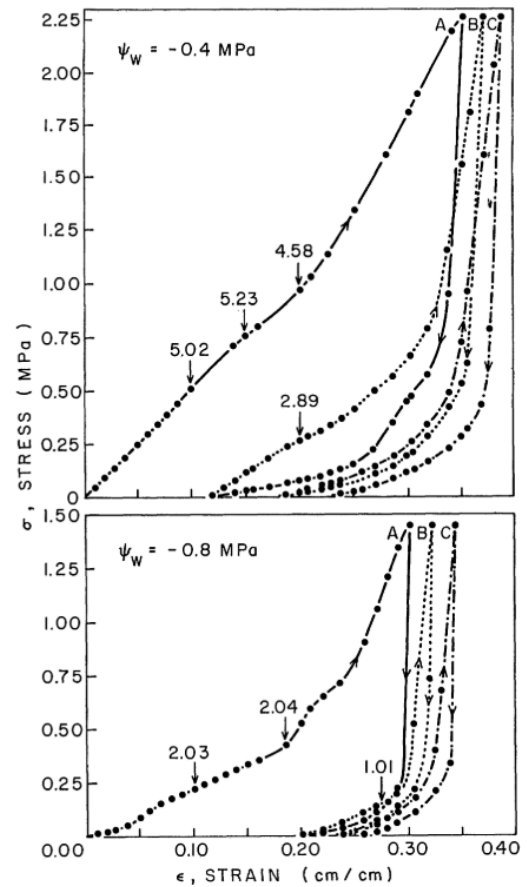
(b) Tensile stress versus tensile strain curves for a hydrated root sample (top) and a root sample partially dehydrated (bottom) of parenchyma cells of potato tubers. As turgor pressure decreases due to dehydration, so does the Youngs Modulus. From Niklas [56]

Figure 38: The contrasting tensile strain versus tensile stress curves of two different plants with different physiology. Boldrin (left) shows an increase in Young's Modulus during dehydration, whereas Niklas (right) shows a decreasing Young's Modulus during dehydration. Both used a tensile test.
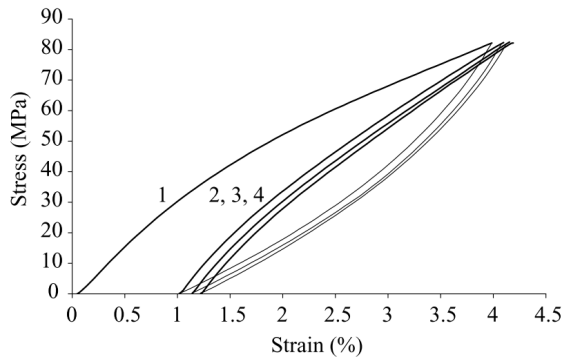
(a) Cyclic loading–unloading curves on sclerenchyma of *Aristolochia macrophylla* show a large residual deformation after the first cycle but almost no plastic deformation in subsequent cycles. Here, elastic and viscoelastic behaviour dominates. The elliptical shape shows hysteresis. From Niklas [53]
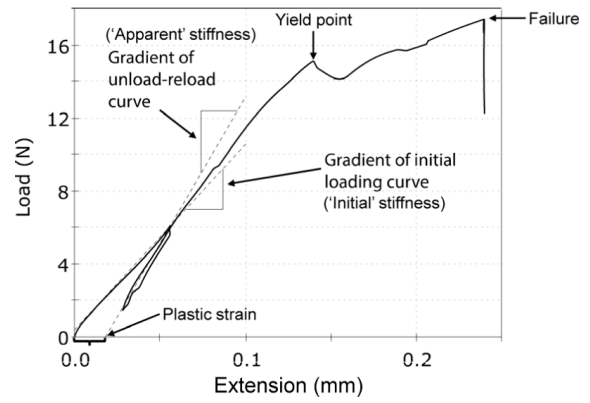
(b) A typical load-displacement curve obtained from a single-cycle tensile test carried out on a basal stem section of *Arabidopsis thaliana*, showing an increase in stiffness and the development of irreversible 'plastic strain' after the first unload. The stress (or strength) at yield and failure can also be determined. From Shah et al. [87]

Figure 39: Viscoelastic behaviour of plants during tensile tests.
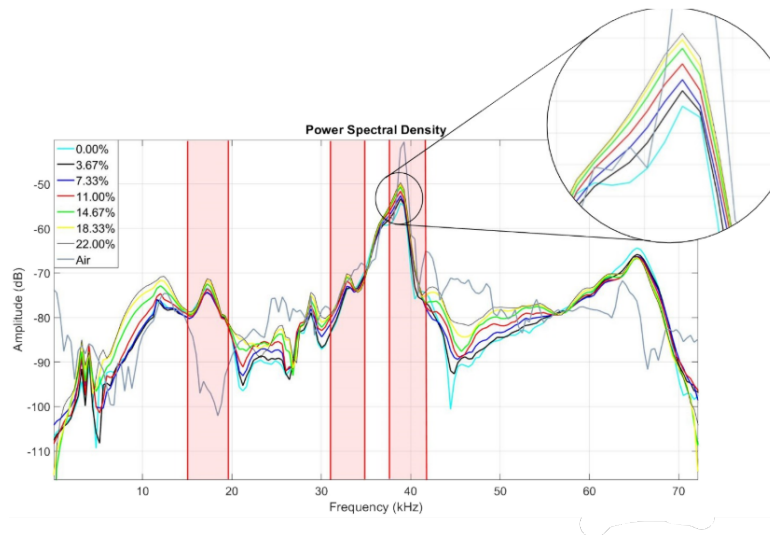
Figure 40: Power spectral densities of the radial response of UAs at multiple percentages of mass lost, indicated with colour. The peak frequencies are depicted with red bars. From the TU Delft bachelor group [61]
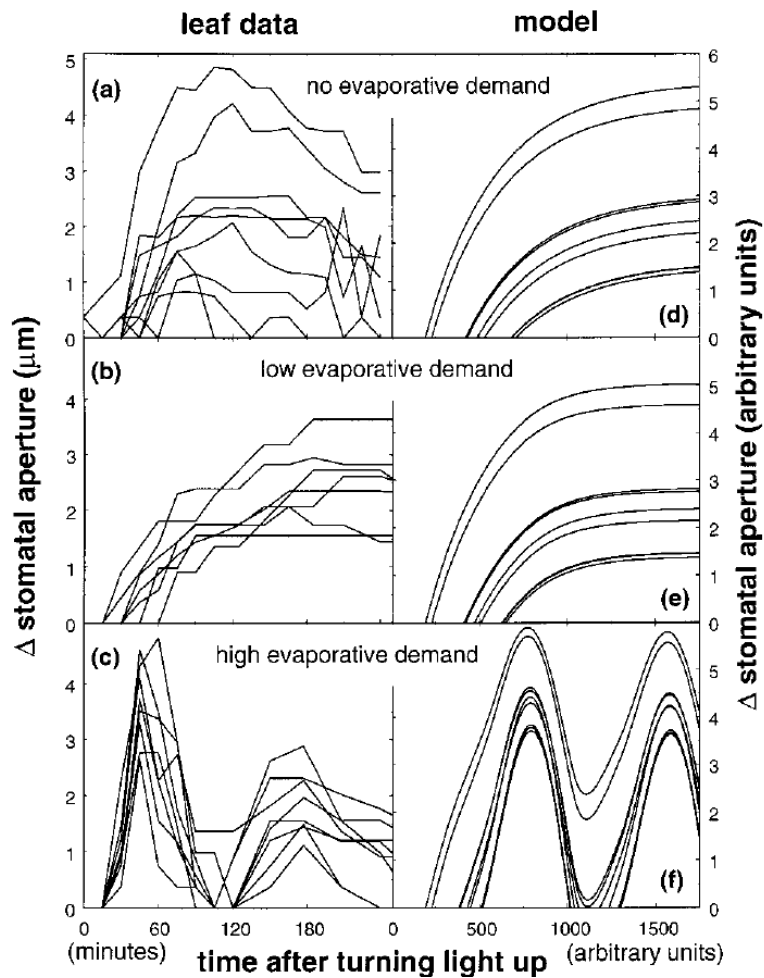
Figure 41: The effect of an increase in light intensity from darkness to 1000 μmol m^{2}s^{-1} on stomatal apertures. Each line is a time-course of the change in aperture of a single stomata from its value before increased light. In **b** with low evaporative demand, a different Spannungsphase for each stomata can be seen. With high evaporative demand (**c**), this difference in delay is not visible. From Mott et al. [62]
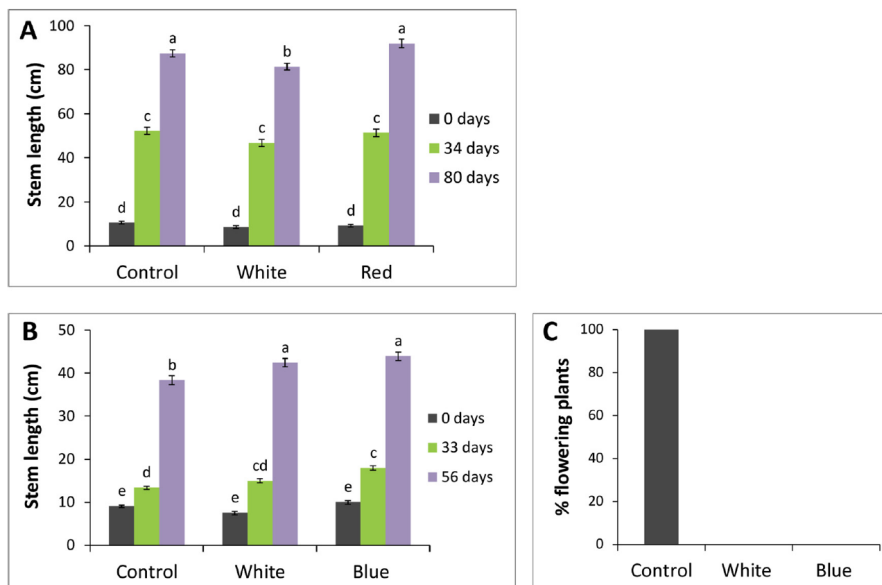
Figure 42: The effects of overnight lighting with no (control), white, red and blue light. On the left, the effect on stem length is shown, and on the right, the effect of flowering is shown. (A) plants were grown under LD conditions and (B) under SD conditions. We can see that the overnight lighting results in somewhat faster growth and inhibition to flowering. From Nissim et al. [70]

Feature	Definition	Unit
t_0	time of first threshold crossing (arrival time)	[s]
N_{AE}	number of signals threshold crossings	[#]
t_{AE}	time between first and last threshold crossing of signal	[μs]
$U_{\max}$	maximum signal voltage	[mV]
t_{peak}	time of maximum signal voltage	[μs]
f_{peak}	frequency of maximum signal contribution	[Hz]
N_{peak}	number of threshold crossings between t_0 and t_{peak}	[#]
Amplitude	$dB = 20\log(U_{\max}/1\mu V) - dB_{preamplifier}$	[dB]
Counts	N_{AE}	[#]
Duration	t_{AE}	[μs]
Rise Time	$t_0 - t_{peak}$	[μs]
Counts To Peak	N_{peak}	[#]
Root mean square (RMS)	$RMS = \sqrt{\frac{1}{T_{RMS}}\int_{t_0}^{t_0+T} U^2(t)dt}$ with a characteristic time T_{RMS} for averaging between 10 - 1000 ms	[mV]
Average signal level (ASL)	$ASL = \sqrt{\frac{1}{T_{ASL}}\int_{t_0}^{t_0+T} Amplitude\, dt}$ with a characteristic time T_{ASL} for averaging between 10 - 1000 ms	[dB]
Average Frequency	$\langle f \rangle = N_{AE}/t_{AE}$	[Hz]
Reverberation Frequency	$f_{rev} = \frac{N_{AE}-N_{peak}}{t_{AE}-t_{peak}}$	[Hz]
Initiation Frequency	$f_{init} = \frac{N_{peak}}{t_{peak}}$	[Hz]
Rise Angle	$\varphi_{rise} = \tan\left(\frac{U_{\max}}{t_{peak}}\right)$	[rad]
Decay Angle	$\varphi_{decay} = \tan\left(\frac{U_{\max}}{t_{AE}-t_{peak}}\right)$	[rad]
Absolute Energy	$W_{AE} = \int_{0}^{t_{AE}} \frac{(U(t))^2}{10k\Omega}dt$ with 10 kΩ input impedance of the recording equipment	[aJ]
Peak Frequency	f_{peak}	[Hz]
Frequency Centroid	$f_{centroid} = \frac{\int f \cdot \tilde{U}(f)df}{\int \tilde{U}(f)df}$	[Hz]
Weighted Peak-Frequency	$\langle f_{peak} \rangle = \sqrt{f_{peak} \cdot f_{centroid}}$	[Hz]
Partial Power	$\int_{f_1}^{f_2} \tilde{U}^2(f)\, df \left/ \int_{f_{start}}^{f_{end}} \tilde{U}^2(f)df \right.$ Frequency range of interest [f$_1$;f$_2$] Frequency range of investigation [f$_{start}$;f$_{end}$]	[%]

Figure 43: Features to describe a signal. From Sause [78]
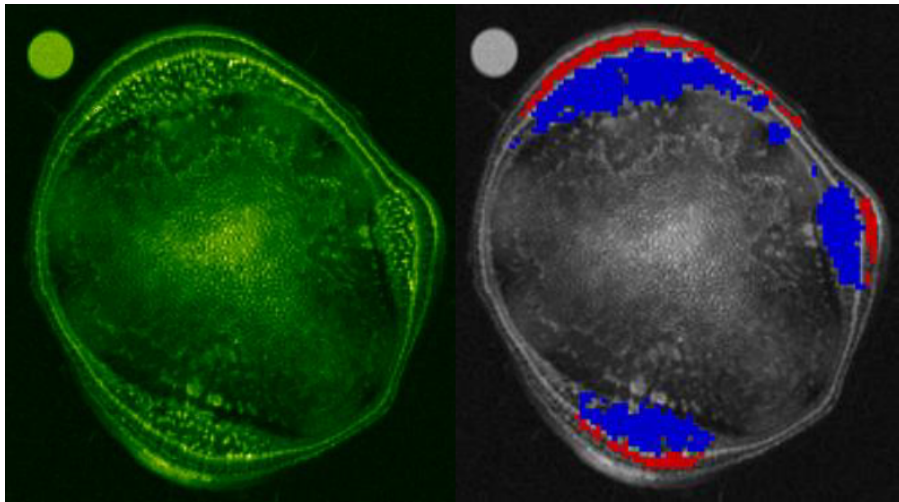
Figure 44: Axial image of plant stem of tomato plant. In the right picture, blue indicates the xylem vessels, red the phloem. From Prusova et al. [88]

C   Additional figures from Greenhouse Experiment
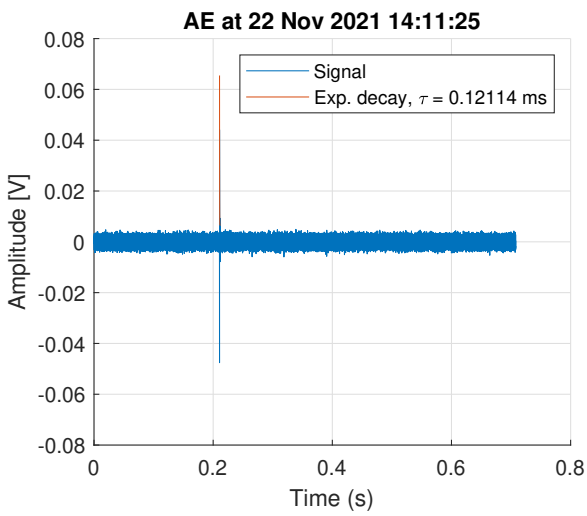
(a) Type I signal (time domain)
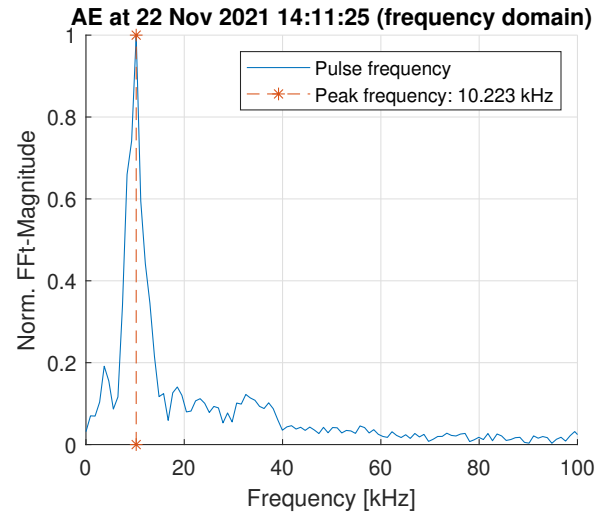
(b) Type I signal (frequency domain)
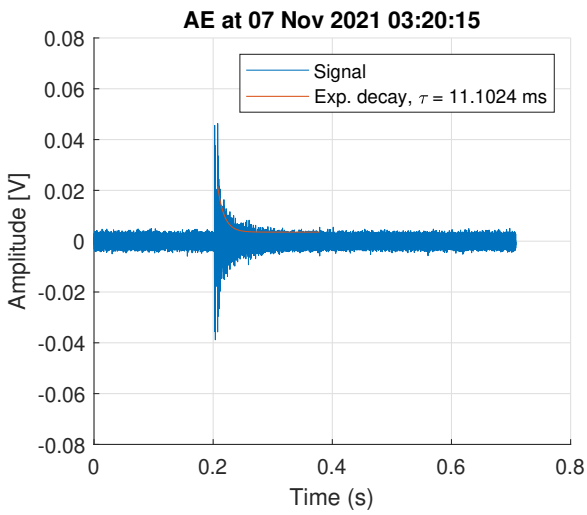
(c) Type II signal (time domain)
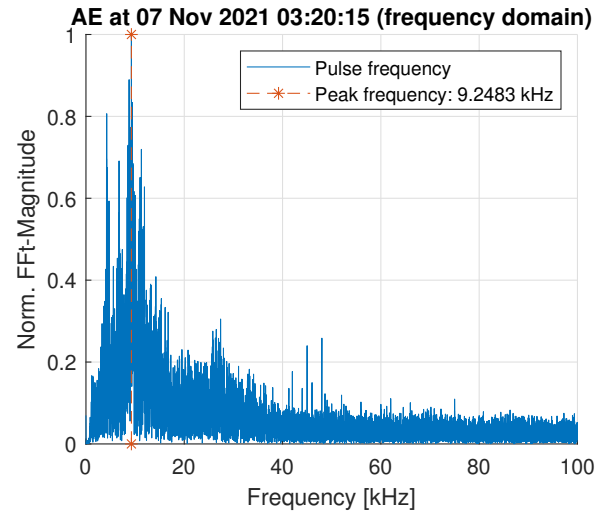
(d) Type II signal (frequency domain)
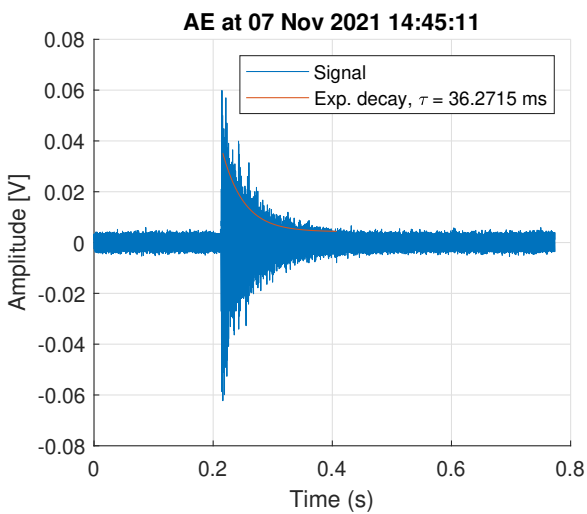
(e) Type III signal (time domain)
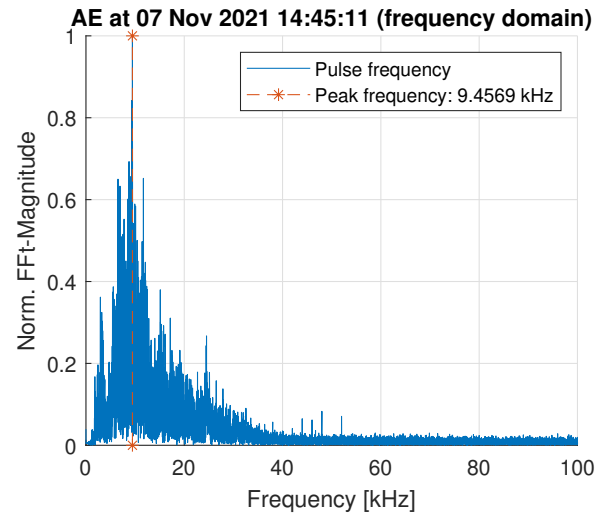
(f) Type III signal (frequency domain)

Figure 45:
Three types of signals form experiment 1
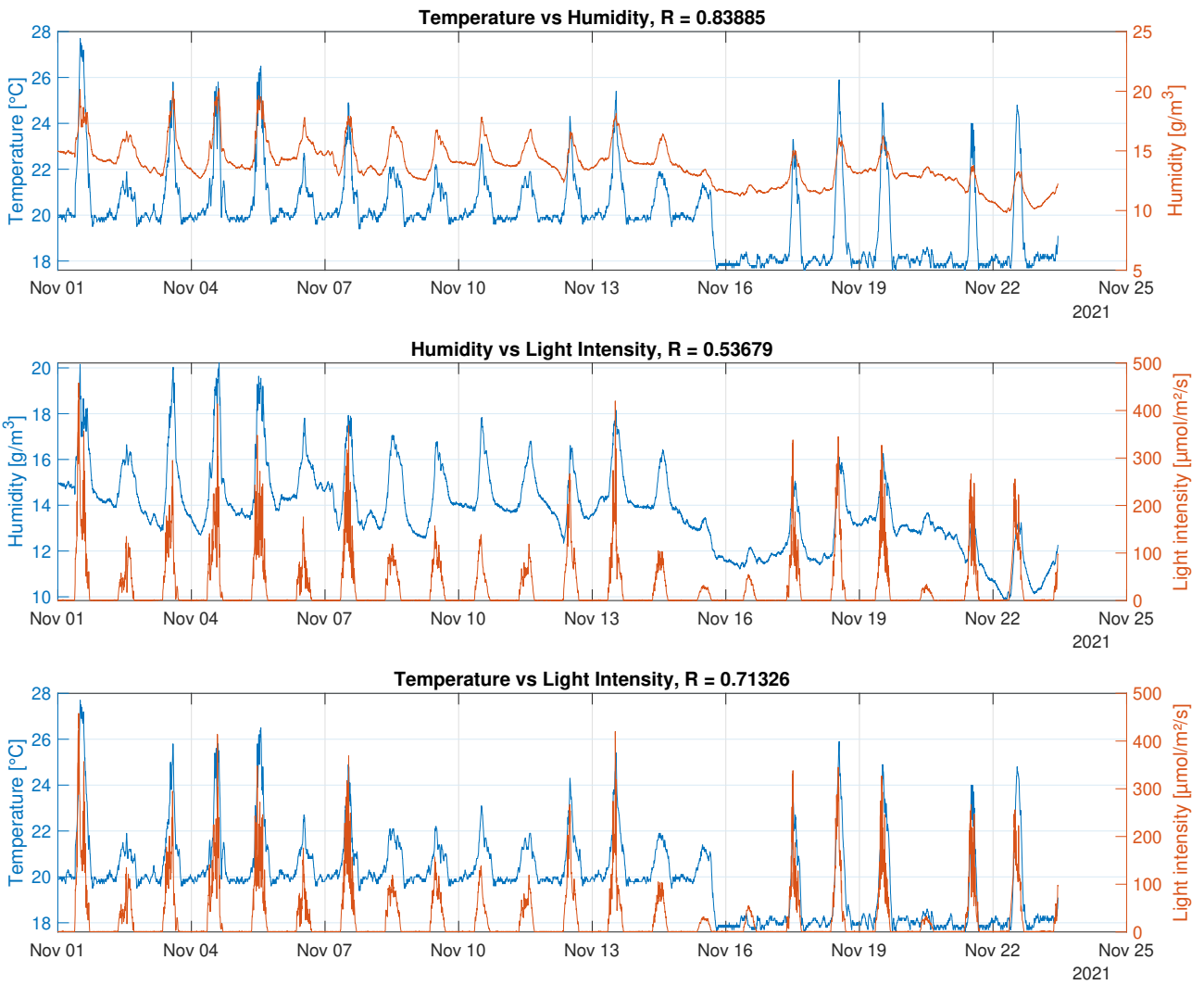
Figure 46: Relations between temperature, light intensity and humidity for total duration of experiment 1. It can be seen that around November 16, the nocturnal heating was decreased by 2 degrees. The R-value on the top of the graph shows the correlation coefficient, which can be interpreted as how well the parameters are in phase.
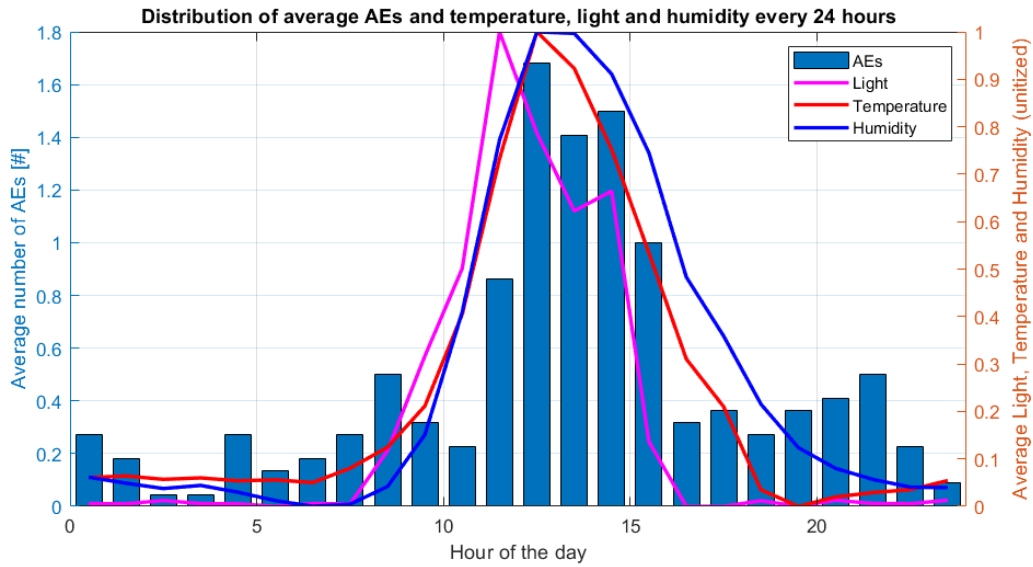
(a) Environmental parameters of total duration of experiment
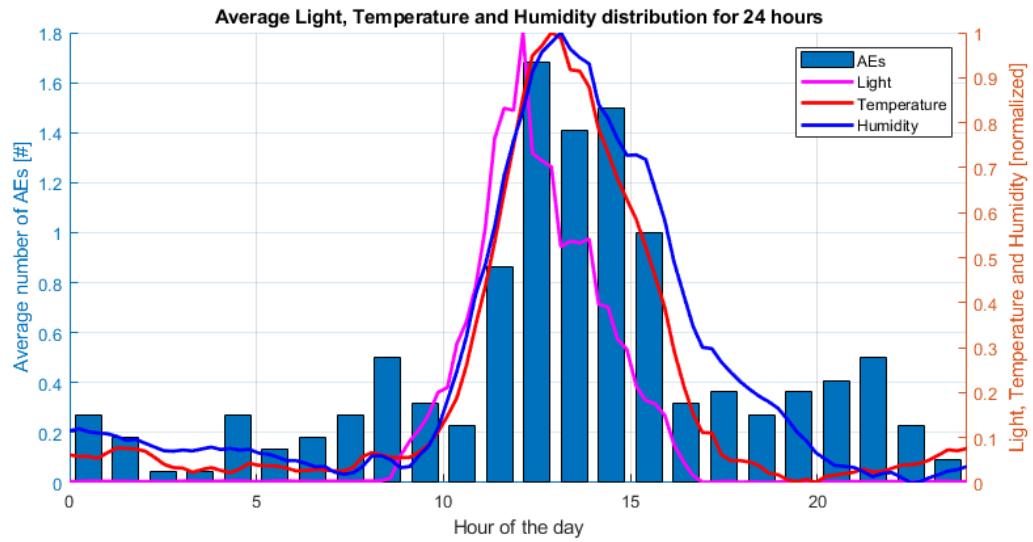
(b) Environmental parameters taken from November 16th and later. This is the same graph as figure 26.
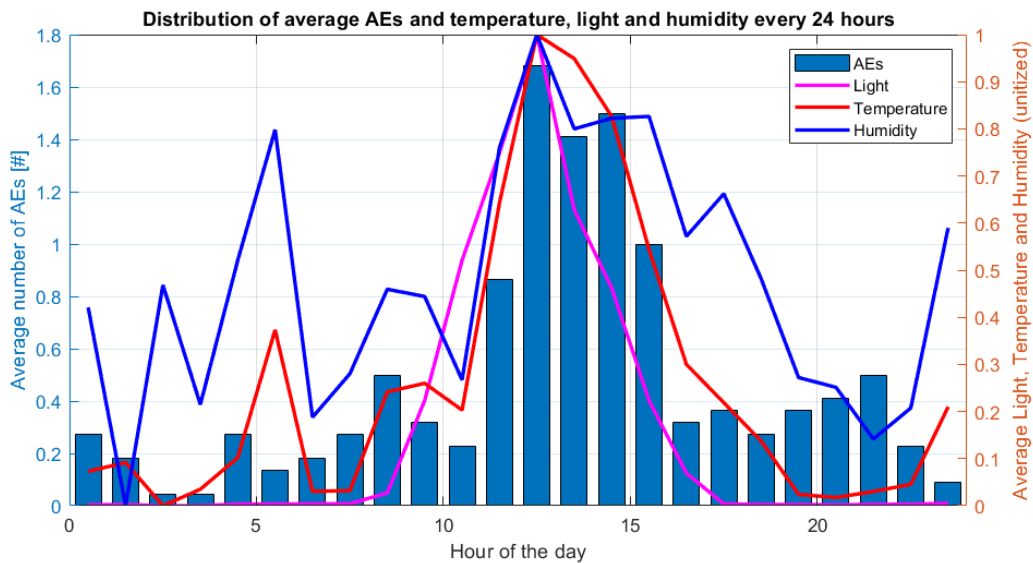
(c) Environmental parameters taken at moment when AE occurs

Figure 47: Relations between number of Acoustic Emissions and temperature, light intensity and humidity from the greenhouse experiment. The environmental parameters have been normalized. The rate of AEs is the same in all plots and are taken from the whole duration of the experiment. The average light, temperature and humidity are calculated in three different ways.
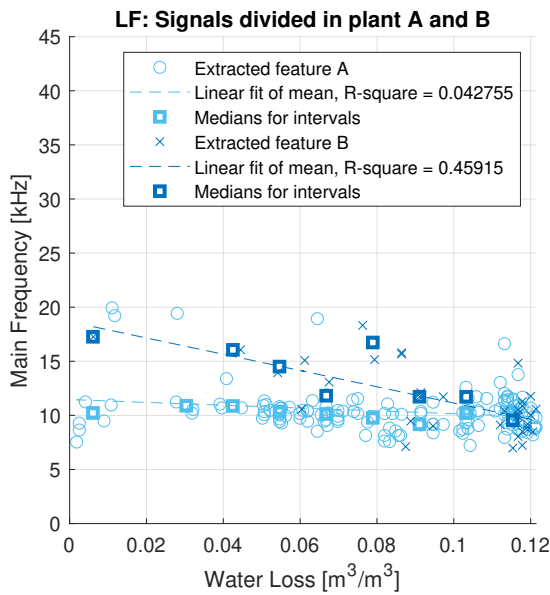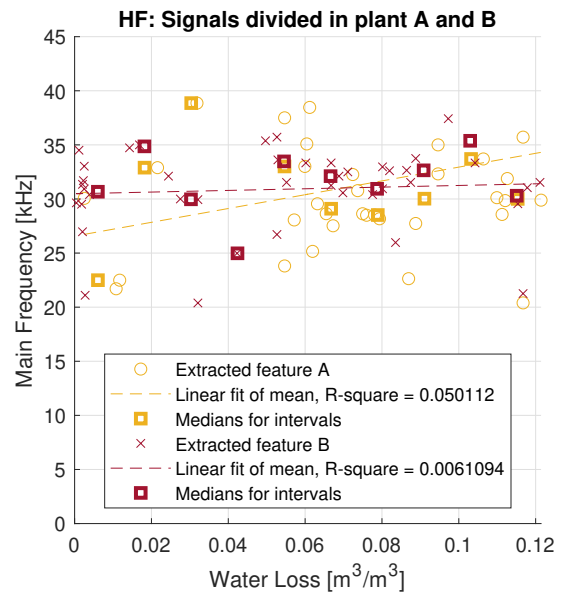
(a) Low frequency signals   (b) High frequency signals

Figure 48: Frequency as function of water loss for low frequency (left) and high frequency (right) signals, divided in plant A and plant B from experiment 1. The dots indicate each datapoint and the squares are the medians over a given interval. The dashed line indicates the linear fit of all datapoints.
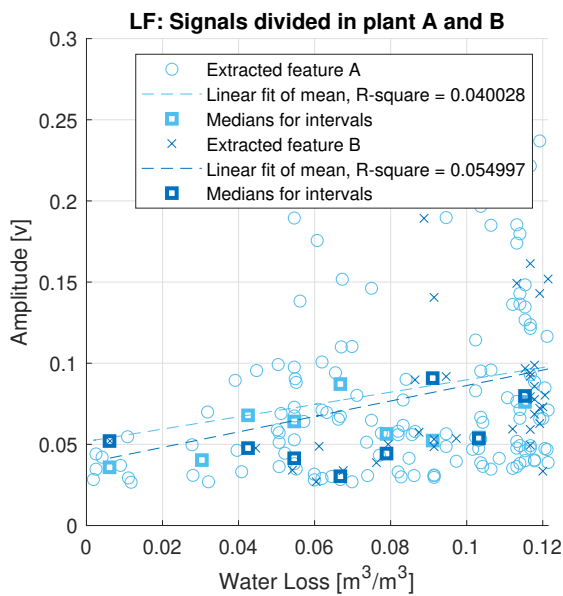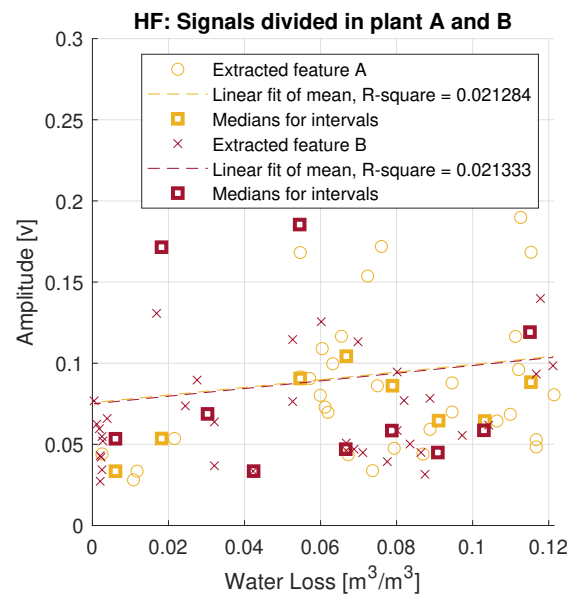
(a) Low frequency signals   (b) High frequency signals

Figure 49: Amplitude as function of water loss for low frequency (left) and high frequency (right) signals, divided in plant A and plant B from experiment 1. The dots indicate each datapoint and the squares are the medians over a given interval. The dashed line indicates the linear fit of all datapoints.
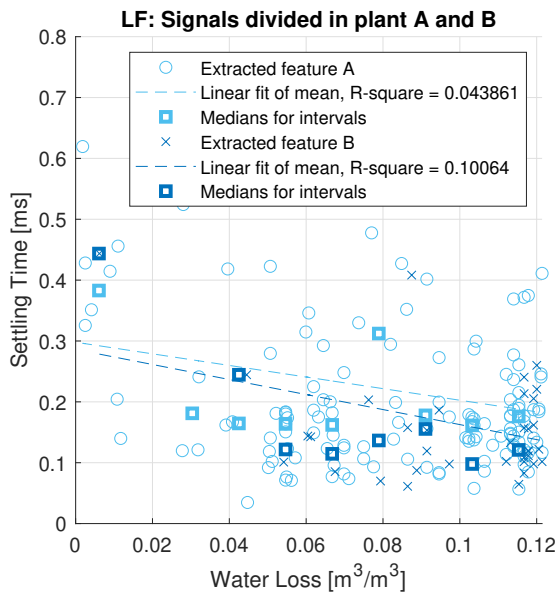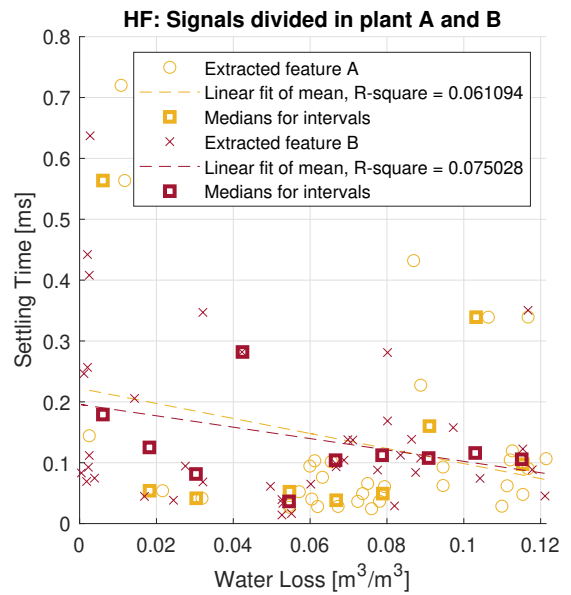
(a) Low frequency signals   (b) High frequency signals

Figure 50: Settling time as function of water loss for low frequency (left) and high frequency (right) signals, divided in plant A and plant B from experiment 1. The dots indicate each datapoint and the squares are the medians over a given interval. The dashed line indicates the linear fit of all datapoints.
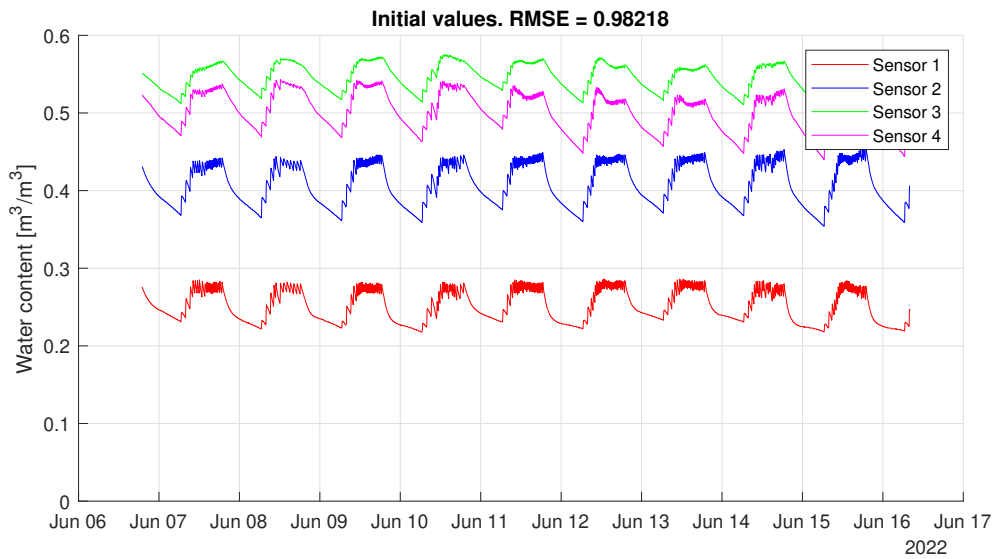
(a) Initial values.
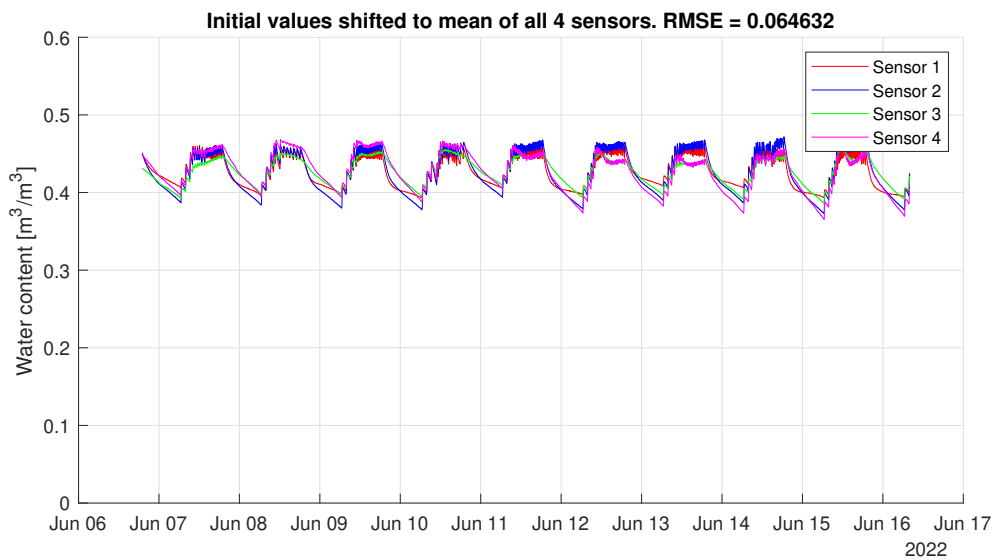
(b) The initial values have been shifted to the mean.
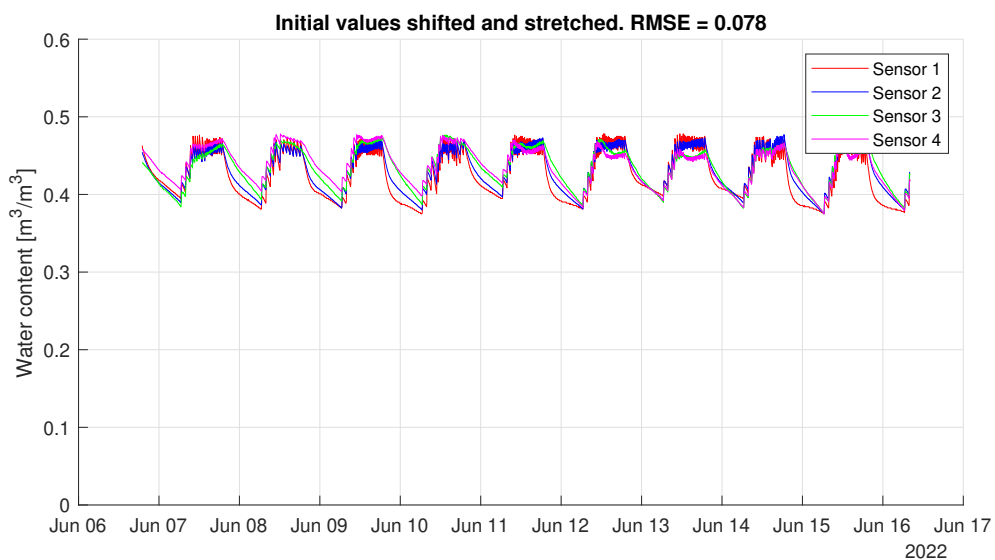
(c) The shifted values have been scaled to the largest range. This does not increase the RMSE

Figure 51: Separate experiment with 4 soil sensors that map the water content. Sensor 1, 2 and 3 were of type TEROS12 and sensor 4 was of type TEROS11. Only shifting the values (and not scaling) results in the smallest root mean square error.
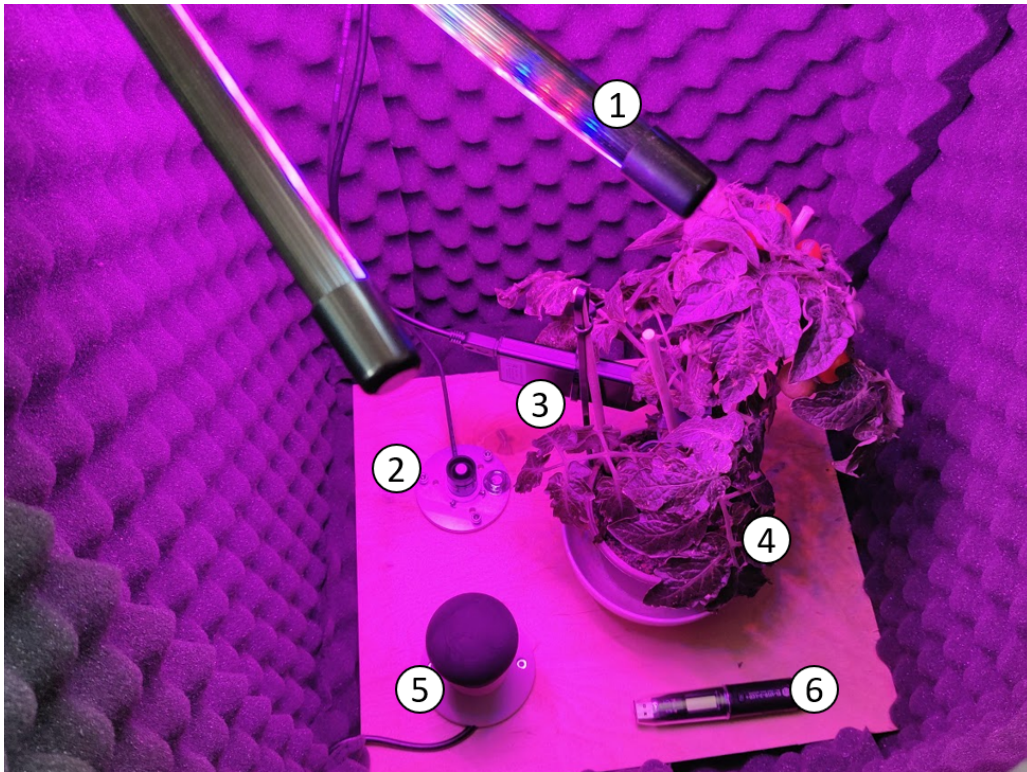
Figure 52: Separate experiment. Photo of the setup used indoor with the plant in an acoustically isolated box. 1: LED light. 2: Light sensor. 3: Ultrasound Microphone. 4: Water content sensor. 5: Heating with light bulb. 6: Sensor for temperature and humidity. No AEs of type I were observed with this setup.

D   Additional figures from climate chamber experiment

(a) Type I signal in time domain.

(b) Type I signal in frequency domain.
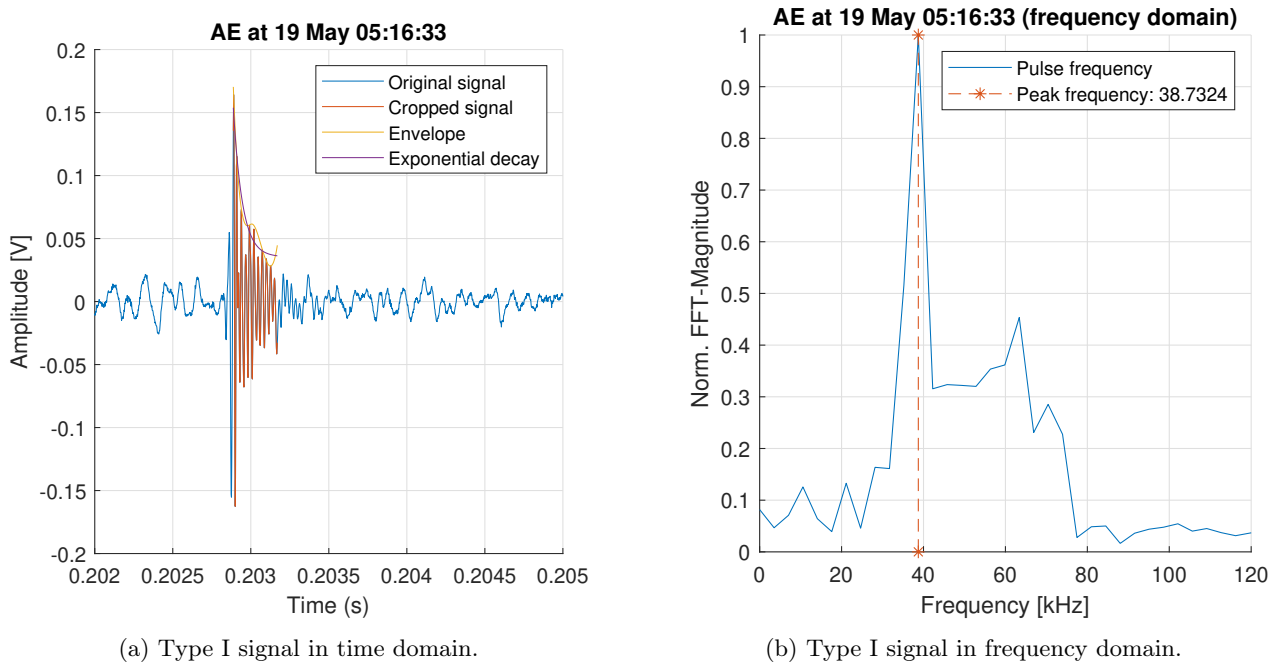
Figure 53: Example of type I signal from experiment 2 in the climate chamber in time- and frequency domain from plant 1B.

(a) Outlier signal (time domain)

(b) Outlier signal (frequency domain)
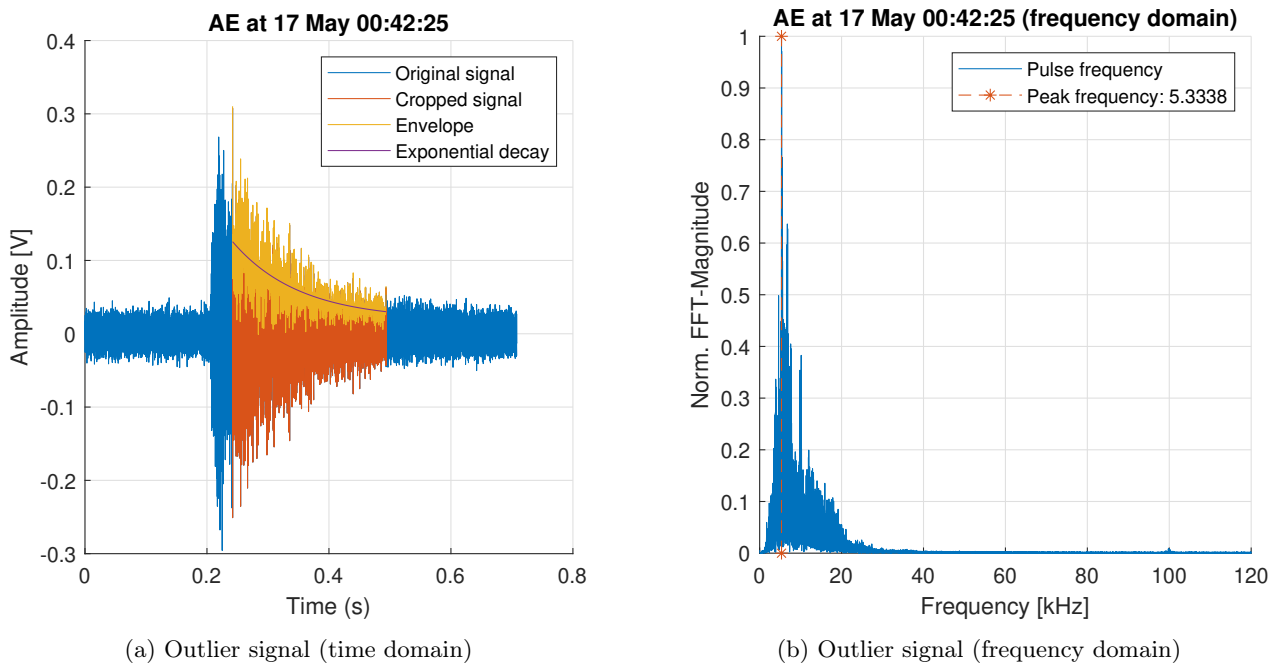
Figure 54: Example of outlier signal from experiment 2 in the climate chamber in time- and frequency domain.
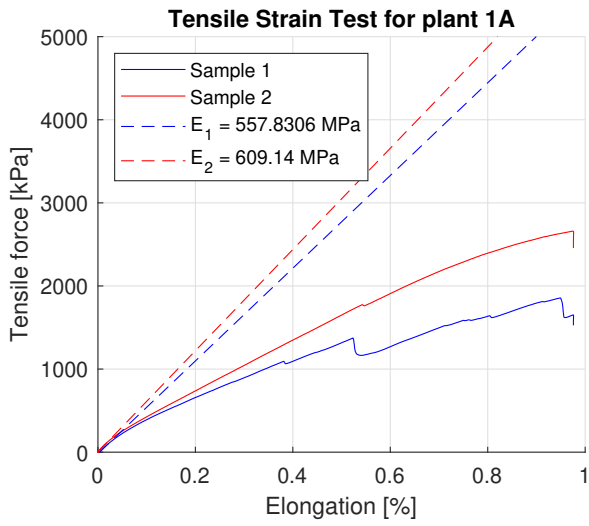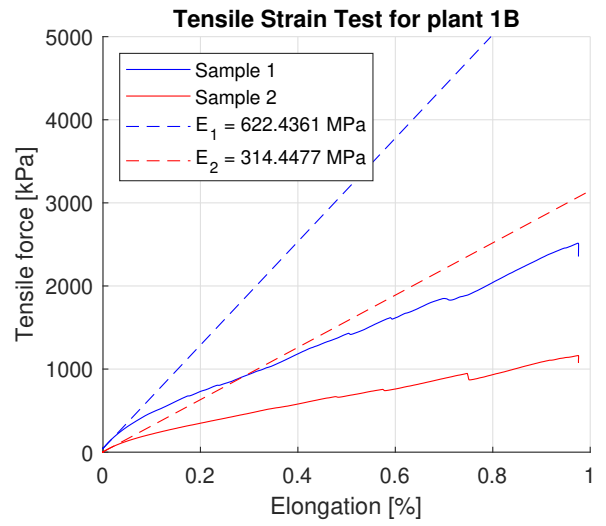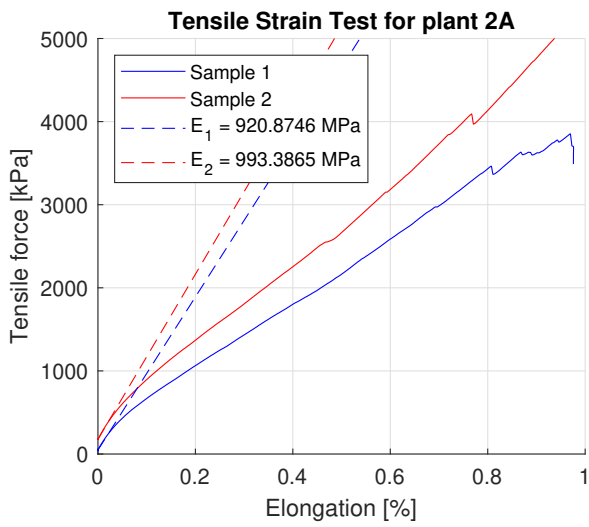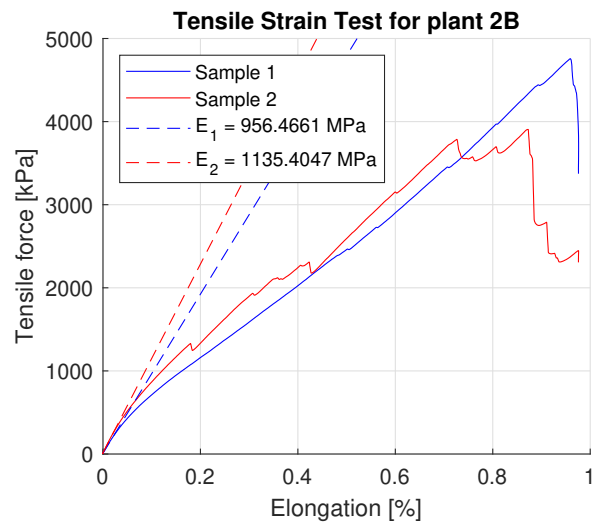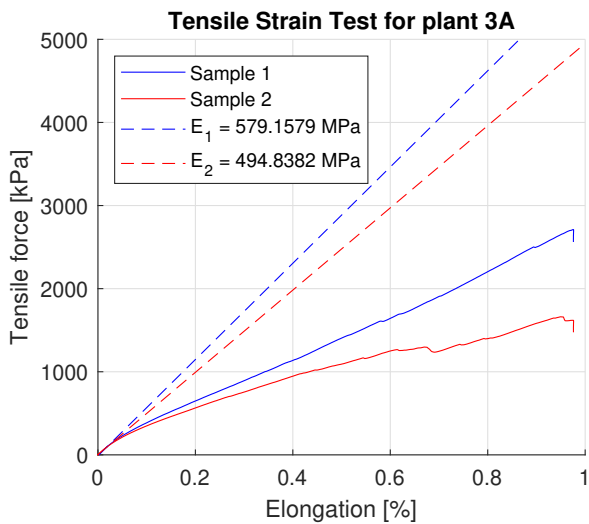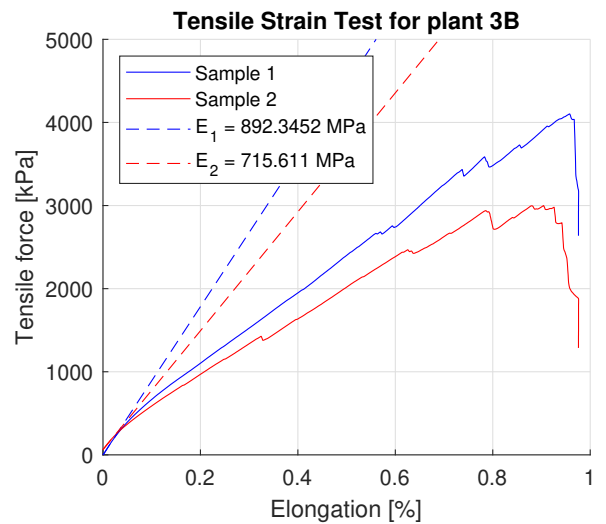
Figure 55:
Tensile force as function of elongation for all six plants from experiment 2. The dotted line is a linear fit for low straining. The slope is the Youngs Modulus. Per plant, 2 samples are taken and analysed.
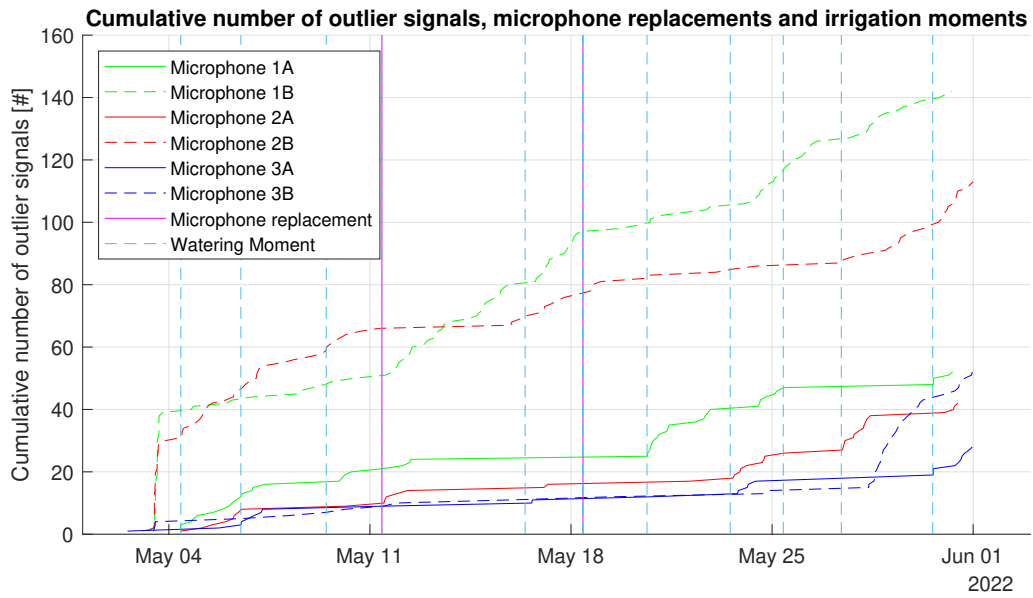
Figure 56: Cumulative number of signals that are not type I from experiment 2. 24 Hours after irrigation, the equipment for plant 1A, 2A and 3A (solid lines) stops working and no signals are recorded (except after irrigation moment 1, 7 and 8). On May 3rd, the microphones of plant 1B and 2B had fallen and on May 28th the microphone of plant 3B had fallen. This resulted in a steep increase of environmental noise signals, as the isolating foam was no longer in place.
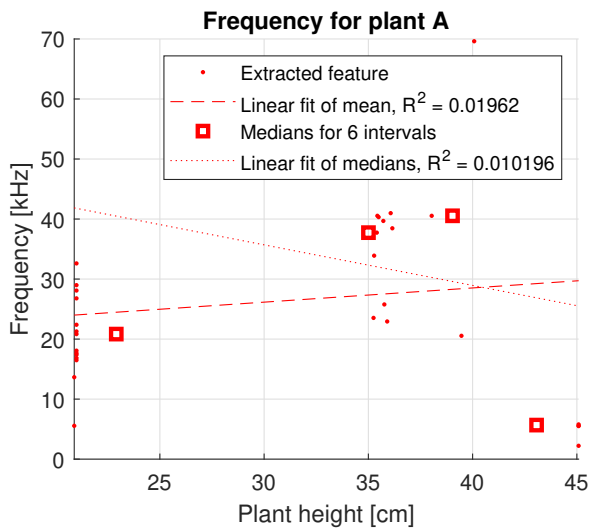
(a) Frequency of Plant 1A
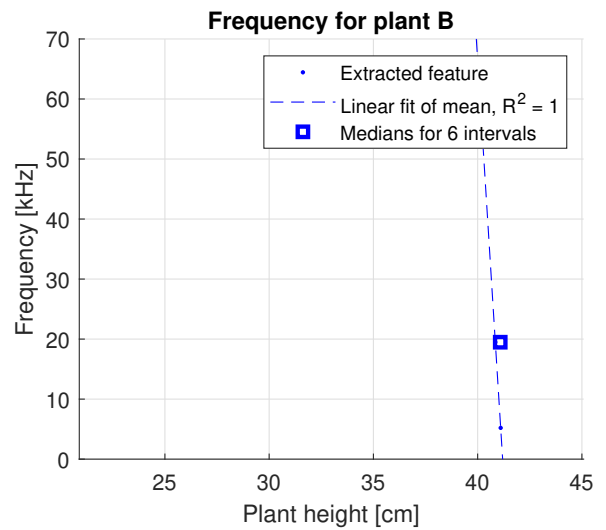
(b) Frequency of Plant 1B
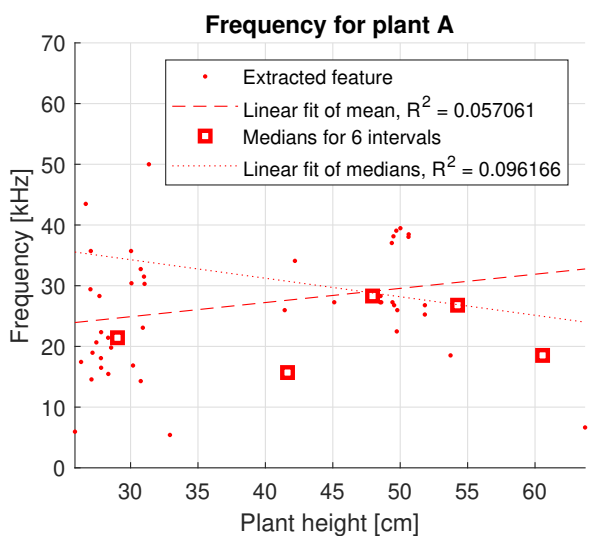
(c) Frequency of Plant 2A
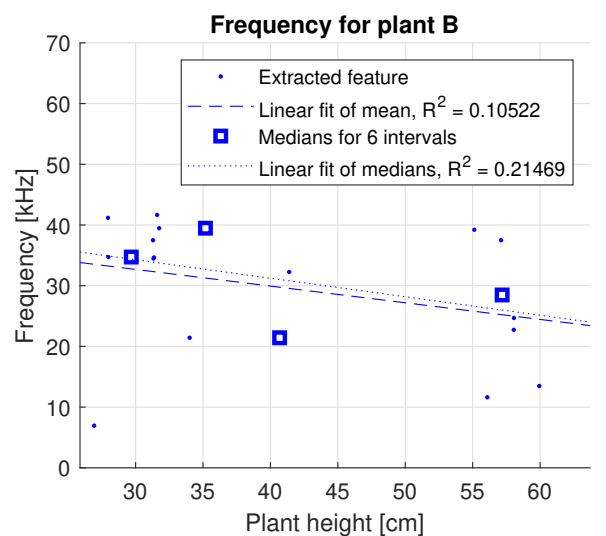
(d) Frequency of Plant 2B
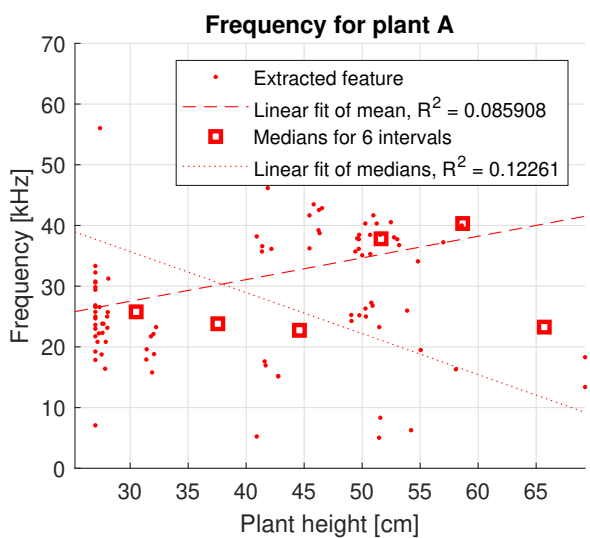
(e) Frequency of Plant 3A
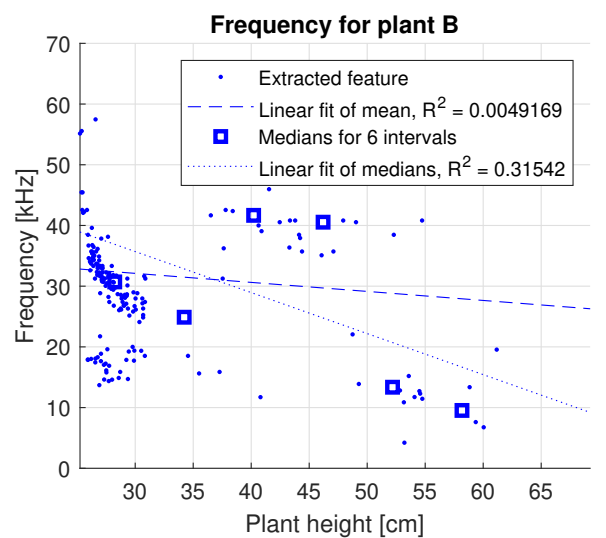
(f) Frequency of Plant 3B

Figure 57:
Frequency as function of plant height for total duration of experiment 2 for all six plants.
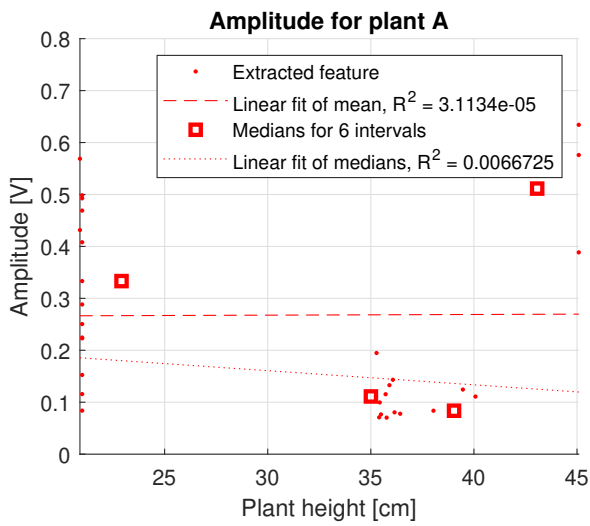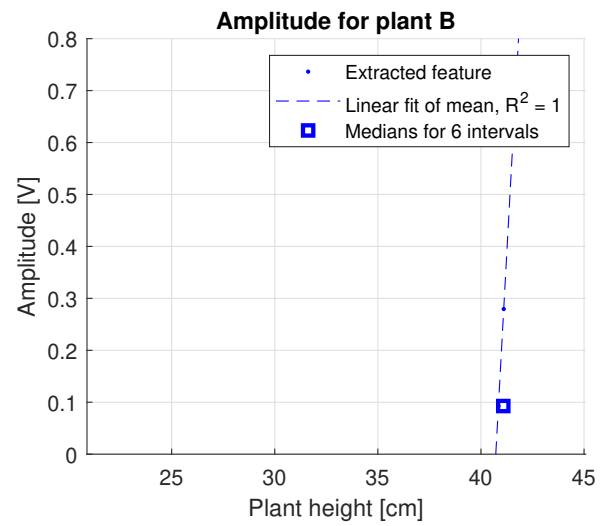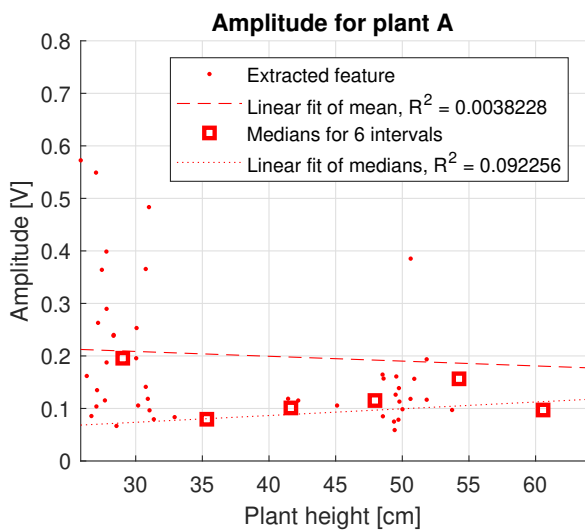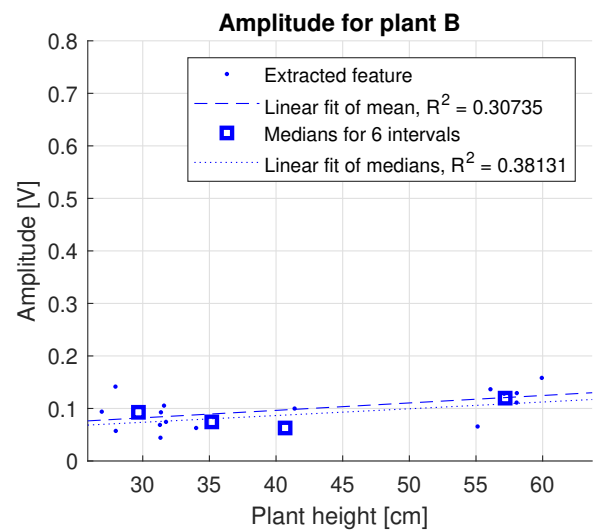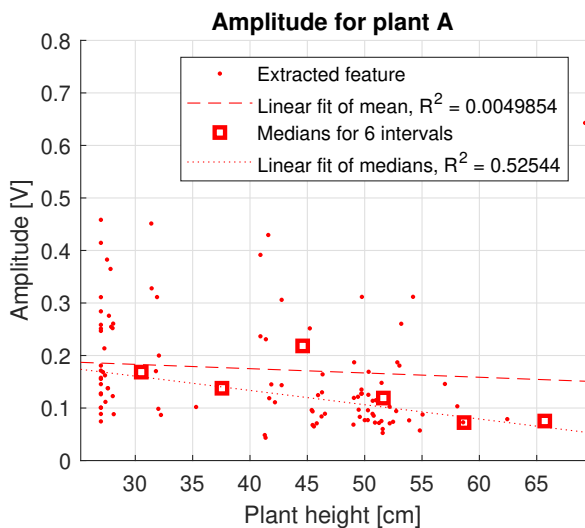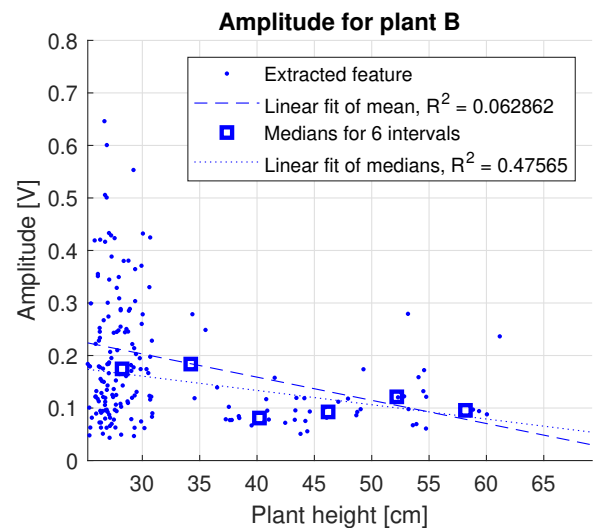
Figure 58:
Amplitude as function of plant height for total duration of experiment 2 for all six plants.
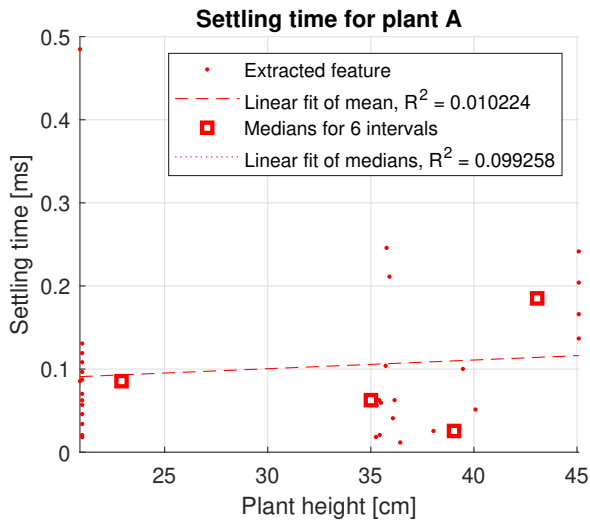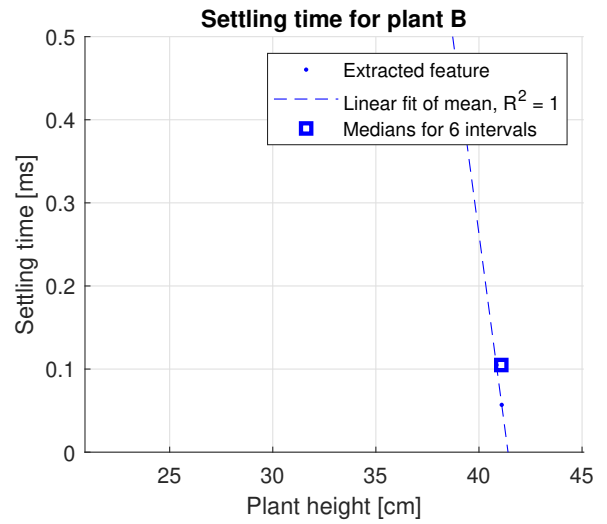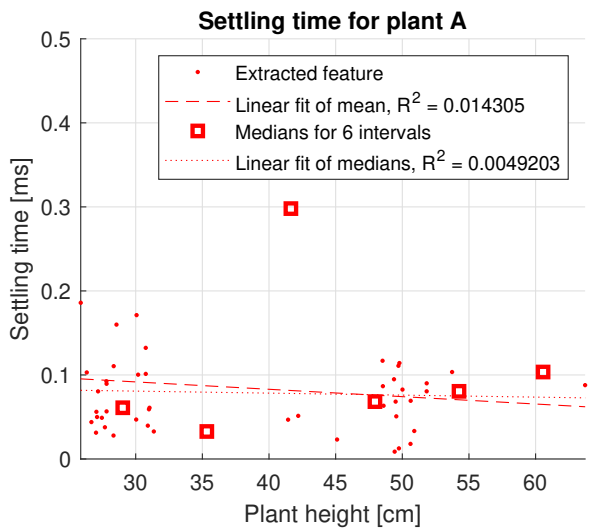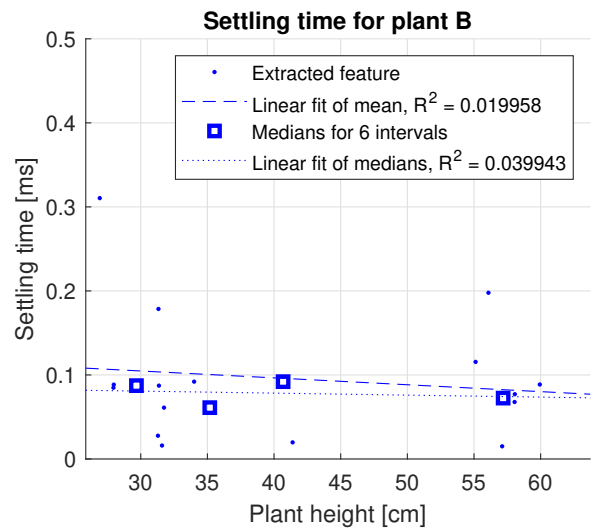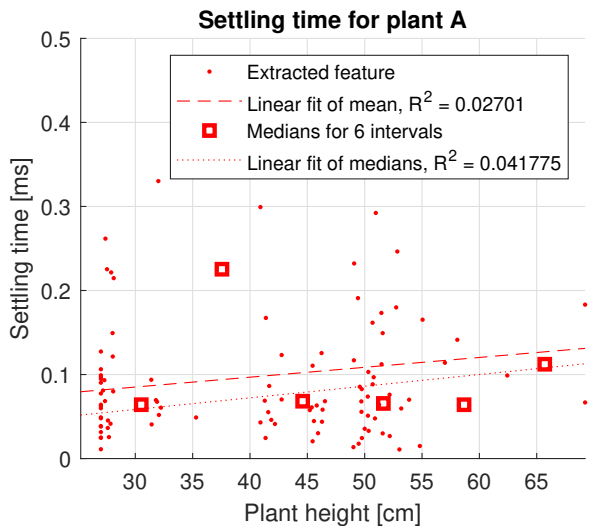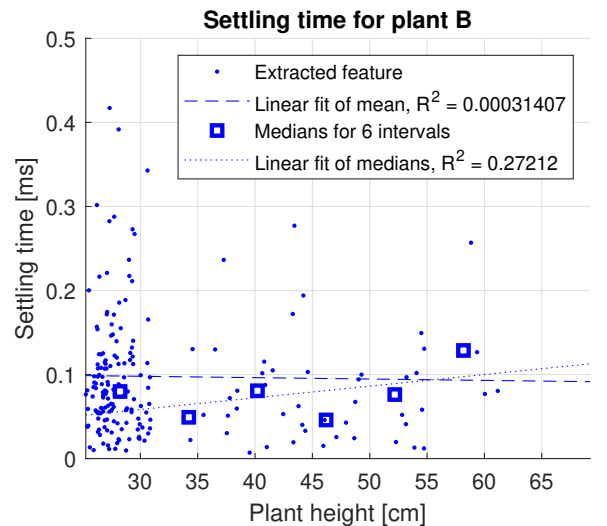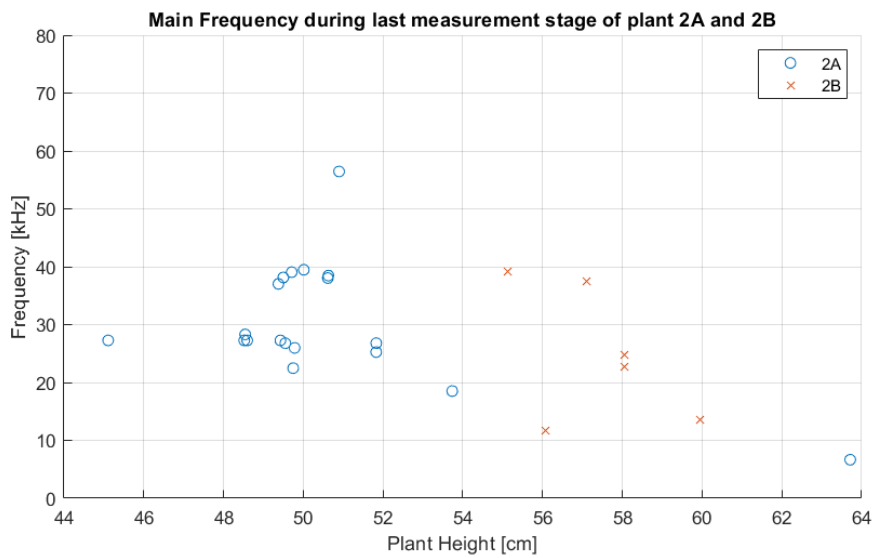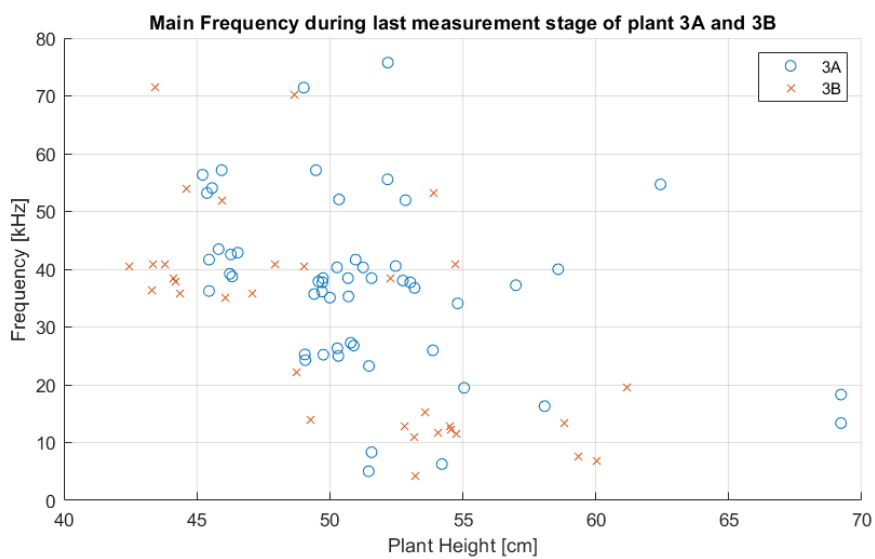
Figure 59:
Settling time as function of plant height for total duration of of experiment 2 for all six plants.
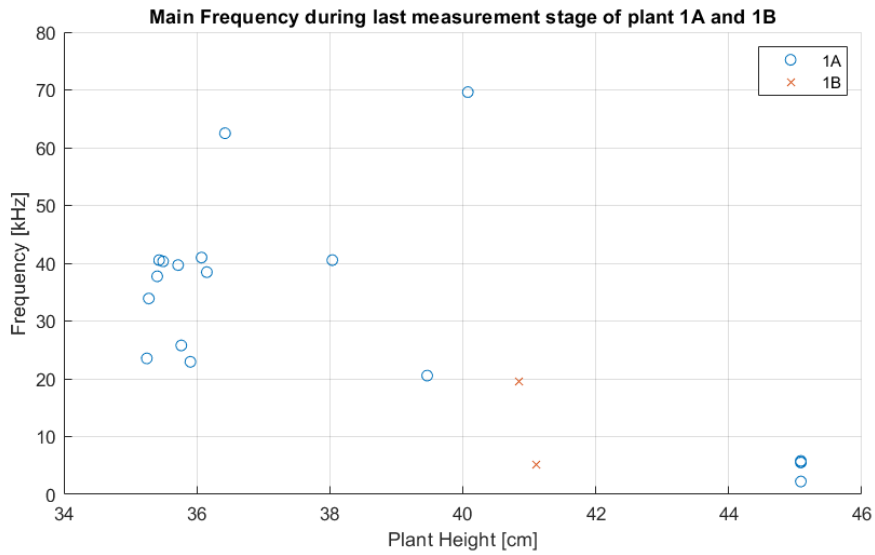
(a) Frequency during last stage of experiment for plant 1A and 1B

(b) Frequency during last stage of experiment for plant 2A and 2B

(c) Frequency during last stage of experiment for plant 3A and 3B

Figure 60: Frequency as function of time in the final stage of experiment 2 (after microphone replacement 2)

Figure 61: Plant 3A on May 11, right after the first microphone replacement of experiment 2. On the position where the microphone and isolating foam have been, the stem obtained a lighter color compared to the rest of the stem due to a decrease in chlorophyll.